8-2018

MICRORNA FUNCTIONS IN UV-INDUCED CUTANEOUS SQUAMOUS CELL CARCINOMA

Tran Nguyen

MICRORNA FUNCTIONS IN UV-INDUCED

CUTANEOUS SQUAMOUS CELL CARCINOMA

by Tran Ngoc Nguyen, B.Pharm.

APPROVED:

Kenneth Y. Tsai, M.D., Ph.D.
Advisory Professor

Elsa Flores, Ph.D.

Hoang Nguyen, Ph.D.

Anil Sood, M.D.

Swathi Arur, Ph.D.

APPROVED:

Dean, The University of Texas
MD Anderson Cancer Center UTHealth Graduate School of Biomedical Sciences

MICRORNA FUNCTIONS IN UV-INDUCED

CUTANEOUS SQUAMOUS CELL CARCINOMA

A

DISSERTATION

Presented to the Faculty of

The University of Texas

MD Anderson Cancer Center UTHealth

Graduate School of Biomedical Sciences in

Partial Fulfillment

of the Requirements

for the Degree of

DOCTOR OF PHILOSOPHY

By

Tran Ngoc Nguyen, B.Pharm.

Houston, Texas

August, 2018

Acknowledgement

Looking back the past 6 years since I started my graduate study at the University of Texas MD Anderson Cancer Center, I am extremely grateful for all the love and support I receive from friends, family and colleges who have made my PhD a very memorable and joyful experience.

First, I would like to thank Vietnam Education Foundation (VEF) for providing me financial support and helps to pursue my graduate study in the United States. At MD Anderson Cancer Center, I had the opportunity to know and discuss with Dr. Kenneth Y. Tsai. His solid knowledge and intuition in the field of cancer genomics had motivated me to join his group at the MD Anderson Cancer Center, and ever since I always knew that his lab was the right place for me. I would like to express my deepest acknowledgement to Dr. Tsai for his strong support from all fronts. Not only providing me with invaluable resources and guidance to lead me through the tough times of my research, his style of mentorship has also helped me to become a very independent researcher, preparing me for the next step of my career. I am also sincerely grateful to my other committee members, Dr. Elsa Flores, Dr. Hoang Nguyen, Dr. Swathi Arur and Dr. Anil Sood for providing insightful comments and suggestions for my research.

Research is a collaborative effort and a substantial portion of my success is rested on the shoulders of my lab members and collaborators. I would like to give a special thank you to Dr. Sadhan Majumder whose lab I have worked in for more than a year. Dr. Majumder is the kindest and most knowledgeable mentor that anyone could ask for. I would like to thank Dr.

Abstract

MICRORNA FUNCTIONS IN UV-INDUCED CUTANEOUS SQUAMOUS CELL CARCINOMA

Tran Nguyen, B.Pharm.

Advisory Professor: Kenneth Y. Tsai, M.D., Ph.D.

Cutaneous squamous cell carcinoma (cuSCC) is the second most common skin cancer, for which long term UV exposure and chronic wounding are the dominant risk factors. Despite these clinically established connections, little is understood about the early molecular response of human skin to UV exposure and its connection to acute wounding and cuSCC. Thus, our goal is to find common and specific signatures driven by UV-exposure and wounding as a means of developing new approaches for treating and preventing cuSCC.

Here, we perform integrated analyses of RNA-seq and miR-seq on 3 datasets: (1) UV-unexposed and acute UV-exposed human skin, (2) public dataset on acute wound healing and (3) our previously published dataset on normal skin and cuSCC from humans. We find that biological signatures and processes regulated by acute UV exposure and wounding has profound similarity.

Through RNA-seq and miR-seq on matched normal skin and cuSCC tumors from humans and a UV-driven mouse model, as well as acute UV-exposed human skin, we were able to identify a group of miRs that change both in cuSCC development and following UV

exposure. We previously reported that miR-21-5p and miR-31-5p overexpression correlates with the development of UV-induced cuSCC in human. This is also true for our analysis where we find that these miRs as well as miR-21-3p are upregulated by more than 6-fold in cuSCC (compared to normal skin) and more than 2.5-fold in UV-exposed skin (compared to unexposed skin). In addition, we identify that miR-340-5p and let-7i-5p are novel candidates that have not been previously linked to either cuSCC development or the UV response of human skin.

This suggests that these changes in miRNA-RNA are important early events that regulated by both UV-exposure and wounding which eventually can promote cuSCC initiation. Thus, our findings suggest that UV-exposed skin, wound and cuSCC share various common signatures, which can be potentially validated as chemopreventive targets for cuSCC.

Table of Contents

List of Figures

List of Tables

Chapter 1: Introduction

1.1 Cutaneous Squamous Cell Carcinoma: Background and Motivation

Cutaneous squamous cell carcinoma is the second most common skin cancer, surpassed only by basal cell carcinoma (1, 2). Annually, an estimated of over 250,000 new cases of cuSCC are diagnosed in the United States (3). In 2012, 3900 to 8700 people in the United Stated died from cuSCC. Although the exact incidence of cuSCC is unknown since it has not been included in national cancer registries, this incidence has been recorded to steadily rise during the last four decades in both men and women (Figure 1) (3). Risk factors for cutaneous squamous cell carcinoma include chronic sun exposure, older age, and impaired immune surveillance with sun exposure being the main etiological factor (4). It is well-established that actinic keratosis (AKs) are pre-neoplastic lesions that can progress to cuSCC. The rate of progression occurs at a statistically low of 10% annually (5).
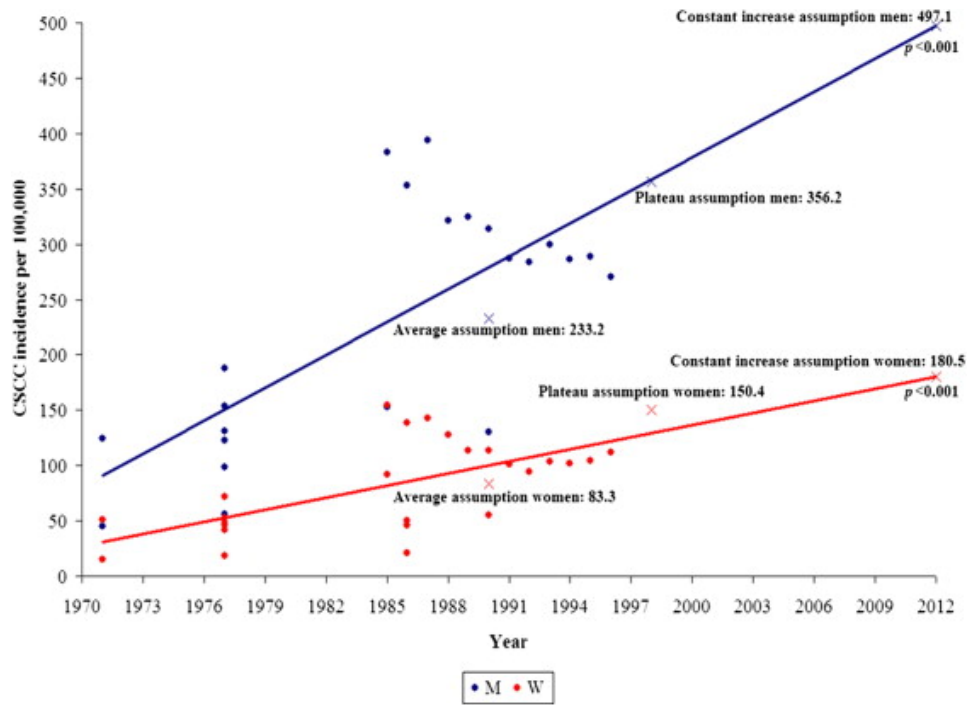
Figure 1

Increase in age-adjusted incidence of cutaneous squamous cell carcinoma in sun zone 2 by gender with average, plateau, and constant increase assumption incidence estimates (X). This figure is reproduced based on previously published figure (3)

From the clinician's perspective, cuSCC is highly curable and more than 95% of cuSCC patients were cured with surgical excision (4). Nevertheless, there is a subset of aggressive cuSCC tumors recur or metastasize, resulting in a 2.1% risk of disease specific death overall (6, 7). In immunosuppressed patients, cuSCC displays more rapid growth, has 13% risk of recurrence, and 5-8% risk of metastasis (8). Once a cuSCC has recurred, it has a much worse prognosis, with risk of metastasize to lymph nodes and distant organs cited as high as 45% (9).

Given its steep rise in incidence, limited therapeutic options for advanced or metastatic disease and potential for poor outcomes, cSCC is emerging as a public health problem. Thus, understanding the genomic signatures of cuSCC can help identify potential predictive biomarkers that can dictate prevention and upfront treatment approaches.

1.2 High-risk cutaneous squamous cell carcinoma

Cutaneous squamous cell carcinoma (SCC) includes many subtypes with widely varying clinical behaviors, ranging from easy-to-manage indolent to aggressive tumors with significant metastatic potential.

It is well documented that immunosuppressed patients due to solid organ transplantation are at greater risk of developing cSCC, with an estimated 65-fold increase compared to the general population (10). The cuSCC to basal cell carcinoma ratio is reversed in the immunosuppressed population. While cuSCCs make up 20% and basal cell carcinomas make up 80% of NMSCs in immunocompetent patients (10, 11). These cancers are more aggressive, with an increased risk of metastases (12). Recurrence and mortality rates are also higher in patients who are immunosuppressed (5%) than those who are immunocompetent (1%) (13, 14).

3

In addition to immunosuppressed patients, patients who suffer from chronic skin injuries, such as wounds, or burns, are at increased risk of developing aggressive cSCC (13). Included in this subgroup are patients with a genetic predisposition to skin injury, including epidermolysis bullosa, xeroderma pigmentosum, and congenital dyskeratosis (13, 15, 16).

1.3 Genomic background of cuSCC development

Like other cancers, the development of cuSCC is likely a multi-step process, involving sequential acquisition of genetic changes. The genomic profile of AKs, the precursors of cuSCC, significantly overlaps that of cuSCC (17). Previously reported, cuSCC tumors features very high background mutation rate with a significant enrichment in UV signatures (Figure 2) (17, 18). UVB exposure is known to cause C>T transitions often following a pyrimidine base. The mutation spectrum of cuSCC is quite similar to that of head and neck cutaneous squamous cell carcinoma (HNSCC) except for the UV signature. In cuSCC, high frequencies of inactivating mutation were found to occur in major tumor suppressors *TP53*, *CDKN2A*, *NOTCH1* and *NOTCH2* (17-19).

1.4 UV spectrum of solar radiation (UVR)

Ultraviolet (UV) rays are a form of invisible energy given off by the sun. Based on wavelength solar UV radiation (UVR) is divided into three ategories, UVA (320-400nm), UVB (280-320nm) and UVC (100-280nm). Minute amount of UVC reaches the earth surface by penetrating the ozone layer of atmosphere and for this reason UVC is not physiologically relevant for studies of human skin cancer. On the other hand, UVA rays account for the majority

(95%) of the UV radiation reaching the earth's surface; terrestrial radiation from the midday sun comprises about 95% UVA and 5% UVB [17]. UVA is mainly responsible in the aging of the cells and some DNA damage. On the other hand, UVB rays cause direct DNA damage and responsible for sunburns. UVA rays can penetrate deeply into the skin and mainly cause dermal compartment damage while UVB damage is mainly in the epidermal compartment. UV radiation can cause an increase in collagen breakdown and abnormal deposition of elastin [18, 19]. This process and it's pathological manifestation is referred to as solar elastosis. In addition, UV radiation can cause an increase in free radicals resulting in damage of cellular functions and DNA damage. Moreover, UV radiation can suppress the immune system by inducing release of certain cytokines, inhibiting antigen presentation, and enhancing leukocytes apoptosis [20].
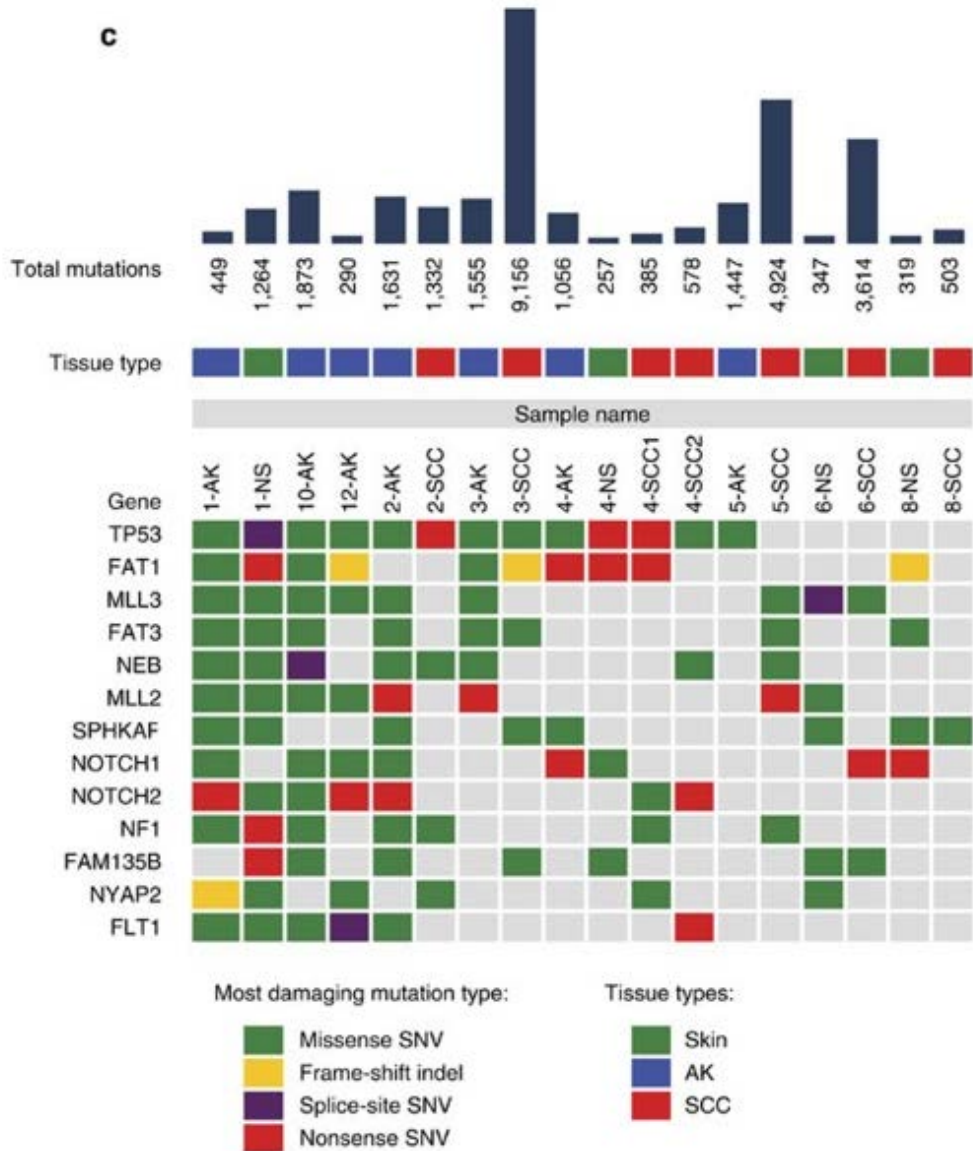
Figure 2

Key mutations in cSCC. Total number of mutations per patient is shown on the top. Inactivating mutations include nonsense, frameshift, and splice site events. This figure is reproduced based on previously published figure (17).

6

At the chromosomal level, several studies have shown that cuSCC can display complex karyotypes with large numbers of allelic imbalances (20, 21) .Moreover, widespread gains and losses of chromosomal fragments have been reported to be already present in AKs (22).

It has been challenging to identify drivers of progression to cuSCC from normal skin as multiple studies show little overlap in differentially expressed (DE) genes in their genome-wide transcriptional profiles. Majority of the studies have employed cuSCC cell lines or small cohorts of unmatched normal skin, AKs and cuSCC tissues on several platforms known to have potentially high annotation error rates (23-26). Using normal skin, AKs and cuSCC tissues derived from patients received immunosuppressive drugs, Hameetman at el. suggested that the NFκB1 and TNF pathways activated as early as AKs stage while RAS and MYC oncogenic pathways appear to be specifically activated in cuSCC (23). Using cross-species approach on sporadic cuSCC in human and UV-induced cuSCC in mouse, our lab has identified several key early transcriptional drivers of cuSCC include E2F, ELK1 and NFY (17). These early findings serve as foundation for further transcriptomics studies of UV-induced cuSCC.

1.5 UV-induced hairless mouse model

In cuSCC research, there are currently two types of mouse model being widely used. The differences lie on how the tumors were induced. The first one is the two-stage chemically induced skin carcinogenesis model (27). In brief, a subcarcinogenic dose of carcinogen 7,12-dimethylbenz[a]-anthracene (DMBA) (Figure 3) was applied onto the mouse skin, followed by repeated application of tumor promoting agent 12-*O*-tetradecanoylphorbol-13-acetate (TPA). This model allows the initiation and promotion stages can be distinctly separated both

operationally and mechanistically. In lesions initiated by this method, mutations in *Hras1 (*A →

T (182) transversion in codon 61) *Kras*, and *Trp53* were observed (28-31). Although the

chemically-induced mouse model proved to be extremely useful and faithful in creating

papillomas and cuSCCs, the need for a mouse model that better captured the genomic features

of human UV-induced cuSCC emerged.
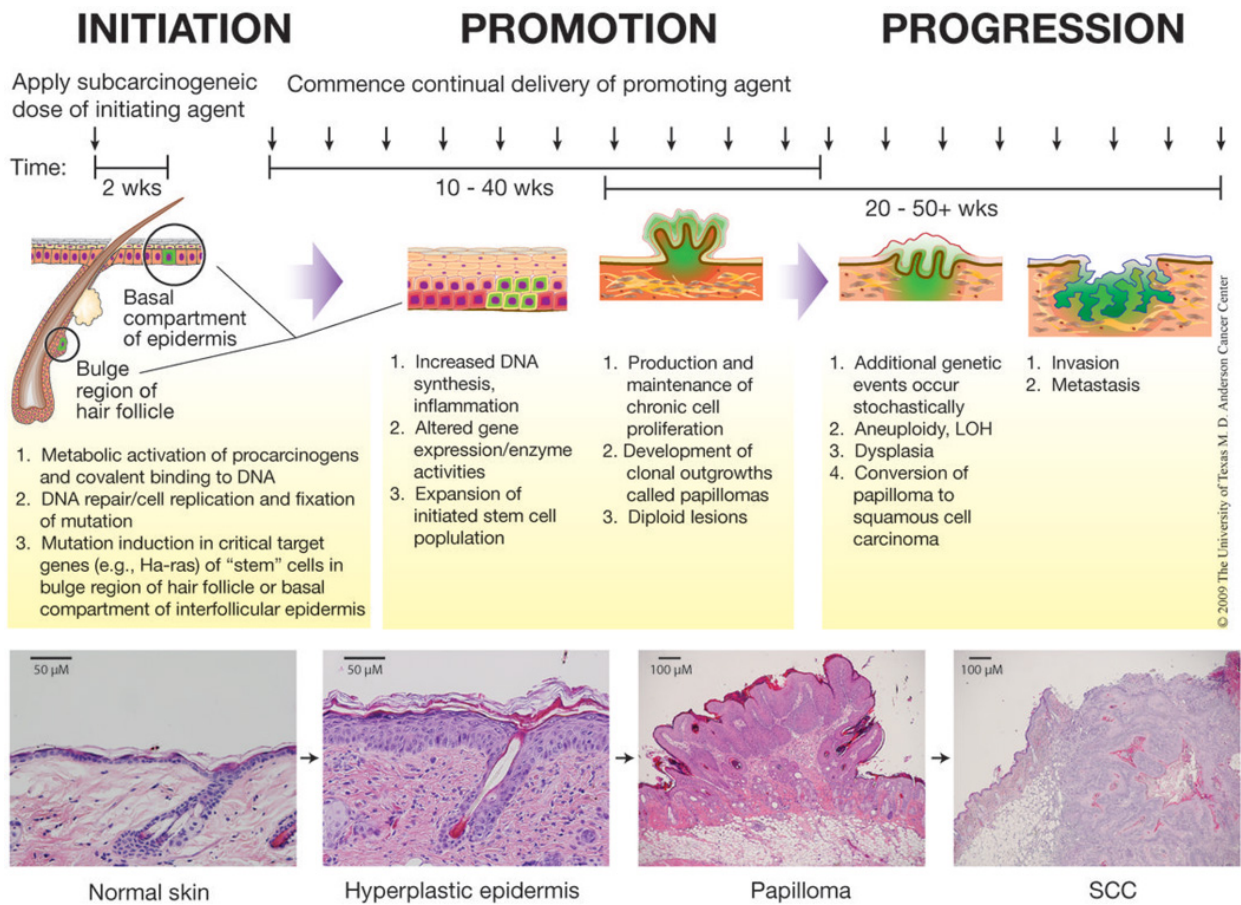
Figure 3

Two-stage model of skin carcinogenesis in mice

This figure is reproduced based on previously published figure (27).

During initiation, topical application of a sub-carcinogenic dose of a mutating agent induces mutations in target genes in keratinocyte stem cells. Repeated topical application of a promoting agent begins two weeks after initiation and continues for the duration of the study. Papillomas begin to arise after approximately 6–12 weeks of promotion and a fraction begin to convert to SCC after approximately 20 weeks. Representative H&E stained sections of normal skin, hyperplastic skin, a papilloma, and a SCC are presented. All mice were handled in accordance with institutional and national regulations. This figure is reproduced based on previously published figure (27).

The second cuSCC mouse model is UV-induced SKH1 hairless mouse model. Tumors induced in these mice resemble both at the morphologic and molecular levels, UV-induced skin malignancies in human. Although there are various strains of hairless mice, outbred albino SKH1 is the strain most extensively used for Wound healing, acute photobiologic responses, and skin carcinogenesis. We chose this model to avoid chronic irritation as a confounding variable in our studies that is due to depilation of mice. In addition, with this model we can eliminate the effects of hair cycle on skin carcinogenesis.

Murine Hr gene locates at the 70Mb on mouse chromosome 14. In mice, *Hr* gene encodes a ~130kDa protein (32). The HR protein is a transcriptional co-repressor, binding to thyroid hormone, vitamin D, and retinoic acid receptor-related orphan receptors but not to retinoic acid or glucocorticoid receptors (33). Embryonically*, Hr* is expressed in various tissues and highly expressed in both hair follicle and interfollicular keratinocytes of epidermis by birth. The mutant allele that is carried by SKH1 mice is autosomal recessive, *hr*, which has an

9

aberrant splicing due to stable integration of a retrovirus into the 6th intron of the gene. In human, two autosomal recessive diseases are associated with *Hr* mutations. Various studies have shown that for normal hair growth *Hr* is necessary and sufficient (34). Hair growth in hairless mice is normal during the first hair cycle; however, mice rapidly lose hair starting cephalically and proceeding caudally(34). During consecutive hair cycles, follicles develop abnormally with characteristic histological findings of utriculus, deep dermal cysts, and sebaceous gland hyperplasia (34).

Each mouse can produce multiple skin tumors, independent of one another, and this feature can be used to discern the rate of development and individual aggressiveness of each tumor. Tumor progression starts from epithelial hyperplasia which then progresses to papilloma and eventually into carcinoma. From this progression sequence, we can identify markers for tumor initiation, promotion and progression. Hairless mice have been shown to be sensitive to development of UV-induced carcinoma that have similar pattern of mutations as human cuSCC. Of important note, haired mice are less susceptible to UVR immunosuppressive effects than nude mice. In the SKH-1 Hairless mouse model of UV-induced cuSCC, *p53*, *RAS*, and *CDKN2A* are similarly affected as seen in human cuSCC [7-16].
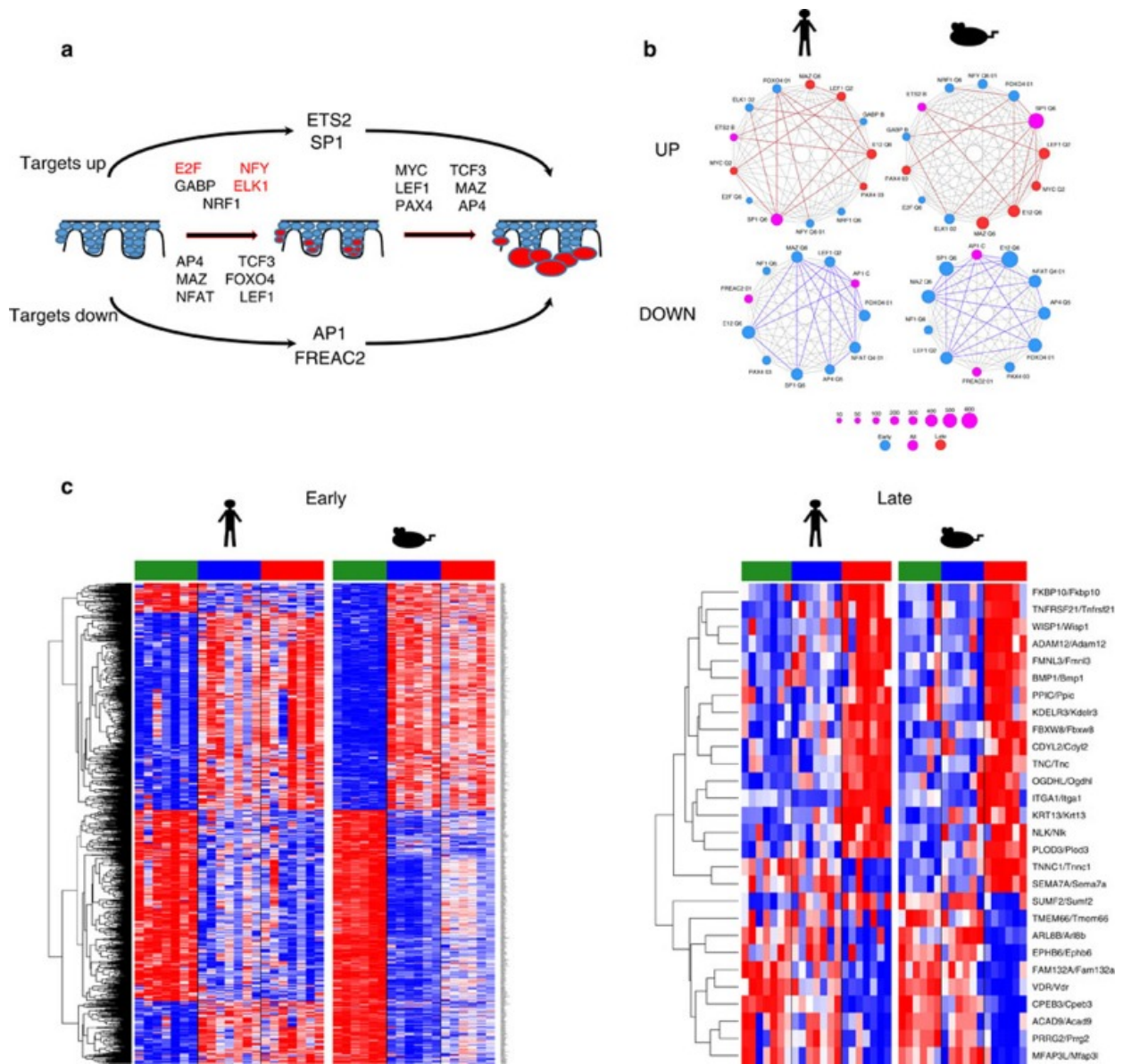
Figure 4

Cross-species transcription factor motif analysis reveals major drivers of cuSCC development.

(a) Global view of transcription factors with target genes enriched across the entire NS/CHR to AK/PAP to cuSCC progression sequence. Directionality reflects the significant

upregulation (above the line) or downregulation (below the line) of predicted targets of the listed transcription factors. Some factors have targets that are enriched in opposite directions across distinct transitions. The transcription factors highlighted in red were identified in both TRANSFAC and LME-based analyses. (b) Network analysis demonstrates that core transcriptional drivers are highly interconnected in both human (left) and mouse (right). The bolded lines delineate connections that are significant by Fisher exact test ($P<10−4$). (c) The LME model of mRNA expression changes across cuSCC development in both species demonstrates that the vast majority of significant gene expression changes occur in the early transition from NS/CHR to AK/PAP. This figure is reproduced based on previously published figure (17).

1.6   MicroRNA landscape in UV-induced cutaneous squamous cell carcinoma

1.6.1. MicroRNA biogenesis

MicroRNAs (miRNAs) comprise a class of non-coding regulatory RNAs of 20-25 nucleotides that regulate transcription of numerous genes mainly by binding to complementary sequences on the 3′ untranslated regions (3′-UTRs) of the target genes. miRNA biogenesis is a complex but fairly well understood process. The biogenesis of miRNAs initiated in the nucleus and complete in the cytoplasm. In the nucleus, primary transcripts (pri-miRNA) are transcribed by RNA polymerase II and cleaved into precursor miRNAs (pre-miRNAs) by the ribonucleases Drosha and DGCR8. Then, pre-miRNAs are exported into the cytoplasm for additional cleavage by a ribonuclease called Dicer. The mature miRNA is a part of the RNA-induced silencing

12

complex (RISC) where they bind to a specific seed sequence on the 3'UTR of target genes. If the 3′-UTR site is fully complementary to the miRNA, the mRNA is targeted for degradation (35). Since the first discovery of miRNAs in the early 1990s, a large amount of studies have focused on uncovering the biological relevance of these small RNAs in skin cancer initiation, development and metastasis.
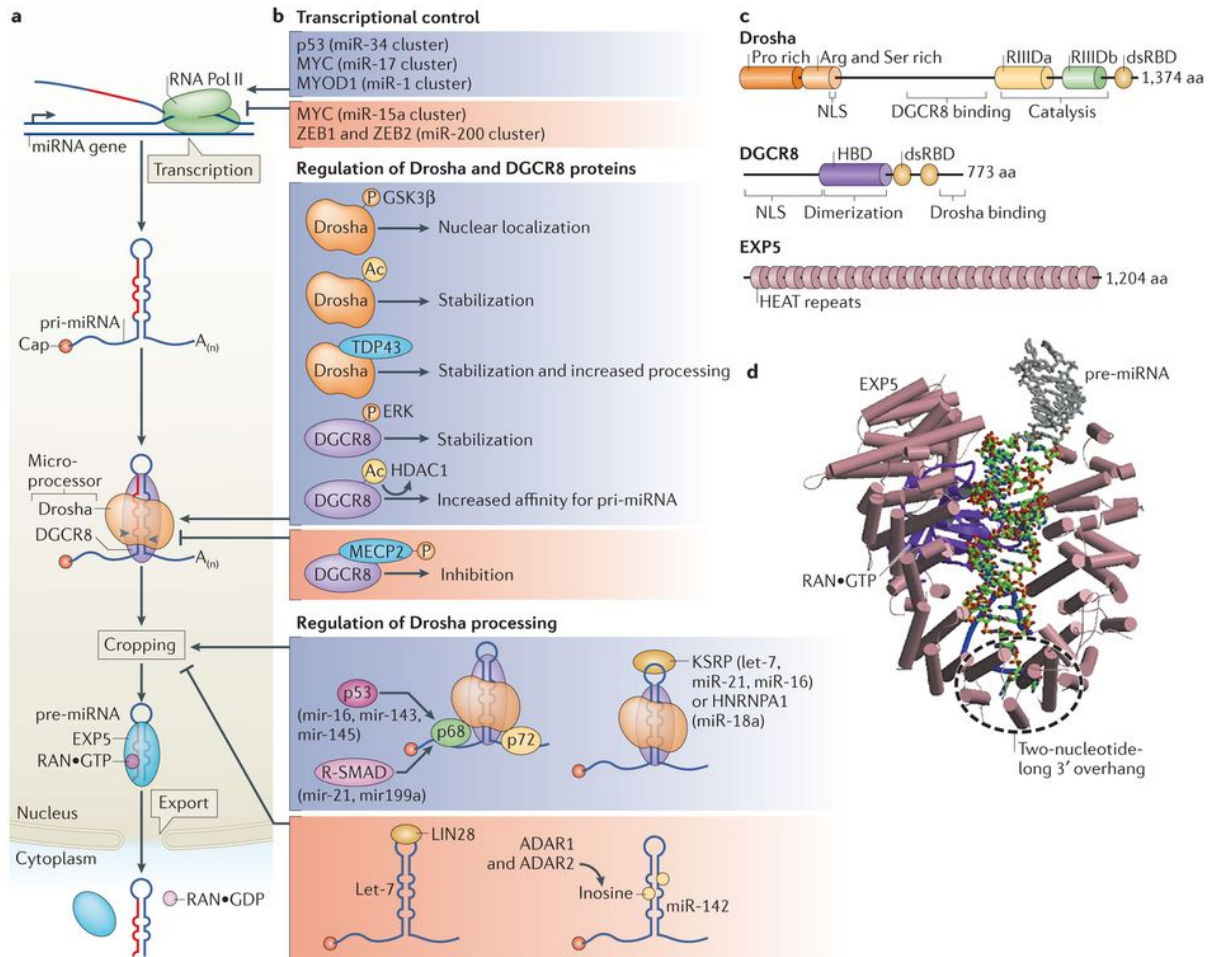
Figure 5

Nuclear events in the miRNA biogenesis pathway. This figure is reproduced based on previously published figure. (36)

1.6.2. MicroRNAs in skin cancer

Current data established the crucial roles of some miRNAs in controlling the transition of skin stem cells along certain differentiation lineages (37-39). Here, miRNAs are involved in controlling the expression of key regulators of stem cell activity in normal healthy skin and hair follicles. miR-203 regulates the p63-dependent proliferative potential of epithelial precursor cells during keratinocyte differentiation by repressing DeltaNp63 (40). miR-125b control stem cell proliferation, fate commitment and differentiation (38). miR-31 ensures proper hair follicle growth by targeting a number of growth regulatory molecules and cytoskeletal components of the WNT and FGF signaling pathways (41).

A large body of literature shows that miRNAs are abnormally expressed in tumors. While tumors often overexpress oncogenic miRNAs (e.g., miR-155, miR-21 and miR-17~92 miR family) that promote cancer cells tumorigenesis, certain tumor suppressor miRNAs are regularly downregulated in cancers (e.g., let-7, miR-16) (42, 43). Due to this, miRNAs might represent important diagnostic tools in cancer as well as possible targets for anticancer treatments. Much research in the area has found that in many cases, a specific microRNA can be oncogenic in one cancer and tumor suppressor in another cancer. For example, anti-inflammatory miR-223 promotes gastric cancer metastasis by targeting *EPB41L3* while suppresses proliferation and migration of nasopharyngeal carcinoma cells through *MAFB* (44,

45). Therefore, the need to characterize miRNA-mRNA regulatory networks in specific cancer settings is crucial.

Like in other cancers, miRNAs have been associated with the initiation and progression of squamous cell carcinoma of the skin by multiple studies. miR-21 was found to be the only miRNA consistently overexpressed in 540 clinical samples in of cancer patients. The importance of miR-21 in tumor development has been documented in multiple studies including melanoma (46). A significant upregulation of miR-31, a proto-oncogene like miR-31 was observed. miR-31 can have tumor-suppressive and oncogenic roles in different tumor types. In colorectal cancer, miR-31 expression is associated with the progression of the disease (47).

An adequate amount of evidence points to the conclusion that miRNAs play an important role in biology of cuSCC. Specific miRNAs might be used as diagnostic and prognostic markers but also to develop targeted or personalized anti-cuSCC treatments. Understanding in detail the function of miRNAs in cuSCC will open new opportunities for modern medicine and clinical application.

1.6.3. MicroRNA target identification

Computational prediction tools continue to be the first routine step in identifying miRNA targets. These tools are usually based on the phylogenetically conserved complementarity of miRNAs to their potential target genes (48). However, seed pairing may not be an fully accurate predictor (49). Therefore, the interaction between microRNA and its target genes must still be validated to reveal the functions of microRNA. The validation method involves well-established techniques, such as qRT-PCR, luciferase reporter assay and western

15

blot (50). Western blot and qRT-PCR measure the expressions level of protein and the mRNA level, respectively. Reporter assays are dependable methods for elucidating the direct interaction between microRNA and its target gene (51).

There are currently two types of miRNA targets prediction tools: databases with experimental data and computational algorithms. The most highly cited experimental public database is miRTarBase (52) and miRWalk with miRTarBase being more frequently updated. These experimental databases collect data using various methods including: PCR, Western blot, proteomics, microarray, etc. (Table 2).

Database name	Number of entry	Version/year	Reference
TarBase (53) (54)	miRNA–gene interactions:65 814 Species :24 Paper curate: 10,000	TarBase (2006) Tarbase 5 (2008) Tarbase 6.0 (2012) TarBase (2014)	http://diana.imis.athenainnovation. gr/DianaTools/index. php?r=tarbase/index
miRecords (55)	miRNA-gene interaction: 2705 miRNA: 664 gene:1907 from 9	miRecords (2008) last updated April 2013	http://mirecords.biolead.org/

	animal Curated from low through put experiment:2028		
miRGator (56)	Mature miRNA: 1856 Validated target:4745 Predicted target :6 218 792	miRGator (2008) miRGator (2011) miRGator (2013)	http://mirgator.kobic.re.kr/ http://genome.ewha.ac.kr/miRGator/
miRWalk (57)	858,750,070 interactions between 11,748 miRNAs and 308,700 genes	miRwalk 1.0 (2010) miRWalks2.0 (2014)	http://www.umm.uni-heidelberg. de/apps/zmf/mirwalk/
miRTarBase (52)	Species: 18 Target genes: 22,563 miRNAs: 3786 miRNA–target interactions: 366,181 Articles: 4966	miRTarBase 1.0 (2010) miRTarBase 4.0 (2014) miRTarBase 5.0(2015) miRTarBase 6.0(2016)	http://mirtarbase.mbc.nctu.edu. tw/index.php

		miRTarBase 7.0(2017)	
miRSel (58)	Human (2112 pairs) Mouse (895 pairs) Rat (231pairs) Other organism: (452 pairs)	miRSel (2010)	http://services.bio.ifi.lmu.de/ mirsel/
starBase (59)	miRNA-circRNA: 9000 miRNA-pseudogene: 16 000 protein–RNA: 285 000	StarBase (2011) Starbase (2014)	http://starbase.sysu.edu.cn
PMTED (60)	miRNA:1897 Target: 5449 Species:12 Experiment:311 Assay:3492	PMTED (2013)	http://pmted.agrinome.org/
ComiRNet (61)	5 million MTIs miRNA: 934 mRNA:30,835	ComiRNet(2015)	http://www.comirnet.di.uniba.it

	biclusterhierarchies:15		
MtiBase (62)	Gene: 15,546 miRNA: 4420 4 400 000 CDS - 470 000 5′UTR miRNA target sites SNP influence 290,000 CDS and 28,000 5′UTR miRNA target sites	MtiBase(2015)	http://mtibase.sysu.edu.cn

Table 1.

miRNA target databases based on experimental data

Current prediction algorithms based on structural characteristics can be categorized into three groups: *ab initio*, machine learning and hybrid approaches (63, 64). The *ab initio* algorithms are based on computational models that do not use the experimental data directly but instead, make the prediction based on the structural features extracted from data. This approach usually leads to high false positive. Machine learning approaches, on the other hand, use computational algorithms that rely directly on experimental data for training. However, negative interactions with experimental support are usually discarded. The limitations of *ab initio* and

machine learning algorithms, have led to the development of hybrid algorithms with features from both methods incorporated. A summarizing table of algorithms can be found below.

Database name	Class	Reference
miRanda (65)	*ab initio* weighted dynamic programming algorithm	http://www.microrna.org
TargetScan (66) (67) (68)	*ab initio* ranked base on hierarchy (6mer offset < 6mer < 7mer-A1 < 7mer-m8 < 8mer)	http://www.targetscan.org/
PicTar (69)	*ab initio* targets are ranked based on a score derived using a hidden Markov model	http://pictar.mdc-berlin.de/
RNA22 (70)	*ab initio* pattern discovery using Markov chain	http://cbcsrv.watson.ibm.com/rna22.html
RNAhybrid (71)	*ab initio* computes the minimum free energy	http://bibiserv.techfak.uni-bielefeld.de/rnahybrid/
PITA (72)	*ab initio*	http://genie.weizmann.ac.il/pubs/mir07/
EiMMo (73)	*ab initio* Bayesian method	(http://www.mirz.unibas.ch/ElMMo2/

DIANA (74)	*ab initio*	http://diana.cslab.ece.ntua.gr/microT/
miTarget (75)	SVM	http://cbit.snu.ac.kr/xmiTarget/introduction.html
Ensemble Algorithm (76)	SVM	a post-processing step for miRanda
NBmiRTar (77)	Naïve Bayes classifier	post-processing step to miRanda
MirTarget2 (78)	SVM	http://mirdb.org
MiRTif	SVM Combines sets from miRanda, PicTar and TargetScan	http://mirtif.bii.a-star.edu.sg/
MTar (79)	SVM	http://www.rgcb.res.in/downloads/Mtar.rar
TargetSpy (80)	automatic feature selection HITS-CLIP	http://www.targetspy.org/
mirSVR (65)	miRanda followed by a support vector regression	http://www.microrna.org
mirror (81)	unified platform generated from several *ab initio* predictors	http://www.proto.cs.huji.ac.il/mirror/search.php

| miREE (82) | hybrid algorithm | http://didattica-online.polito.it/eda/miREE/ |

Table 2

miRNA target prediction tools based on mathematical models

Identifying the target of a specific miRNA is crucial in understanding the role of the miRNA in biological processes. MiRNA, however, can target thousands of genes (66, 83). Over the better part of the last two decades, experimental and computational prediction tools have been developed to facilitate microRNA research (63, 64). Although each has predictive power, they all have limitations based on the scoring and integration of features into the tool. Understanding the principle of these prediction methodologies will aid in the appropriate tools selection and tool output interpretation.

1.7 Pathway analysis for genome-wide association study data: An overview

High-throughput experiments (e.g. microarray, next-generation sequencing, or proteomics) have transformed biomedical research by enabling comprehensive monitoring of a biological system. Analysis NGS data typically yields a useful list of differentially expressed genes or proteins. However, this gene list of thousands of rows often fails to provide insights into the underlying biology of the condition being studied. To reduce the complexity of the data, one approach has been to group long lists of individual genes into smaller sets of related genes

22

or proteins. Researchers have developed a large number of pathway databases (e.g. KEGG (84), Ingenuity, MSigDB, Wikipathways) to help with this task. The pathway databases describe biological processes, components, or structures in which individual genes and proteins are known to be involved in, as well as how and where gene products interact with each other (Table 1) (85-87).

PDB Name	Pathway focus	URL	Y.O.R.	Formats
EcoCyc	M,S	biocyc.org	1995	SBML, BioPAX
KEGG	M,S,D	kegg.jp	1996	BioPAX
RegulonDB	GR	regulondb.ccg.unam.mx	1997	BioPAX
MetaCyc	M	metacyc.org	1999	SBML, BioPAX
STRINGDB	PPI	string-db.org	2000	PSI-MI
PANTHER	S,D,PS	pantherdb.org	2004	SBML, SBGN, BioPAX
Gene Ontology	PPI,M,S	geneontology.org	2000	
REACTOME	M,S,D	reactome.org	2005	SBML, SBGN,

				BioPAX, PSI-MI
MSigDb	M,S,GR	broadinstitute.org/gsea/ msigdb	2005	
Ingenuity Knowledge Base[*]	PPI,PCI,M,S,GR, D	ingenuity.com	2005	
NCI PID	S,D	pid.nci.nih.gov	2006	BioPAX
WikiPathways	M,S,D	wikipathways.org	2008	BioPAX
Small Molecule Pathway DB	M,S	smpdb.ca	2009	SBML, BioPAX
ConsensusPathDB	PPI,PCI,M,S,GR	consensuspathdb.org	2009	BioPAX, PSI-MI
Pathway Commons	PPI,PCI,M,S	pathwaycommons.org	2010	BioPAX

Table 3

Pathway databases. A brief example of the diversity of available PDBs found online. The second column shows the kind of biological focus pursued by each database: (PPI, protein-protein intereactions; PCI, protein-compound interactions; M, metabolic; S, signaling; GR, gene regulation; D, diagrams; PS, protein sequence). The last column addresses the standard pathway languages adopted to provide data. Additionally, in the third column the links to web sites are

24

supplied. YOR, Year of release. *Commercial database. This table is reproduced based on previously published data.

1.7.1 Over-Representation Analysis (ORA): First Class pathway analysis

ORA approach has become a routine task in functional genomics studies. The basic hypothesis in ORA is that relevant pathways can be detected if the proportion of differential expressed genes, within a given pathway, exceeds the proportion of genes that could be randomly expected. The confidence level of overlapping is calculated using statistical methods such as hypergeometric, chi-square, or binomial distribution. Popular tools implementing this idea include DAVID (88), BINGO (89), and GeneMania (90).

Despite the availability of a large number of tools and their widespread usage, traditional ORA have a number of limitations. First, the different statistics used by ORA are independent of the measured changes (85). This means that these tests consider the number of genes alone and ignore any values associated with them such as fold-changes or significance of changes. By discarding this data, ORA treat each gene with equal weight or importance and assume that each gene is independent of the other genes. Assuming independence between genes amounts to "competitive null hypothesis" testing, which ignores the correlation structure between genes (85). For example, a gene may act as the regulator of a number of genes inside the same pathway, and the perturbation of this gene may have a larger impact on the pathway than the perturbation of its target genes do. Consequently, the estimated significance of a pathway may be biased or incorrect. Second, ORA uses arbitrary user cut-off threshold, that leaves out potentially important information and generates result variability (91). To date, there is no rule

25

of thumb for establishing a cut-off threshold. Finally, ORA assume that each pathway is independent of other pathways, which is contrary to the acknowledgement of interaction between pathways (86, 92). To find a more precise model of biological systems, pathway analysis has to evolve to address the discussed limitation. This led to the second class of pathway analysis method.

1.6.2 The Second Generation: Functional Class Scoring (FCS)

These methods work under the main hypothesis that although large changes in gene expression have significant effects on a pathway, weaker but coordinated changes in the genes that assemble the pathway have an impact on the overall pathway state. In this way Functional Class Scoring (FCS) methods use all the available measurements in NGS data to evaluate their enrichment scores, but still using pathways as gene sets to perform their computations. FCS methods use a three-step framework that consists of gene-level statistics, pathway-level statistics and assessment of the statistical significance of the pathway-level statistic.

An important improvement of FCS methods over ORA is that they are built to use all available measurements from NGS data. They do not need an arbitrary cut-off threshold of differentially expressed genes. Also, they can detect differences between pathways that are barely passing the differentially expressed thresholds and the ones that are passing them with significance levels. They can also detect coordinated associations between genes and their belonging pathways.

26

One of the first and most popular methods deploying the FCS approach is the Gene Set Enrichment Analysis (93), which was developed by researchers from the Broad Institute for gene expression analysis from microarray data. In brief, GSEA uses a list of ranked genes in accordance to their differential gene expression between two biological states (93). Then, evaluates their distribution on pre-defined gene sets, (i.e., gene sets from the MSigDB) thus computing an enrichment score (ES) for each set of genes (through a Kolmogorov-Smirnov pathway-level statistic) to determine whether it shows statistically significant, concordant differences between two biological states (93).

Another popular FCS tool is Ingenuity Pathway Analysis (IPA) canonical pathway owned by QIAGEN (Hilden, Germany). IPA charges a user fee and maintains their own knowledge base to compare gene expression data to. They, however, incorporate causal analytics tools in their 'Upstream Regulator Analysis', 'Mechanistic Networks', 'Causal Network Analysis' and 'Downstream Effects Analysis'. In particular, IPA uses two measurements that address two independent aspects of the inference problem: an enrichment score (Fisher's exact test) that measures the overlap significance, and a Z-score assessing the match of observed and take direction of change into account. Here, Z-score serves as both a significance measure and a predictor for the activation state of the regulator (94). This is a significant advancement over traditional FCS tools which just look for statistical enrichment in overlap to sets of genes.

Although an improvement over ORA, FCS has several setbacks. First, they do not take the relationships between pathways components or pathway network configuration into account

(95). This issue has been partially addressed by Ingenuity causal network analysis (94). Second, similar to ORA, FCS analyzes each pathway independently from each other, not accounting for overlapping between them or the influence they can exert over another (92). This concern has been partly addressed by Enrichment Map, which groups dependent gene-sets into network clusters, enabling researchers to quickly visualize major enriched functional themes. Enrichment map utilizes GSEA output results and was developed as an add-on application in the Cytoscape software (96). However, the remaining unbridged gaps suggest opportunities in the field to explore.

1.6.3   The Third Generation: Pathway Topology (PT)-Based Approaches

Beside simple gene lists, publicly available pathway databases also provide vast amount of information about genes that interact with each other in a given pathway, how they interact (e.g., activation, inhibition, etc.), and where they interact (e.g., cytoplasm, nucleus, etc.). ORA and FCS methods dramatically under-utilize the knowledge that such pathways are meant to capture. Thus, if the pathways are perturbed with new connections between the genes, so long as they contain the same set of genes, ORA and FCS will return exactly the same results.

The key hypothesis of pathway topology (PT)-based analysis is that interactions found in pathway topology, annotated in pathway databases, bear information for interpreting correlated changes between pathway components. PT-based methods can be seen as extensions of the ORA and FCS methods, as they perform along the same initial steps. The main difference comes the use of pathway topology to compute gene-level statistics (85).

PT-based methods that consist of multiple scoring steps, are difficult to generalize and are beyond the scope of this dissertation. A detail overview of existing methods are published previously (87). The most popular commercial tool that incorporates topology in the pathway analysis is MetaCore (oftenly regarded as GeneGO, Thomson Reuters, http://www.thomsonreuters.com). Here, MetaCore use only the differentially expressed gene list without associated expression value as input for its two propriety knowledge bases: an interaction database and canonical pathways (87).

PY-based methods have certain common limitations. One problem is that true pathway topology is highly specific to the phenotypes and condition being studied. However, this information is fragmented in pathway data bases (85). As annotations improve, these approaches are expected to become more useful. Currently, there is no analysis method that takes advantage of the information stored in all of these different pathway database sources. Promising developments include the incorporation of multiple component types and interaction types, each with specific properties (87).
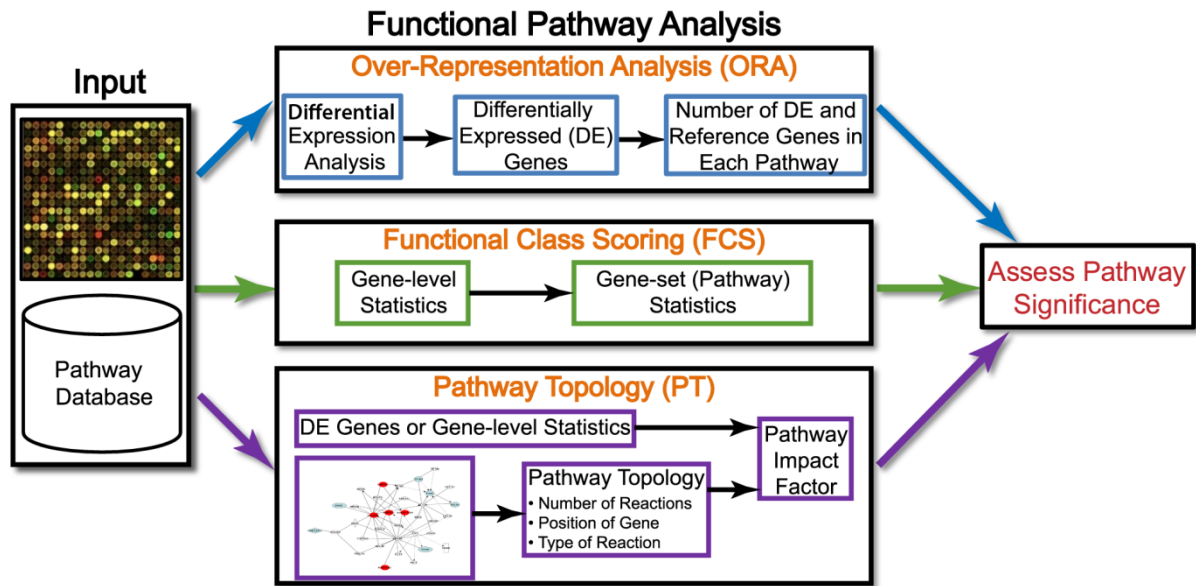
Figure 6

Overview of existing pathway analysis methods using gene expression data as an example. Note that this overview is equally applicable to molecular measurements using proteomics, and any other high-throughput technologies. The data generated by an experiment using a high-throughput technology (e.g., microarray, proteomics, metabolomics), along with functional annotations (pathway database) of the corresponding genome, are input to virtually all pathway analysis methods. While ORA methods require that the input is a list of differentially expressed genes, FCS methods use the entire data matrix as input. In addition to functional annotations of a genome, PT-based methods utilize the number and type of interactions between gene products, which may or may not be a part of a pathway database. The result of every pathway analysis method is a list of significant pathways in the condition under study. DE, differentially expressed. This figure is reproduced based on previously published figure (85).

With efforts to understand vast amount of data generated by high-throughput experiments, thousands of computational pathway analyses tools have been developed over the better part of the last two decades. Each tool has pros, cons and even 'niche'. Thus, it is important for biology researchers to understand the basis of how they are built and be conscious of the limitations when applying these methods on their high-throughput data.

1.8 Papillomavirus-related cutaneous squamous cell carcinoma

Papillomaviruses (HPVs) are small non-enveloped icosahedral viruses that infect the keratinocytes of skin and mucosa. HPVs are represented mainly by the beta and gamma genera, which are widely present in the skin of normal individuals. In recent years, the impact of viruses to cutaneous oncogenesis has increasingly gained recognition. Cutaneous HPVs that belong to the beta genus (β-HPV) have been found to act as co-carcinogen with UVR. Mechanistic studies have previously shown that UV can trigger the promoter activity of the cutaneous types HPV5, 8, 20, and 77 (97, 98). Exposure to UV could also favor replication of β-HPV types by inducing local immunosuppression (99). Furthermore, immunosuppressed individuals show a markedly increased incidence of β-HPV–positive SCC (100).

1.9 Dissertation outline

It is well accepted that miRNAs are often deregulated and plays major roles in tumor development. The aim of this dissertation is to better understand the role of miRNAs and their targets in cuSCC development in order to identify biomarkers for prediction and prevention of this second most common skin cancer.

31

Chapter one provides a general introduction to cuSCC risks, genomic backgrounds, mouse models, details of miRNA biogenesis and available miRNA prediction tools. We also discuss the method of pathway analyses that were used on our next-generation sequencing data. In chapter two, we provide information on methodologies and materials used in this study. In chapter three, we investigated the transcriptomes of UV-exposed skin, wound healing skin and cuSCC tumors based on the knowledge that cuSCC mostly arise from chronic UV-exposed skin and wound areas. We discovered that their transcriptomes overlap significantly. Thus, we were able to use common transcriptomic features shared by these three tissues to identify potential candidates for biomarkers evaluation. In chapter four and chapter five, we characterized the functions of important miRNAs in cuSCC and identified novel functional targets that are regulated by the miRNAs.

Chapter 2: Materials and methods

Cell Culture

Normal human epidermal keratinocytes (NHEK) were purchased from Lonza and maintained in KGM-Gold Keratinocyte Basal Medium (Lonza). SRB1, SRB12, and COLO16 were a gift from Dr. Jeffrey Myers UT MD Anderson Cancer Center (Houston, TX). SCC IC1, SCCT1, SCCT2, SCCT3, SCCT8, SCRDEB2, SCRDEB3 and SCRDEB4 were provided by Dr. Andrew South at Thomas Jefferson University (Philadelphia, PA). HaCaT cells, an immortalized human keratinocyte line cell was obtained from Dr. Norbert Fusenig at German Cancer Research Center. CuSCC cell lines were maintained in DMEM/F12 (1:1), supplemented with with 10% FBS, RM+ supplement (101) and 1% pen/strep. All lines were STR profiled to confirm distinct identities.

Quantitative RT-PCR

miRNAs and mRNAs were detected by Taqman quantitative reverse transcription PCR (qRT-PCR) method. Expression of miRNAs were normalized by RNU6B. Expression of mRNAs were normalized to GAPDH. All primers were purchased from Thermo Fisher, USA (Cat. # 4427975, Assay ID 000480).

Western blot analysis

50μg of total protein were electrophoresed on 10% SDS-PAGE gel and transferred to PVDF membrane as previously described (6, 127). Blots were then probed with anti-ΔNp63 (619002, Biolegend, 1:500), E-cadherin (3195, Cell Signaling, 1:1000), Vimentin (ab92547, Abcam, 1:1000), Twist1 (sc-81417, Santa Cruz, 1:250), Lef1 (2230S, Cell Signaling, 1:1000), Snail (3879S, Cell Signaling, 1:1000), Zeb (sc-10572, Santa Cruz, 1:500), Smad2 (sc-101153, Santa Cruz, 1:500), Smad3 (9523S, Cell Signaling, 1:1000), phospho-Smad2 (ab53100, Abcam, 1:500), and phospho-Smad3 (9520S, Cell Signaling, 1:500) overnight at 4^OC. Horseradish peroxidase conjugated- secondary antibodies against either murine or rabbit IgG (Jackson lab) were incubated with the blots for 1 hour at room temperature. Actin (A5060, Sigma) or Hsp90 (ab13495, Abcam) was used as loading control. Detection was performed using ECL Plus Kit (Amersham) or Licor system.

Apoptosis assay

TMRE (Invitrogen) was used as a measure of mitochondrial membrane potential, Annexin V-FITC or Annexin V-APC (Invitrogen) as a probe for apoptosis, and Cytox Blue (Invitrogen) as an indicator for dead cells. At 6, 24, or 48 hours post-irradiation, both floating and adherent cells were collected and stained with TMRE, Annexin V and Cytox Blue. Data

were collected and analyzed using a flow cytometer (FACScalibur, Becton Dickinson) and FlowJo Software (Tree Star). Data were analyzed and charts were plotted using GraphPad Prism software.

Confluence-based proliferation aassay

0.2×10^4 cells per well were plated onto 96-well plates. The plates were read with the IncuCyte (Essence Bioscience) every 6 hours for 96 hours. Cell confluency or density was measured using IncuCyte Zoom software.

Overexpression and inhibition of miRNA in cuSCC cells and keratinocytes

5×10^5 cells per 60 mm dish were transfected with 40 nM microRNA inhibitors (ThermoFisher) or 3 nM microRNA mimics (ThermoFisher) using Lipofectamine RNAi Max (Invitrogen) according to manufacturer's protocol. The cells were collected 48 hours post-transfection for further analysis. The microRNA inhibitors used to target microRNAs are as followed: miR-21-5p, miR-21-3p, miR-181a-5p and negative control (4464077) (ThermoFisher). The microRNA mimics purchased from ThermoFisher are miR-21-5p, miR-21-3p, miR-181a-5p

and negative control mimics (4464058).

Lentivirus-based GFP-tagged vectors for hsa-miR-181a (lenti-miR-181a OE) or scramble control (lenti-miR-00 control) were purchased from System Biosciences (SBI) lenti-miRNA vector bank. Transduction efficiency was assessed by GFP intensity and Taqman qRT-PCR.

Overexpression and depletion of TGFBR3

To overexpress TGFbR3, we purchased pDONR223-TGFBR3 (Addgene, plasmid # 23478) donor vector which contained TGFBR3 ORF. Then, the TGFBR3 ORF was cloned into pcDNA4.1/V5 expressing vector using Gateway technique. All vector sequences were validated by Sanger sequencing. TGFBR3 expression was validated by western blot.

To deplete TGFBR3, we use GIPZ Human TGFBR3 shRNA (GE Dharmacon, Clone ID V3LHS_352448 and V3LHS_352450). GIPZ non-silencing lentiviral shRNA (GE Open Biosystems, Cat. # RHS4348) was used as control. The shRNA lentivirus was prepared with 293T cells and psPAX2/pVSV.G packaging plasmids, and then was transduced to target cells. Following transduction, cells were puromycin-selected and sorted to obtain cells with high-level suppression TGFBR3 suppression were validated by Taqman qRT-PCR.

Trans-well Invasion Assay

Cells were treated with mitomycin C 2 hours prior to the assay, then 4.5×10^5 cells were suspended in serum-free media and seeded on a 8μM pore size control insert (Corning, Cat. # 08-774-162) or the insert coated with matrigel (Corning, Cat # 08-774-122). Complete media

contain 30% FBS was added to the lower compartments as a chemo-attractant for cells. Thereafter, cells were allowed to move for 48 hours. Cells remaining on the upper side of the membrane were removed. Those that invaded to the bottom side of the membrane were fixed and stained with Diff-Quik Stain Set (Siemens B4132-1A). The membranes were air-dried and mounted for photography. Cells from ten random fields were counted.

miRNA *in situ* hybridization (ISH)

In situ hybridization was conducted by the MD Anderson Center for RNA interference and non-coding RNAs. Skin squamous cell cancer tissue arrays (Cat # SK 801b and # SK 802a) were purchased from US Biomax, Inc. (Rockville, MD).

Plasmid construct and luciferase reporter assay

The pEZX-MT05 expression vector harboring the human TGF☐R3 3' UTR cDNA (GeneCopoeia, Cat. # HmiT066530) was used as DNA template. Site-directed mutagenesis was carried out using the QuickChange II XL Site-Directed Mutagenesis Kit (Catalog #200521, Agilent Technologies), following the Manufacturer's instruction. The mutagenic primers were synthesized by IDT and the oligonucleotide sequences of these primers are listed in Table X. The success of the designed mutations was verified by DNA sequencing.

HaCaT cells were transfected with wild-type and mutant reporter vectors along with scrambled control. 72 hours after transfection, the cell culture medium was collected for the

assay. The luciferase reporter assays were performed according to the manufacturer's guidelines for the Secrete Pair Dual Luminiscence Assay Kit. Luciferase activity was normalized to secreted alkaline phosphatase.

Soft agar and colony formation assays

Following plating of bottom agar (0.6% Bacto Agar) with media we plated 2500 to 10,000 cells per well and they were embedded in top agar (0.3%) and plated in 24-well plates. Control or lenti-miR-overexpression media was replaced every 48 hr for 4 to 6 weeks. Cell colonies were stained with 1% crystal violet, imaged and quantified.

Protein extraction and Western blot analysis

Protein lysates were prepared in RIPA buffer (Sigma, Cat # R0278) supplemented with Halt Protease & Phosphatase Inhibitor Cocktail (Thermo Scientific, Cat #1861281). Primary antibodies were obtained from Cell Signaling and Thermo Scientific. Westerns were imaged using the Licor Odyssey CLx system.

Animals and in vivo model of human cutaneous squamous cell carcinoma

NOD CRISPR *Prkdc Il2r gamma* (NCG) mice (6 to 8 weeks old; Charles River) were housed and monitored in our Animal Research Facility. All experimental procedures and protocols had been approved. RDEB2 cells were transfected with control inhibitor and miR-181a inhibitor. 24 hours post-transfection, cells were trypsinized for xenografting. Mice were

subcutaneously inoculated with 3 x 10^6 SCC RDEB2 cells. Once tumors become palpable, measurement was taken every other day. Mice were sacrificed 11 days after inoculation.

mRNA-Seq analysis

The mRNA-seq paired-end reads were aligned to the human reference genome, GRCh37/hg19, using the TopHat2 alignment software (102, 103). The overlaps between aligned reads and annotated genomic features, such as genes/exons were counted using HTSeq software (104). Hierarchical clustering analysis, using the Pearson correlation coefficient as the distance metrics and the complete linkage, and principal component analysis (PCA) were performed using the R statistical system. Genes significantly different between the control and different time points of acute UV treatment were determined using the R package DESeq (105). Since multiple genes were tested simultaneously, the Benjamini-Hochberg method was used to control false discovery rate (FDR). For further integration of mRNAs and miRNAs, and detection of enriched transcription factor targets, we used a cutoff of Q-value<0.05 and fold change exceeding 1.25x.

smallRNA-Seq Analysis.

This work was performed with collaboration with laboratory of Dr. Preethi Gunaratne, PhD (University of Houston, Biology & Biochemistry). As previously described (17), Illumina small RNA adapter sequences were trimmed from the reads, and reads of length below 10nt or ending in homopolymers of length 9 nt or above were discarded. Total usable number of reads

for each sample was calculated. The reads were mapped to the miRBase (106) reference using BLAST; the abundance of each expressed microRNA was quantified as a fraction of the usable reads, and expressed as parts per million We determined differentially expressed microRNAs imposing a fold-change of 1.25x and t-test comparison (p<0.05) using the R statistical system. We employed principal component analysis (PCA) to examine sample structure; further visualization of microRNA significant in one or multiple comparisons was carried out using the R statistical system.

Integrative mRNA-miRNA functional pair analysis.

We determined enriched miRNA-mRNA pairs using the SigTerms methodology. Essentially, by applying a one-sided Fisher exact test and using the TargetScan (107) predicted microRNA targets, we determined the miRNAs for which the gene targets are significantly enriched (FDR-adjusted q<0.25) in the gene signature. Finally, we determined the conserved enriched miRNAs and the conserved miRNA-mRNA pairs conserved with respect to acute UV treatment.

TMT-base proteomics

Sample Preparation. Cells were lysed in denaturing lysis buffer containing 8M urea, 20 mM HEPES (pH 8), 1 mM sodium orthovanadate, 2.5 mM sodium pyrophosphate and 1 mM β-glycerophosphate. A Bradford assay was carried out to determine the protein concentration. Equal amount of heavy and light proteins were mixed together. The mixed proteins were

40

reduced with 4.5 mM DTT and alkylated with 10 mM iodoacetamide. Trypsin digestion was carried out at room temperature overnight, and tryptic peptides were then acidified with 1% trifluoroacetic acid (TFA) and desalted with C18 Sep-Pak cartridges according to the manufacturer's procedure.

TMT Labeling. 400 microgram of peptide from each sample was labeled with TMT reagent. The label incorporation was checked by LC-MS/MS and spectral counting. 98% or greater label incorporation was achieved for each channel. The 6 samples were then pooled and lyophilized.

High pH Reversed Phase Peptide Separation. After lyophilization, the peptides were re-dissolved in 400 micro liter of 20 mM Ammonium Formate, (pH 10.0). The high pH reversed phase separation was performed on a Xbridge 4.6 mm x 100 mm column packed with BEH C18 resin, 3.5 µm, 130Å. (Waters) The peptides were eluted as follows: 5% B (5 mM Ammonium Formate, 90% acetonitrile, pH 10.0) for 10 minutes, 5% - 15% B in 5 minutes, 15-40% B in 47 minutes, 40-100% B in 5 minutes and 100% B held for 10 minutes, followed by re-equilibration at 1% B. The flow rate was 0.6 ml/min, and 24 concatenated fractions were collected. Speedvac centrifuge was used to dry the peptides.

LC-MS/MS. A nanoflow ultra high performance liquid chromatograph (RSLC, Dionex, Sunnyvale, CA) coupled to an electrospray bench top orbitrap mass spectrometer (Q-Exactive plus, Thermo, San Jose, CA) was used for tandem mass spectrometry peptide sequencing experiments. The sample was first loaded onto a pre-column (2 cm x 100 µm ID packed with C18 reversed-phase resin, 5µm, 100Å) and washed for 8 minutes with aqueous 2% acetonitrile and 0.04% trifluoroacetic acid. The trapped peptides were eluted onto the analytical column, (C18, 75 µm ID x 25 cm, 2 µm, 100Å, Dionex, Sunnyvale, CA). The 90-minute gradient was

programmed as: 95% solvent A (2% acetonitrile + 0.1% formic acid) for 8 minutes, solvent B (90% acetonitrile + 0.1% formic acid) from 5% to 38.5% in 60 minutes, then solvent B from 50% to 90% B in 7 minutes and held at 90% for 5 minutes, followed by solvent B from 90% to 5% in 1 minute and re-equilibrate for 10 minutes. The flow rate on analytical column was 300 nl/min. Sixteen tandem mass spectra were collected in a data-dependent manner following each survey scan. Both MS and MS/MS scans were performed in Orbitrap to obtain accurate mass measurement using 15 second exclusion for previously sampled peptide peaks..

Data Analysis. MaxQuant (version 1.5.2.8) was used to quantify the TMT reporter ion intensities (108). The MaxQuant output was normalized with modified iterative rank-order normalization algorithm (109).

Statistical analyses

All biological experiments were repeated at least three times. Numerical data were analyzed using a one-way analysis of variation. The statistical significance between treatments was assessed by one-tailed Student's *t*-tests or Paired Wilcoxon tests.

Chapter 3: Integration of transcriptomic data identifies UV exposure and wound-related biomarkers of cutaneous squamous cell carcinoma

3.1 INTRODUCTION

Skin is the largest organ in the body in terms of surface area and plays vital roles in protecting the skin from potential environmental risks. Skin cancer, 20% of which is cutaneous squamous cell carcinoma (cuSCC), is the most common malignancy in the United States. Because its incidence is rapidly increasing, cuSCC poses as a significant public health and economic burden (110). UV radiation is recognized as the main etiological agent that stimulates initiation and progression to sporadic cutaneous squamous cell carcinoma (19, 111). Although not as common, a subset of high-risk cuSCC, which occurs in chronic wound area in recessive dystrophic epidermolysis bullosa (RDEB) patients, is more lethal. In fact, metastatic cuSCC is the main cause of death among RDEB patients (112). Since UV exposure and wounding are the two main factors that lead to cuSCC initiation, study of the acute molecular dermal responses shared by them can be beneficial to establish solid cuSCC prevention strategies.

UV exposure triggers immune response and causes multiple alterations to the composition and architecture of the dermal extracellular matrix (ECM) (113). In melanoma, UV radiation induced the expression of FAP through transforming growth factor-b1 (TGF-b1) release, which mediated ECM degradation and enabled tumor dissemination (114). Similarly, non-healing RDEB wounds, precursors of cuSCC, are characterized by increased inflammation

43

and high TGF-b1 activity (112). A causal relationship between UV exposure and wound healing was highlighted by the benefit of UV irradiation in wound care. Beside germicidal effect, UV light exposure induced release of cytokines, growth factors and fibronectin, which enhance the wound healing process. A few clinical and animal studies have shown that low dose UV treament is effective in managing acute and chronic wounds (115). Even so, the similarity in UV exposure and wound healing response and how that can be employed to prevent cuSCC initiation were not reported.

In the current study, using miRnome and transcriptome profiling in acute UV-exposed human skin, we first integrated differentially expressed miRNAs and mRNAs in functional pair analysis. We further predicted significantly enriched biological pathways related to acute UV exposure using GSEA (93). We then integrate miRNA and RNA profile of acute UV-exposed skin to equivalent published profiles of wounding skins (116, 117). Our combinatorial analyses show for the first time that acute UV-exposed skin (at 24h) and wounding skin (at 3 day) share remarkable resemblances in their miRNA and RNA profile. GSEA showed that ECM remodeling pathways and GPCR related pathways were positively enriched while while PPAR activity decreased. Finally, we compare the miRnome and transcriptome of acute UV-exposed skin and wound to those of cuSCC. We found that not only differentially expressed genes from these 3 tissues overlap but they also share similar enriched pathways.

3.2 RESULTS AND DISCUSSION

3.2.1 Identification of acute UV-exposed differentially expressed genes and microRNAs in unexposed human skin

UV radiation is a complete carcinogen that can initiate genetic mutations in human skin (19, 111, 118). Additionally, UV can trigger genome-wide transcriptional instability that affects thousands of genes. Many studies of UV-induced transcriptome have focused on *in vitro* approach where cultured human primary keratinocytes were irradiated with UVB (119). These approaches did not reflect the actual systemic response of human skin to UVR nor did they closely mimic the solar spectrum in reality. To address these issues, we interrogated normally sun-protected human buttock skin after an acute does of two MED of solar stimulated light (SSL). We then obtained the snap frozen whole skin samples pre- and post-UV in 8 healthy subjects with similar types of skin (Fitzpatrick skin type II or III). The solar simulator delivered 8.7% of UVB and 91.3% of UVA (120) and the average ($\pm$ standard error) dose delivered was 4.6 ± 0.5 J/cm^2 of UVA and $51.5 \pm$ mJ/cm^2 of UVB.
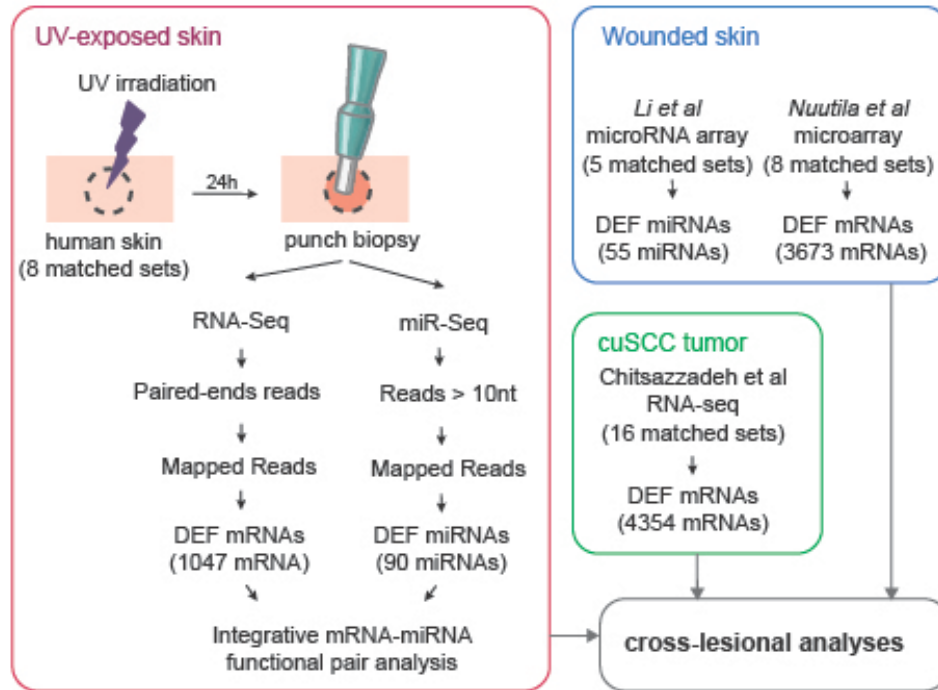
Figure 7

Study pipeline of integrating existing transcriptomes of UV-exposed skin, cuSCC tumors and public transcriptomic data sets of wound healing skin

RNA-Seq and microRNA-Seq was used to measure the changes in genes and microRNA expression at 6 hours and 24 hours post-SSL. The data were represented as the fold change (FC) in transcript levels, calculated by dividing the average read counts in the UVB group by those in control (pre-SSL) for each gene. The total number of differentially expressed genes and microRNAs at 6 hour and 24 hour post-SSL were reported in Table 4. The differentially

46

expressed microRNAs were reported in Appendix 1 and 2. We found that oncomiR miR-21 was highly expressed (miR-21-3p: 4.9-fold, p-val = 8.65E-07 and miR-21-5p: 1.96-fold, p-val = 4.84E-05) in 24 hour post-SSL human skin which agreed with previous studies where miR-21 were shown to be induced by UV irradiation in skin and cultured keratinocytes (121) (122) (123). Noticeably, inflammatory miR-223 which involved in rheumatoid arthritis and proriasis progression were most significantly upregulated (7.7-fold, p-val = 5.5E-09) in 24 hour post-SSL human skin. As an oncomiR, miR-223 promoted breast cancer cell invasiveness (124) and stimulated proliferation, migration and invasion of gastric cancer cell lines (45). Since the functions of miR-223 in UV-induced skins or skin cancers are unknown, this miRNAs can potentially be further explored.

Timepoints	Total	Up-regulated	Down-regulated
Differentially expressed genes			
6 hour post-SSL	767	552	215
24 hour post-SSL	3021	1633	1388
Differentially expressed miRNAs			
6 hour post-SSL	5	1	4
24 hour post-SSL	89	50	39

Table 4

Differentially expressed miRNA gene counts among different conditions

We were interested in identifying functional miRNA-mRNA pairs that were regulated by UV exposure. Given that miRNAs function by suppressing their target genes, we used functional pair analysis method where upregulated miRNAs were paired with downregulated predicted mRNA targets and vice versa. In total, we identified 45 pairs of upregulated miR-downregulated mRNAs and 37 pairs of downregulated miRs- upregulated mRNAs.

To investigate the effect of acute UV exposure through miRNAs on the molecular pathways, we use paired target mRNAs in GSEA C2 canonical pathway analyses. Here, the 5 highest upregulated miRNAs and their downregulated predicted target genes were found to be involved in Immune System, Signaling by GPCR and Matrisome pathways. Interestingly, 5 highest downregulated miRNAs and their upregulated predicted target genes were also found to be involved in the same mentioned pathways (Figure 8). These pathway analyses suggested that in acute UV-exposed human skin, Immune System, Signaling by GPCR and Matrisome pathways were important and were indirectly regulated by miRNAs.

A

hsa-miR-223-3p

REACTOME IMMUNE SYSTEM

REACTOME SIGNALING BY GPCR

hsa-miR-212-3p

hsa-miR-132-5p

NABA MATRISOME

hsa-miR-21-3p

hsa-miR-665

KEGG PATHWAYS IN CANCER

B

hsa-miR-2116-3p

hsa-miR-152-5p

NABA MATRISOME

REACTOME IMMUNE SYSTEM

REACTOME SIGNALING BY GPCR

hsa-miR-23a-5p

hsa-miR-30c-1-3p

hsa-miR-27b-5p
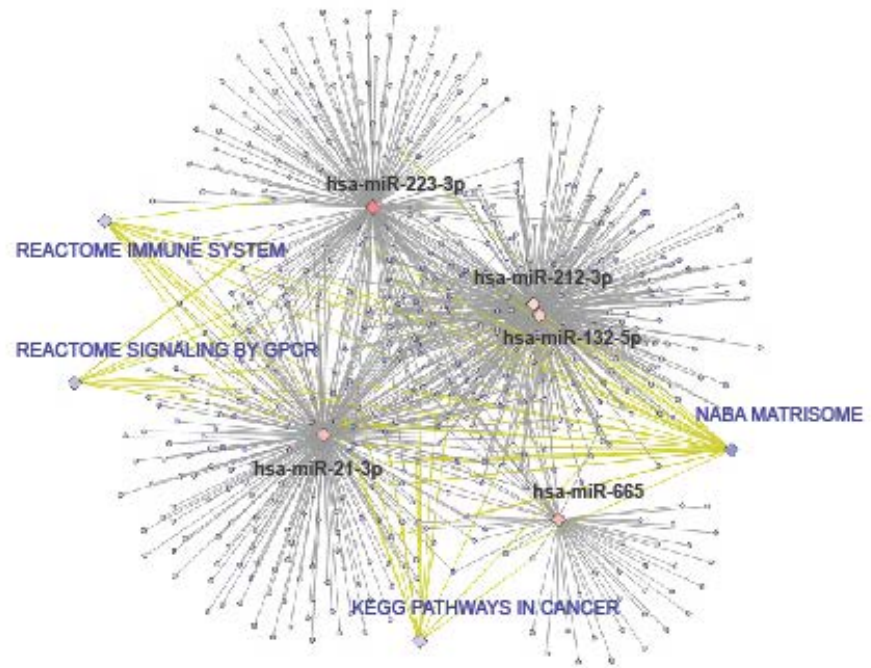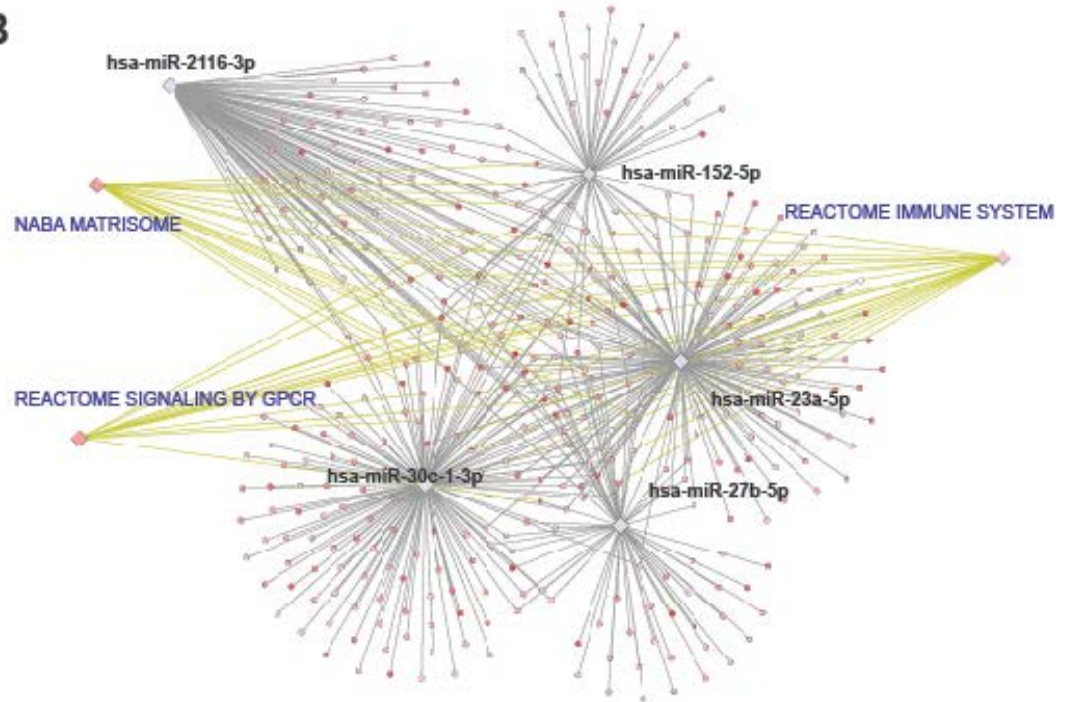
Figure 8

Integrated functional pair analyses reveals canonical pathways regulated by differentially expressed miRNAs and their predicted targets

3.2.2   Integrated analysis revealed correlation in the microRNA and mRNA expression between acute wounding skin and UV-exposed skin

SCC can arise from chronic wounds in epidermolysis bullosa (EB) individuals who are clinically characterized by generalized skin fragility, blistering of mucous membranes and compromised wound healing (125). With an effort of using integrated analyses as a solid foundation for better target prediction for cuSCC prevention, we sought to compare the transcriptome of acute UV-exposed skin with acute wound-healing skin and cuSCC tumors. The rationale is that cuSCC tumors can arise from chronic UV-exposed skin and chronic wounds.

To address this, we used previously published data that showed miRNAs dynamic changes during the inflammation phase of human skin wound healing (116). This Taqman MicroRNA low-density array data set was acquired from 5 healthy donors at 0 hour and 24 hours after injury (116). Interestingly, we found that the expression pattern of miRNA in acute UV-exposed skin was strongly correlated with acute wound healing skin at 24 hour time point (Figure 9). Inflammatory miR-223 is the highest increased miRNA in both data sets after 24 hour, suggesting strong inflammatory response at this time point in following UV-exposure and injury. Among the upregulated miRNA, miR-132 has been extensively characterized in wound-healing but not in UV response. This correlation suggests that published data in wound healing studies can be used as reference for UV response studies. Complete data on miRNA expression can be found in Appendix 1 and 2.

50

Figure 9

Transcriptome and miRNAome of UV-exposed skin, wound healing skin and cuSCC show significant similarity. (A) Comparative miRNA expression level analysis between UV-exposed skin and wound healing skin. (B) Comparative gene expression level analysis between UV-exposed skin and wound healing skin. (C, D, E) PCA of transcriptome of UV-exposed skin, wound healing skin and cuSCC.

To study whether the mRNA expression of UV-exposed skin, wound healing skin and cuSCC tumors share the similar correlation as miRNA, we again used another published transcriptomic data set on wound healing skin (117). This study employed 8 burnt patients who underwent skin grafting. Their skins were biopsied immediately before and after harvesting and during the wound healing process 3 and 7 days thereafter. The biopsied tissues were subjected to genome-wide microarrays. We used data from 3-day wound healing since it shows strong transcriptomic correlation with UV-exposed skin and cuSCC tumors. Overlapping analyses showed significant overlap in differentially expressed genes among three data sets (Figure 9). Specifically, 84% of DE genes in UV-exposed skin overlapped with DE genes in cuSCC. 87% of DE genes in wound healing overlapped with DE genes in cuSCC (Table 5).

Data set	DE genes in UV (n= 1047)	DE genes in Wound (n= 3673)	DE genes in cuSCC (n= 4354)
Overlap percentage among DE genes in 3 data sets (n = 630)	60%	17%	14%
Overlap percentage between DE genes in UV and Wound (n =727)	70%	20%	
Overlap percentage between DE genes in cuSCC and Wound (n =3184)		87%	73%
Overlap percentage between DE genes in	84%		20%

cuSCC and UV (n =884)			

Table 5

Overlapping gene counts among UV-exposed skin (24 hour post-SSL), wound healing skin (3 day post-injury) and cuSCC tumors

To better visualize the overall directional changes in 3 data sets, we performed principle components analysis (PCA). The data projected the 2 distinguished clusters of the UV-exposed skin, wound healing skin and cuSCC tumors and their normal control counterparts (Figure 9). To confirm, we projected the transcriptome of normal skin, AKs and cuSCC tumors and observed that the transcriptome of AK spanned those of normal skin and cuSCC. This observation agreed with previous study from our lab where we showed the transcriptomic of AK spanned the spectrum of normal skin to cuSCC (17). Overall, these results showed that there was a strong unprecedented correlation between the mRNA and miRNA expressions of UV-exposed skin, wound healing skin and cuSCC tumors.

3.2.3   Pathway analyses revealed correlation in the microRNA and mRNA expression between acute wounding skin and UV-exposed skin

The global functional impact of UV-exposure *vs.* wounding *vs.* cuSCC on skin was determined by using 3 approaches: integrated GSEA analyses (Figure 10), upstream regulator predictions through IPA (Figure 11), and canonical pathways prediction also through IPA (Figure 11). Using pathway analyses with different algorithms and annotations allows us to better select central and key pathways that are being affected. IPA determines overlaps between

53

the provided gene lists and the curated databases, looking for overlaps that are bigger than that expected by random chance (94). In contrast, GSEA is a tool that uses every data point in its statistical algorithm (126) (93). Genes are ranked by from most up-regulated to most-down-regulated. The two rank metrics commonly used are p-value and fold-change. The test assess whether ember of a gene set appear enriched at one end of the profile. To test enrichment, GSEA performs permutations of the profile, calculating the enrichment of the gene set 1000 times or more to estimate p-value empirically (126) (93).

Figure 10

Canonical pathway analyses revealed important common pathways in UV-induced skin, wound healing skin and cuSCC tumors (q=0.05). Each circle represents a gene set. Each circle is

divided into three sections which represent one of three dataset. Blue color represents pathway downregulation. Red color represents pathway upregulation.

When using integrated GSEA using the C2 canonical pathway gene set, we sought to identify unique and common pathways affected by acute UV-exposed skin, wound healing skin and cuSCC tumors. We focus on the common pathways because these are the pathways that were modified following UV-exposure and wound-healing that persisted in cuSCC tumors. We reason that by focusing on these pathways, we can identify ways to predict early development of cuSCC. Here, we observed that ECM related pathways, GPCR signaling, Cytokine and Chemokine signaling, immune system signaling and Cell cycle signaling were significantly and positively enriched. This suggested that these pathways were activated in acute UV-exposed skin, wound healing skin and cuSCC tumors.

Using IPA canonical pathway analysis, although we were able to detect unique and common pathways, we decided to focus on the common pathways modified in acute UV-exposed skin, wound healing skin and cuSCC tumors because of the above rationales. Unsurprisingly, we found that p53 signaling was activated (Figure 11). Immune response pathways such as Oncostatin M signaling, Interferon signaling, acute phase response signaling were activated (Figure 11). The IPA upstream regulator analysis examines how many known targets of transcription regulator are present in the provided data sets with the direction of change taken into consideration. Here, upstream regulator predicted that in cuSCC tumors, there was an activation of tumor promoters while an inhibition of tumor suppressors (Figure 11). Two

transcriptional factors that were commonly predicted in three data sets were OSM and TNF-a (Figure 11).
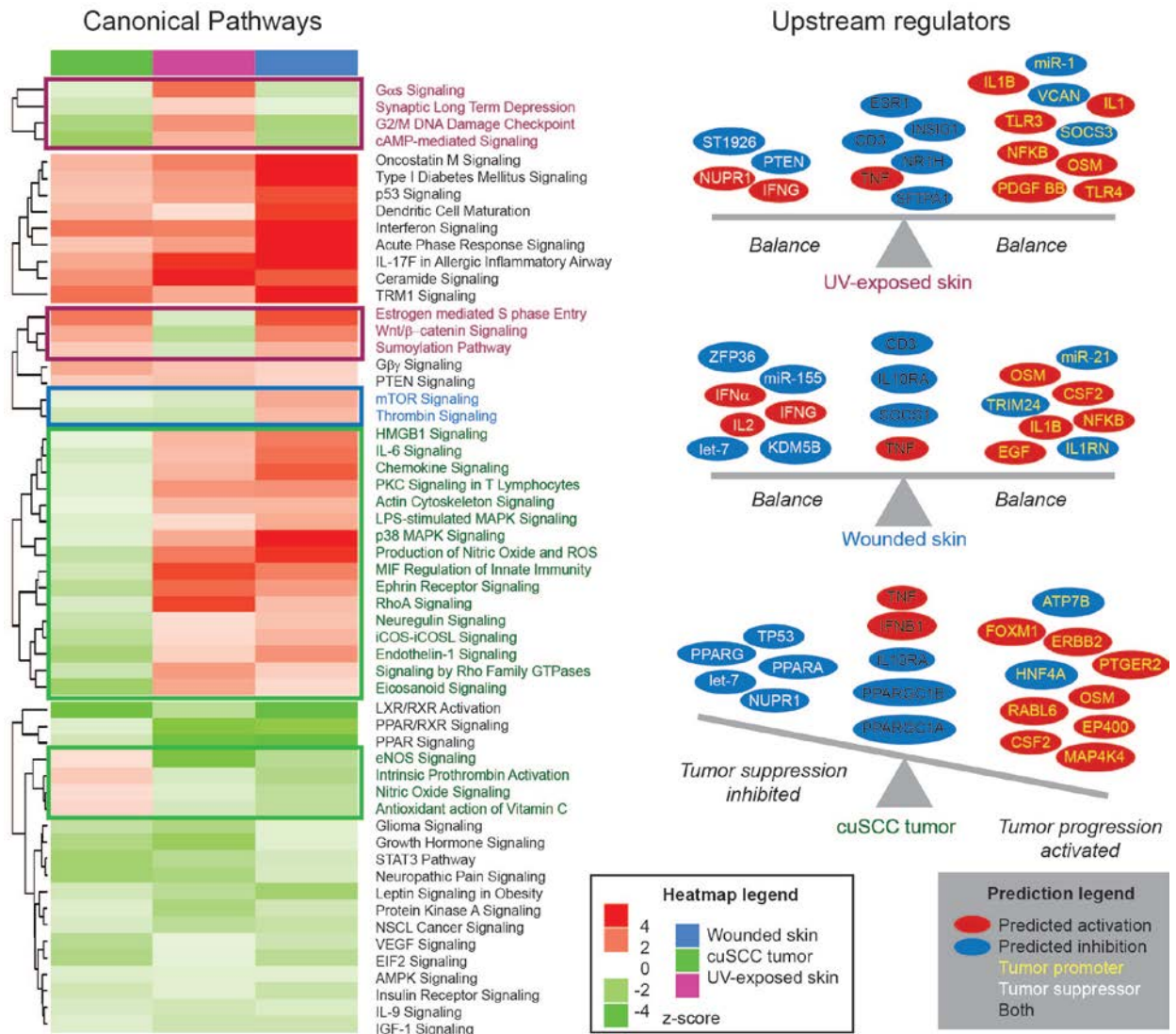
Figure 11

Ingenuity pathway analysis (IPA) identifies deregulation of Oncostatin M pathways and suggests possible important role of OSM and TNF upstream regulators. (A) Unique and

common IPA canonical pathways shared by three data sets. (B) Identified upstream regulator in three data sets.

3.2.4 Oncostatin M is a potential marker for cuSCC early development

Oncostatin M supports diverse homeostasis processes including liver repair, cardiac-tissue remodeling, and hematopoiesis. However, overproduction of OSM is thought to promote a variety of pathologies, including skin and lung inflammation, and several forms of cancer (127) (128). Nevertheless, the role of OSM in cutaneous squamous cell carcinoma has remained unclear (127) (128). Here, in cuSCC tumor, pathway mapping using GeneGO suggested that OSM can exert its effect through TIMPs and MMPs to regulate ECM remodeling; through Cyclin D1 and VEGF to modulate growth and through CCL2 to regulate inflammatory response (Figure 12).
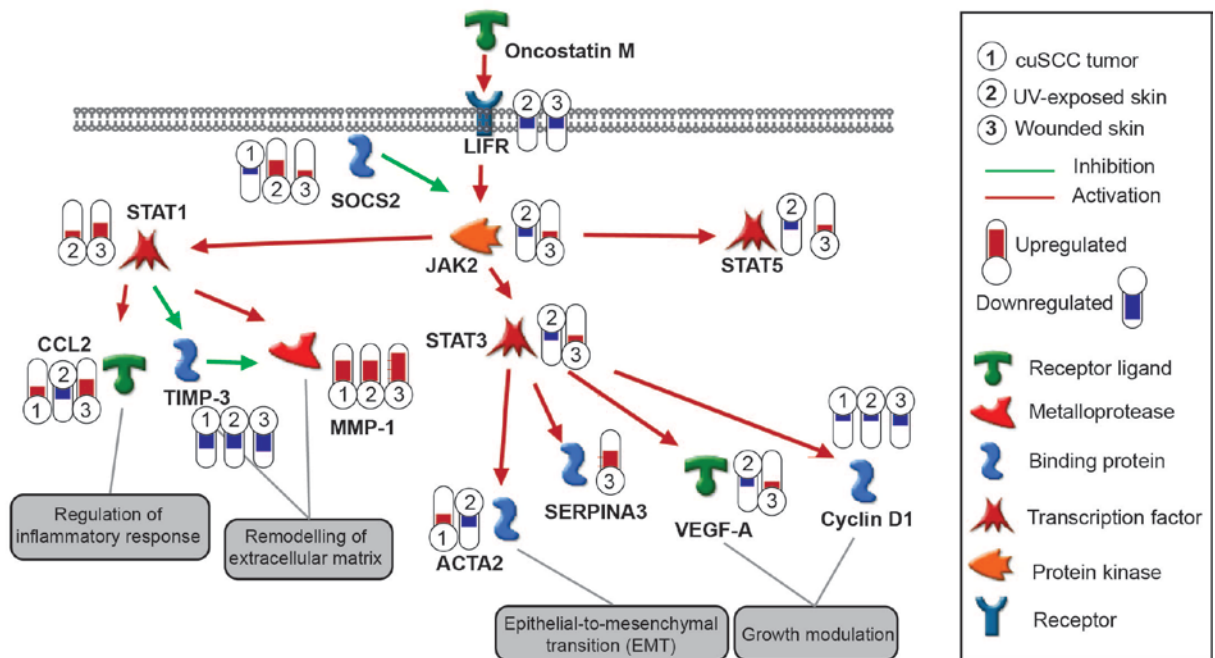
Figure 12

Oncostatin M downstream networks. GeneGO pathway generator identify possible downstream molecular targets and cellular processes regulated by Oncostatin M.

Next, we sought to validate whether expression of OSM and its downstream targets affect survival in SCC. We used TCGA data from HNSCC with TP53 mutation because genetically, this type of carcinoma most closely related to cuSCC. The Kaplan-Meier survival curves showed that high OSM expression related with shorter overall survival time in comparison with low OSM expression (p-value = 0.005) (Figure 13). In addition, survival analysis based on expression of Oncostatin M signaling downstream upregulated targets ACTA2, MMP1, CCL2 showed that high expression of these genes related to shorter overall survival time (Figure 14, **Error! Reference source not found.**) in HNSCC patients with TP53 mutation.

GSE65858
SURVIVAL MEASURE - OVERALL SURVIVAL
OSM GENE EXPRESSION
TP53_MUTATION - POS
COHORT DIVIDED AT MEDIAN OF GENE EXPRESSION

HR: 2.1(1.25-3.52)|PVAL: 0.0050408
— HIGH EXPRESSION
— LOW EXPRESSION

3 Years

5 Years

OVERALL SURVIVAL
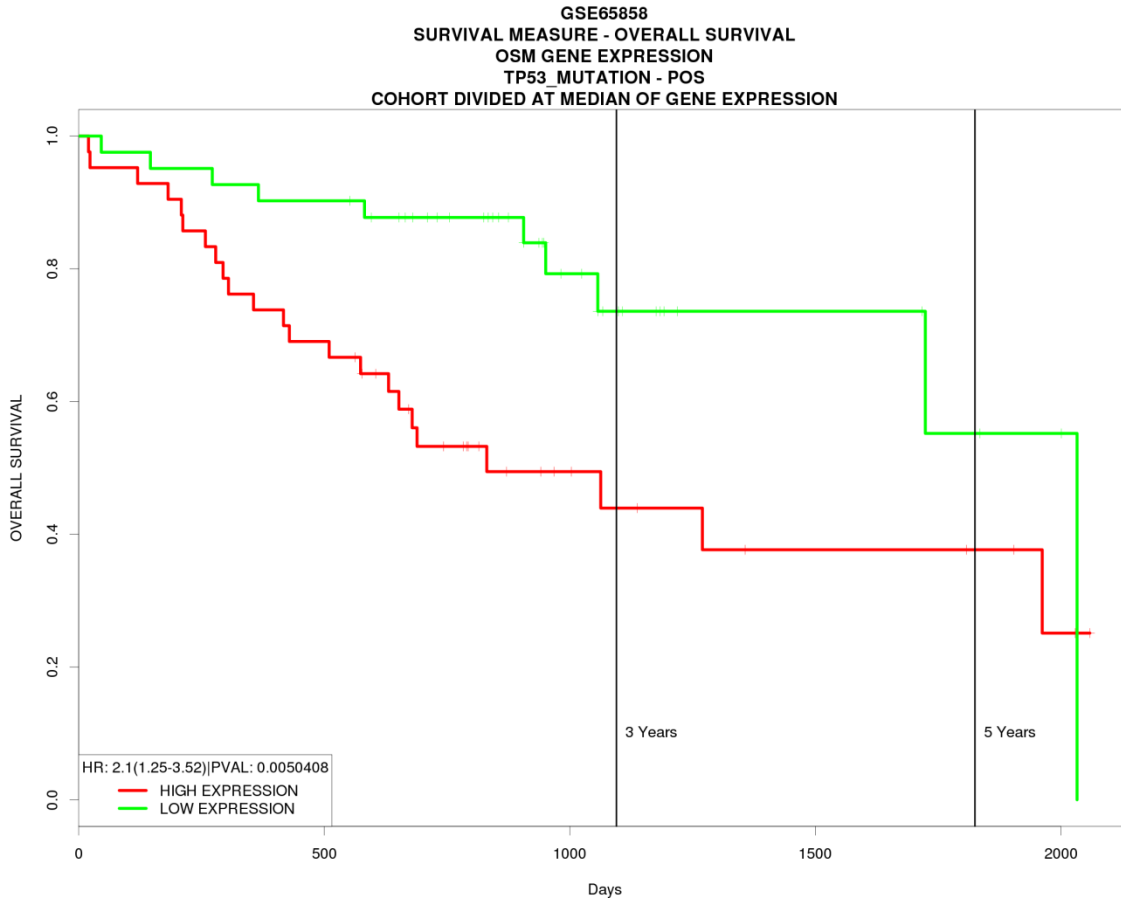
Days

Figure 13

Kaplan – Meier survival analysis of OSM gene expression in HNSCC patients with TP53 mutation. In this cohort, high expression of OSM is associated with shorter overall survival (High: median survival = 831 days; Low: median survival = 2033). Kaplan – Meier curves were generated following bifurcation of gene expression at median (High: n =42, Low: n =41). P-values were calculated according to the log-rank test.

59
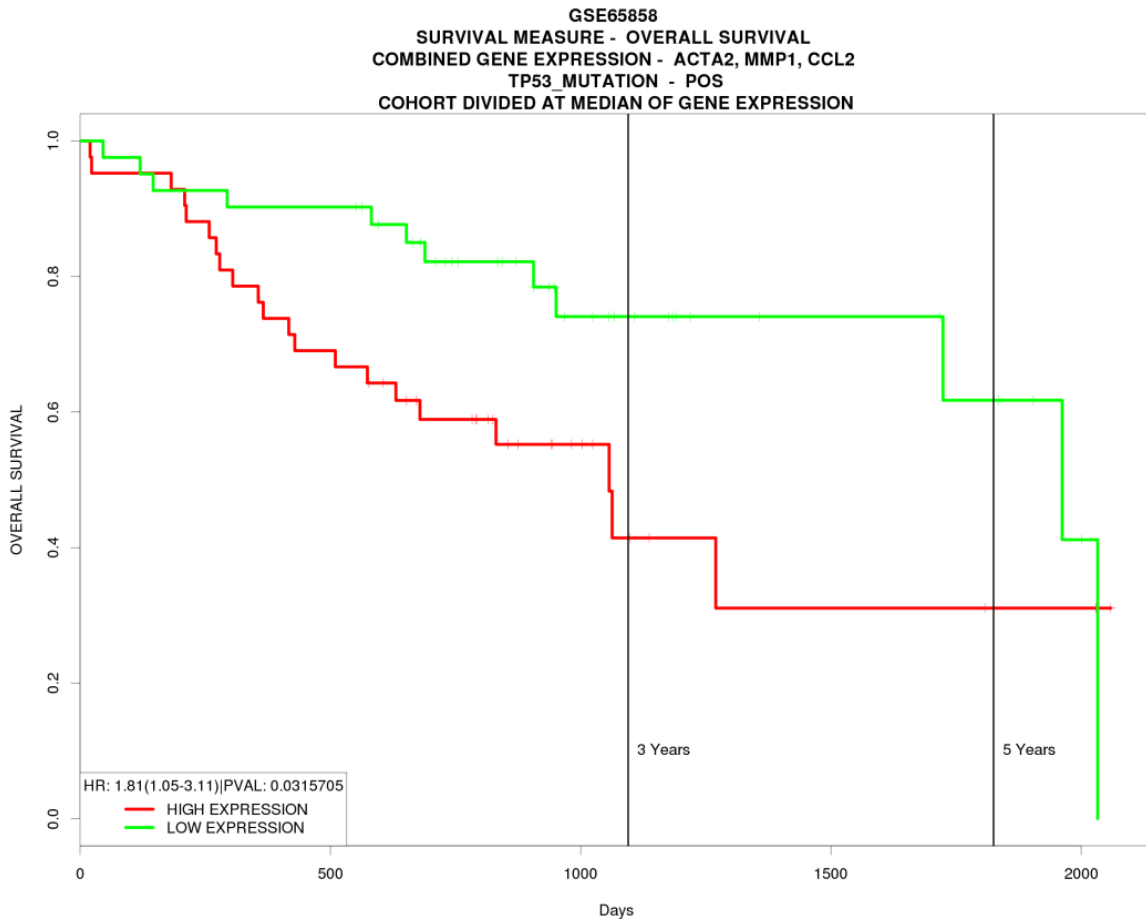
Figure 14

Kaplan – Meier survival analysis of ACTA2, MMP1, CCL2 gene expression in HNSCC patients with TP53 mutation. In this cohort, high expression of OSM is associated with shorter overall survival (High: median survival = 1057 days; Low: median survival = 1962). Kaplan – Meier curves were generated following bifurcation of gene expression at median (High: n =42, Low: n =41). P-values were calculated according to the log-rank test.

3.3   DISCUSSION

UV exposure is the most important risk for skin carcinogenesis. Exposure to UV radiation in early age increased childhood melanoma risk (129). In this chapter, we showed that the transcriptomic deregulation observed in cuSCC was induced early in UV-exposed skin and wound healing skin, which are the two main preconditions of cuSCC development. We show molecular evidences for the transcriptomic correlation between UV-exposed skin and wound healing skin using multiple gene set analysis tools. Previously found, moderate and repeated doses of UV can enhance wound healing process because of its antimicrobial effects (115). Patients with skin injury has greatly benefited from UV light therapy following skin wounding (130). Besides that, UV and wounding has been studied as two separate events even though they might lead to the same consequences of non-melanoma skin cancers. Our findings provide unique evidences showing that transcriptomes of UV-exposed skins and wounded skins largely overlap. Our study also provides rationales for future studies in integrating existing findings in UV radiation and wounding.

UV-exposure and skin injury triggers similar responses in human skin transcriptomes reflecting through several pathways. First, there is activation in pathways associated with inflammatory responses. Although inflammation is the second stage of wound healing, it is unexpected that we observed similar response in acute UV-exposed skin. These inflammatory responses might have resulted from the release of a variety of regulatory mediators including cytokines and chemokines following UV-exposure or skin injuries (131, 132). Here, at the UV irradiated sites or wounded sites, components of innate immune system such as macrophages are also recruited. Previously known, macrophage electrotaxis is mostly dependent on Rho

61

family small GTPases (133). Thus, this might be the explanation for the observed positive enrichment of GPCR signaling that might have been precursors to macrophage recruitment.

OSM is thought to promote a variety of pathologies, including skin inflammation, and various forms of cancer (127, 128). Our analyses using multiple data sets and pathway analysis platforms suggested that Oncostatin M signaling, a pathway found to be modified early in UV-exposed skin and wound healing with its deregulation existed in cuSCC tumors. High OSM gene expression shows significant correlation with overall survival in HNSCC patients with TP53 mutation, which is genetically related to cuSCC. Based on these findings, we aim to characterize OSM functions in cuSCC *in vitro*. Here, our results suggest that Oncostatin M can be further evaluated as a novel target in cuSCC treatment.

Chapter 4: Identifying miR-21 and miR-31 in cutaneous squamous cell carcinoma development

4.1 INTRODUCTION

miR-21 is a well-characterized oncogenic miRNA which was found to be the only miRNA consistently overexpressed in 540 clinical samples of cancer patients (42). However, only a handful of study has been conducted on characterizing miR-21 functions in skin disorders. miR-21 has been linked to the pathogenesis of epidermal hyperplasia in psoriasis through its targets *TIMP-3* (134). *miR-21* knockout mice show no obvious phenotype in development or adulthood, and seem to be protected against cancer development (135, 136). In invasive cuSCC, miR-21 is elevated and thought to induced epithelial mesenchymal transition in cuSCC (137). It has also been shown that miR-21 inhibition increased apoptosis in A431 cuSCC cell lines (138). In immunocompetent individuals, miR-21 and miR-31 is significantly upregulated in their healthy skin suggesting that deregulation of miR-21 and miR-31 happens early in cuSCC development (139).

The functional role of miR-31 is especially complex because miR-31 can have tumor-suppressive and oncogenic roles in different tumor types. However, a handful of studies suggested that miR-31 is oncogenic in cuSCC. A study employing A-431 cuSCC cell lines showed that miR-31 targets RhoTBT1 and regulate cuSCC proliferation and invasion (140). Another study determined that miR-31 regulated cell motility and colony formation ability of tumor cells (141).

Our data shows that while miR-21 was highly upregulated in UV-exposed skin, miR-31 has been shown to increase in the late inflammatory phase of wound healing skin (142). In addition, our microRNA-seq data of shows that miR-21 and miR-31 were the most highly expressed miRNAs in sporadic cuSCC, immunosuppressed cuSCC and Xeroderma pigmentosum cuSCC (Figure). These evidences motivated us to further explore the functions of miR-21 and miR-31 in more cuSCC cell lines and UV-induec cuSCC mouse model. In this study, we hypothesize that deregulation of miR-21 and miR-31 collectively plays a role in the development of cuSCC. We investigated the expression levels of miR-21 and miR-31 in cuSCC cell lines; examine their possible functions and the targets through which they exert their functions.

4.2 RESULTS AND DISCUSSION

4.2.1 Expression of miR-21 and miR-31 in cuSCC tumors

We sought to study the miRNA-expression landscape in cuSCC tumors and normal skin tissues derived from three different groups of patients: (1) Patients with sporadic cuSCC (n= 14), (2) Immunosuppressed patients (n= 5) and (3) *Xeroderma pigmentosum* patients (n= 8). We performed RNA-Seq to evaluate the expression of miRNAs in the tumors and normal skins. While we were able to identified upregulated miRNAs and down regulated miRNAs, we noticed that there is substantial overlap of miRNAs in the miRNA expression spectrum of the three patient groups (Appendix 3). Here, we found that miR-21 and miR-31 are highly up-regulated universally in all cuSCC tumor types compared to normal counterparts. Specifically, in sporadic

64

cuSCC, miR-21 increase 6.1-fold (p-value < 0.05) and miR-31 increases 9.7-fold (p-value < 0.05), compared to normal skin. Notably, several miRNAs identified from this experiment (data shown in Appendix 3) have previously been known to regulate various biological processes related to cuSCC; these include upregulated miR-135b (143-145) and downregulated miR-211 (146-148).
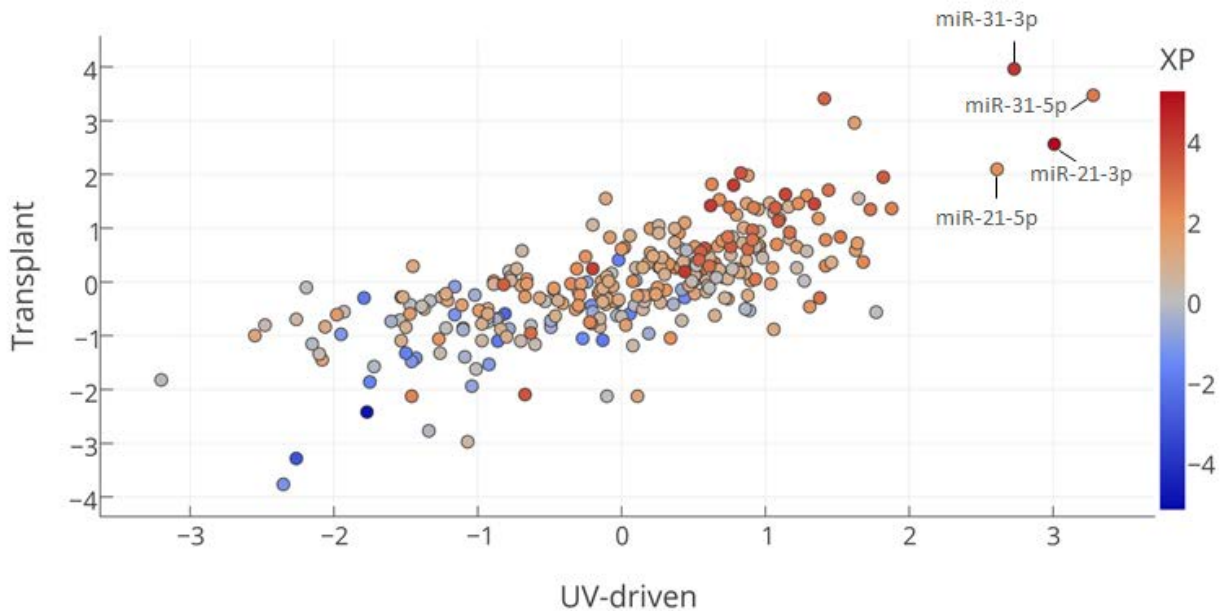
Figure 15

miR-21 and miR-31 were highly upregulated across cuSCC subtypes. X-axis, Y-axis and color represent miRNA expression levels ($\log_2$ fold change) in UV-driven cuSCC, cuSCC in immunosuppressed patients and Xeroderma pigmentosum, respectively. Graph was generated using Plotly open source tool (https://plot.ly/).

Next, we then used qRT-PCR to validate the expression level of miR-21 and miR-31 in normal human keratinocytes (NHEK) and 10 cuSCC cell lines derived from different types of cuSCC tumors (See Introduction). We found that majority of cuSCC cell lines have elevated miR-21 and miR-31 expression level compared to NHEKs (Figure 17). Cell line that has the highest miR-21 expression level compared to NHEK is SCCIC1 (4.4-fold upregulation). Cell line that has the highest miR-31 expression level compared to NHEK is SCC IC1 (13.8-fold upregulation). Taken together, the results of our RNA-seq and qRT-PCR demonstrate that miR-21 and miR-31 expression level are highly upregulated in cuSCC cell lines and cuSCC tumors of different origins, suggesting the important roles of miR-21 and miR-31 in cuSCC development.
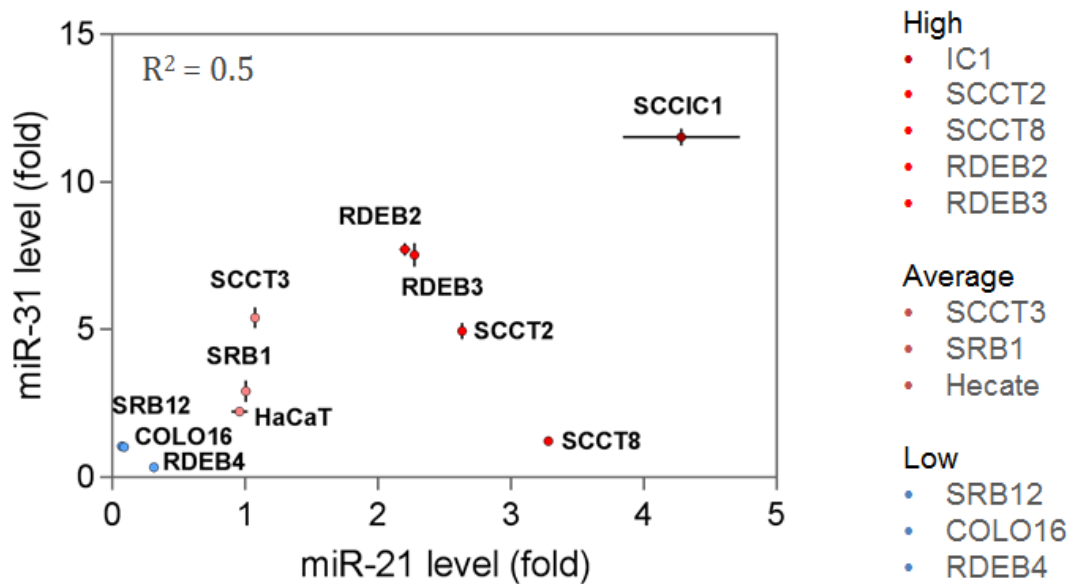
Figure 167

miR-21 and miR-31 expression level in cuSCC cell lines. Taqman qPCR experiments were performed in three biological replicates. Cells were group in three based on miR-21 and miR-31 expression level. Graph shows correlation between miR-21 and miR-31 in each cuSCC cell lines.

4.2.2 Modulation of miRNA expression levels in cuSCC cell lines

In order to study the effect of miR-21 and miR-31, we first established conditions for overexpression and knockdown of both miRNAs. To overexpress, we have used locked nucleic acid (LNA) modified oligonucleotides and transiently transfected it into cuSCC cell lines of interest. To knockdown, we have also used LNA modified antisense nucleotide to inhibit the expression of both miR-21 and miR-31 mature strands. The miRNA expression in testing condition was compared to cells transfected with a mock LNA sequence. We confirmed that the cellular level of established miR-21 and miR-31 targets were decreased following over-expression and increased with inhibition of the miRNAs (**Figure**).
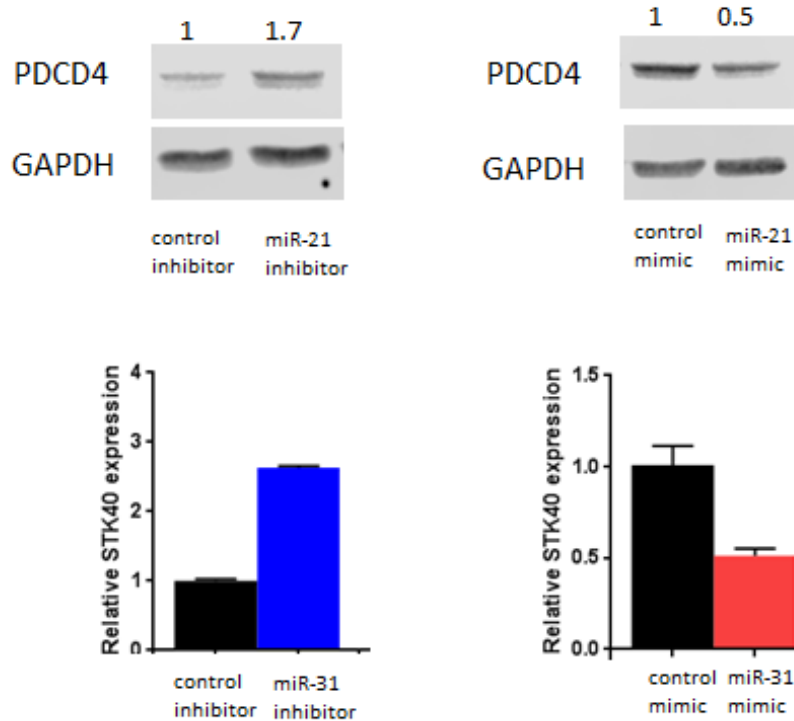
Figure 18

miR-21 inhibitor increase the expression of PDCD4, its established targets by 1.7-fold based on western blot analysis and vice versa. miR-31 inhibitor increase transcriptional level of STK40, a published target of miR-31(149) by 2.6-fold through qRT-PCR and vice versa.

4.2.3 miR-21 and miR-31 synergistically increased proliferation in cuSCC cell lines

To determine whether miR-21 and miR-31 affects the proliferative capacity of cuSCC cell lines, we performed proliferation assays. Cells were transiently transfected miR-21 and miR-31 inhibitors (Thermo Fisher). After 48 hours, transfected cells were re-seeded for Incucyte confluence-based proliferation assay. Cell proliferation was visualized and quantified using time-lapse imaging. We observed that miR-21 inhibitor and inhibitor combination treatment significantly suppressed cell proliferation in majority of tested cells (Figure 17). Interestingly, at

68

96 hour after seeding in SCCT8, which has the high miR-21 expression level, miR-21 inhibitor decreased its proliferation by 39% while inhibitor combination suppressed proliferation by 80% compared to cells transfected with non-targeted control. In line with this, the cell proliferation suppression by miR-21 and inhibitor combination was also observed in SCC IC1, SCC RDEB2 and COLO16. These data indicate that loss of miR-21 contribute to reduction in cuSCC cell proliferation. More importantly, this suggested that miR-21 and miR-31 inhibitor can act synergistically in inhibiting cuSCC tumor proliferation.
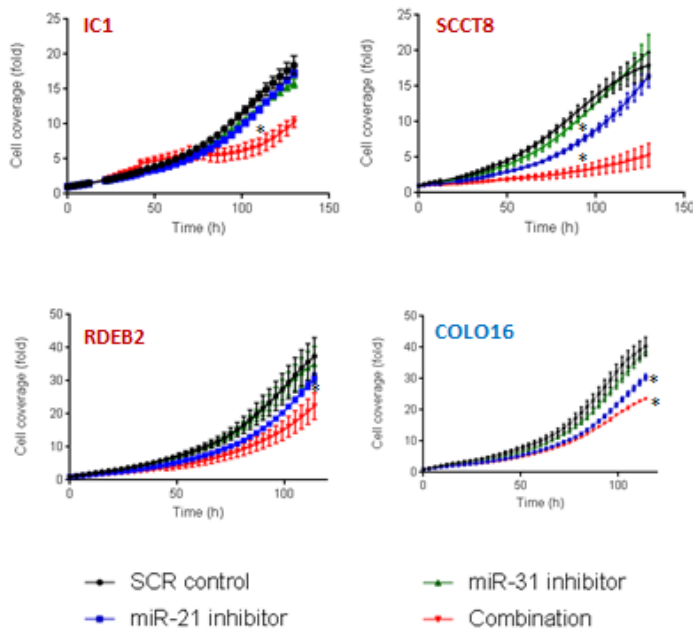
Figure 17

Line graphs showing result of confluence-based cell proliferation assay (Incucyte, Essen Bioscience). Cells were seeded for proliferation assays 24 hour post-transfection with non-targeting inhibitor control, miR-21 inhibitor, miR-31 inhibitor and inhibitor combination.

69

4.2.4 miR-21 and miR-31 synergistically decreased apoptosis in cuSCC cell lines

Generally, miR-21 acts as an antiapoptotic agent as it suppresses the expression of the pro-apoptosis proteins PDCD4, PTEN, and many other (136, 150-152). Here, apoptosis analysis was performed to investigate whether cuSCC call apoptosis could be influenced after miR-21 and miR-31 expression inhibition. We found that miR-21 inhibitor, miR-31 inhibitor and the inhibitor combination induced apoptosis (AnnexinV positive cells) in SCCT8 cell lines by 2.59 ± 0.42 – fold (p-value = 0.0138), 1.51 ± 0.28 - fold (p-value = 0.0596) , 3.53 ± 0.2-fold (p-value = 0.0032) respectively, compared to cells transfected with non-targeted control (Figure 17). We detected significant decrease in apoptosis in all cuSCC cell lines tested. Specifically, in RDEB2, miR-21 inhibitor, miR-31 inhibitor and the inhibitor combination induced apoptosis by 2.73 ± 0.83 – fold (p-value = 0.0285), 1.33 ± 0.5 - fold (p-value = 0.1767), 4.03 ± 0.72-fold (p-value = 0.0067) respectively, compared to cells transfected with non-targeted control (Figure 21). In COLO16, miR-21 inhibitor, miR-31 inhibitor and the inhibitor combination induced apoptosis by 1.92 ± 0.55 – fold (p-value = 0.093), 1.3 ± 0.12 - fold (p-value = 0.3717) , 3.34 ± 0.7-fold (p-value = 0.0214) respectively, compared to cells transfected with non-targeted control (Figure 21).

SCCT8-Annexin+

COLO16-Annexin+

RDEB2-Annexin+
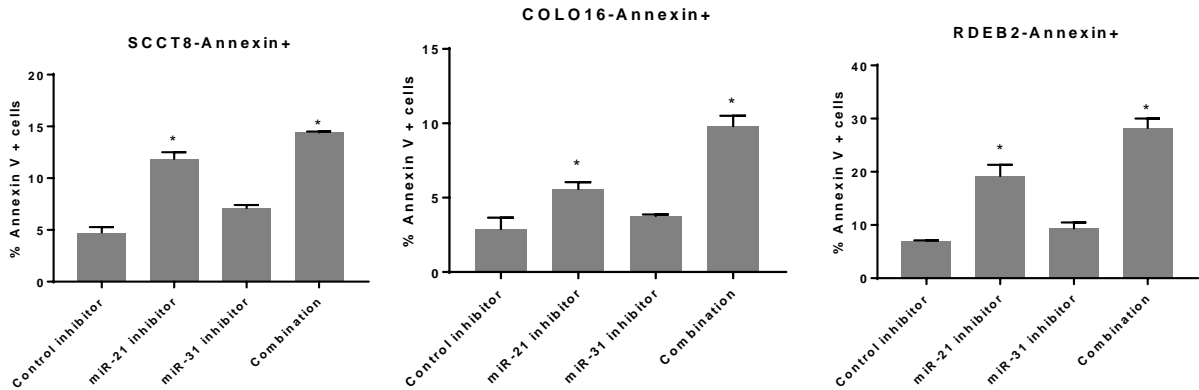
Figure 18

cuSCC cells were transfected with non-targeting inhibitor, miR-21 inhibitor, miR-31 inhibitor and control inhibitor. After 48 hours, cells were labeled with annexin V-FITC and PI was collected on a BD FACS Canto II.

Noticeably, the combination of miR-21 inhibitor and miR-31 inhibitor showed synergistic effect on inhibiting apoptosis in cuSCC cell lines. Specifically, in SCCT8, inhibitor combination increased apoptosis by 27% while total apoptosis increase of miR-21 inhibitor and miR-31 inhibitor was 45%. Taken together, this result provides indication that miR-21 and miR-31 inhibitors have synergistic effect in cuSCC apoptosis. Furthermore, this data provide additional evidence that mir-21 and miR-31 cooperatively act to promote cuSCC development.

4.2.5 Identification of novel targets for miR-21 and miR-31 in cuSCC

TMT-based detection of the proteins was carried out in the transfected SCCT8 with either the mimics of the inhibitor against miR-21, miR-31 and both of them (Figure 22). SCCT8 was chosen based on low heterogeneity often seen in cuSCC cells and strong response to

inhibitor treatment. We successfully detected significantly modulated proteins in three mimic treatment groups and three inhibitor treatment groups (p-value < 0.05).
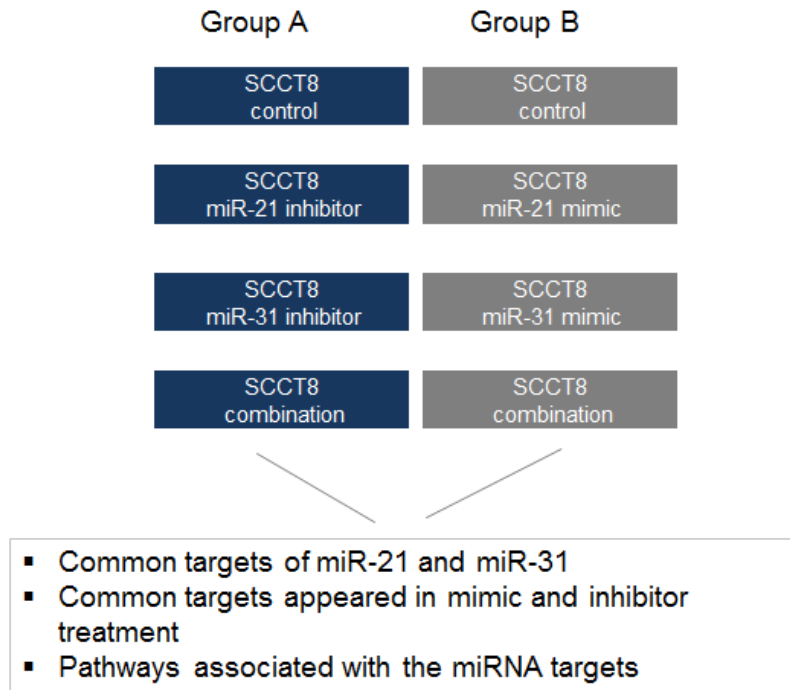
Figure 19

Design of proteomics experiments on SCCT8 to identify miR-21 and miR-31 novel targets in cuSCC. Experiments were performed in three biological replicates.
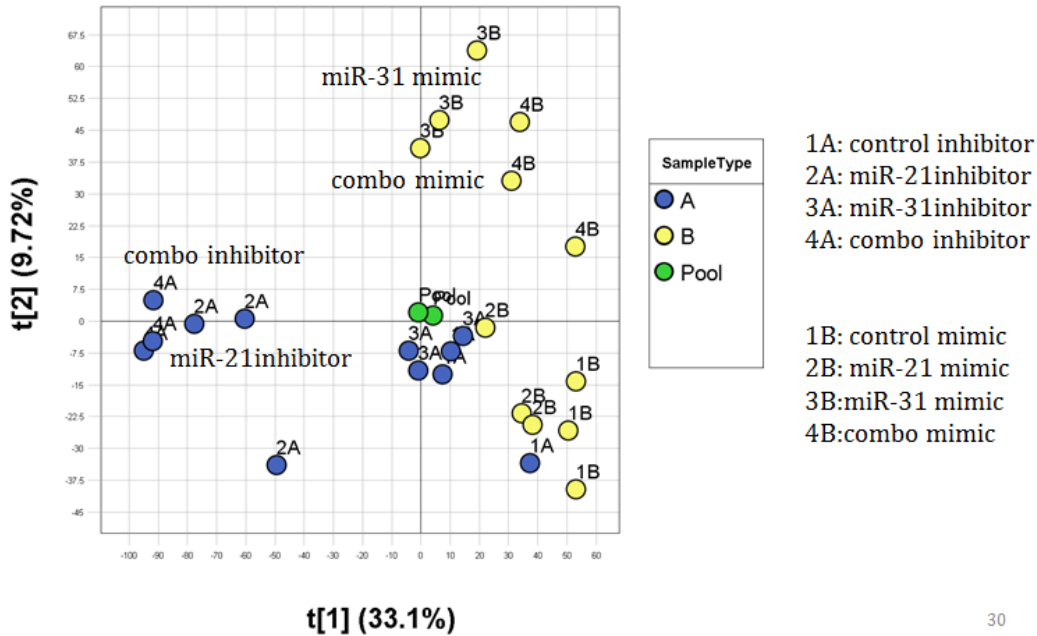
Figure 20

Principle component analysis of identified proteins in eight experimental conditions

We next compared the list of differentially expressed proteins from our proteomics study to their respective list of experimentally and computationally predicted targets of both miRNAs. Computational prediction of targets against miRNAs typically leads to hundreds of predicted targets and is widely held to be susceptible to false positive prediction. We used consensus prediction of targets, considering only targets commonly predicted through at least four prediction programs including TargetScan to generate a list of targets for miR-21 and miR-31 and finally checked for the presence of these targets in our list of differentially expressed proteins identified by proteomics. The consensus target prediction approach led to 1695 targets for miR-21 and 2409 targets for miR-31 respectively. Since number of differentially expressed proteins in miRNA-proteomics experiments is typically much lower than the total number of

predicted targets, we looked for common proteins detected in our experiment and predicted as targets. Given that miRNA functions by suppressing the expression of their target genes, we focused on predicted miRNA targets that increased following miRNA inhibition and decreased following miRNA overexpression. We then looked qualitatively for overlapping differentially expressed proteins in both conditions. In the proteomics study for miR-21, we identified 42 proteins that fulfill these conditions. Here, we were able to identify that several potential functional targets of miR-21 in cuSCC that were shown in Table 6. In the proteomics study for miR-31, we identified 31 proteins that fulfill these conditions. Combining miR-21 and miR-31 potential target results, we found that MTMR12 and MOCS2 can be common functional targets of miR-21 and miR-31 in cuSCC. To validate that the proteomics study were performed properly, we confirm that a known target of miR-21, Isoform 2 of Program Cell Death Protein 4 (PDCD4) increased by 1.8-fold following miR-21 inhibitor treatment and decreased by 1.77-fold following miR-21 mimic treatment, compared to their respective non-targeting controls.

Predicted target	miR-21 mimic treatment ($\log_2$FC)	miR-21 inhibitor treatment ($\log_2$FC)	mimic combination treatment ($\log_2$FC)	inhibitor combination treatment ($\log_2$FC)
ANXA1	-0.43239	0.272606	-0.50538	0.193606
BID	-0.25126	0.555065	-0.34518	0.985248
CAMSAP1	-0.204	0.227075	-0.1243	0.483813
GSS	-0.12422	0.220859	-0.16563	0.132916
GTPBP1	-0.29233	0.256802	-0.40514	0.177748
MTMR12	-1.11217	1.091099	-0.84736	0.512323
MYO1E	-0.1127	0.23083	-0.29566	0.147437
SUB1	-0.18375	0.171702	-0.18377	0.264578
TIMP2	-0.29589	0.411779	-0.6813	0.140253
TP53BP2	-0.13135	0.352458	-0.13234	0.434275

WDR7	-0.14932	0.15522	-0.2135	0.121168

Table 6

Predicted miR-21 targets that increased following miRNA inhibitor treatment and decreased

following miRNA mimic treatment in both single and combination treatment

Predicted target	miR-31 mimic treatment (log$_2$FC)	miR-31 inhibitor treatment (log$_2$FC)	mimic combination treatment (log$_2$FC)	inhibitor combination treatment (log$_2$FC)
AHNAK2	-0.3253	0.167462	-0.24681	0.197691
EXOC8	-0.1111	0.100481	-0.21896	0.219626
HECTD3	-0.44966	0.189476	-0.27191	0.628198
MTM1	-0.16351	0.130448	-0.1562	0.136523
NELFB	-0.15532	0.105361	-0.16493	0.367473
PGM2L1	-0.16709	0.565088	-0.36869	0.616371
PLEKHA1	-0.1872	0.241933	-0.10059	0.317377
SNRNP27	-0.17212	0.398887	-0.20371	0.398308

Table 7

Predicted miR-31 targets that increased following miRNA inhibitor treatment and decreased

following miRNA mimic treatment in both single and combination treatment
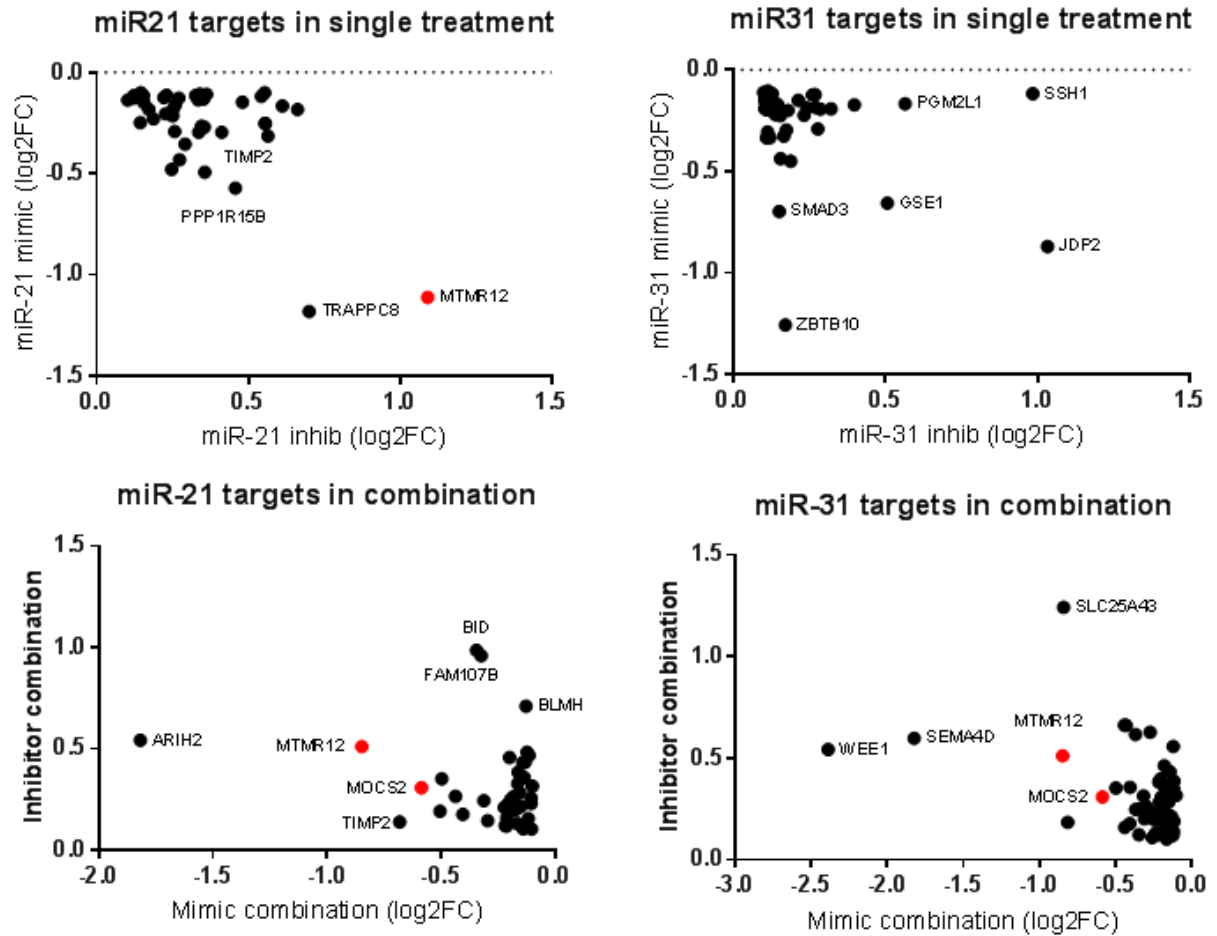
Figure 21

Potential miR-21 and miR-31 targets in cuSCC were identified by using multiple miRNA target prediction tools and integrating data from eight independent experimental conditions.

In order to identify canonical pathways regulated by miR-21 and miR-31, we use GSEA canonical pathway analysis. Then, use Enrichment map (Cytoscape) to integrate the GSEA output of four different conditions: cells treated with miR-21 inhibitor, miR-21 mimic, inhibitor combination and mimic combination. We found that cell cycle pathways were enriched significantly in cells treated with miR-21 inhibitor and inhibitor combination. Specifically,

checkpoints activity at G1/S phase and DNA damage checkpoint was upregulated (Figure 22). On the other hand, the inhibitor treatment seems to further decrease ECM receptor activity and Ribosome activity (Figure 22).

Figure 22

Canonical pathway analyses revealed important common pathways regulated by miR-21 and the combination of miR-21 and miR-31 (node cut-off: q=0.01). Each circle (node) represents a gene set. Each circle is divided into three sections which represent one of three dataset. Blue color represents pathway downregulation. Red color represents pathway upregulation.

Taken together, using the integration of TMT-based proteomics analysis and computationally predicted miRNAs targets, we were able to determine several novel functional targets of miR-21 and miR-31 in cuSCC. Our on-going works include validating these targets *in vitro* and *in vivo*.

4.3 DISCUSSION

The up-regulation of miR-21 in many types of tumor has been known for a long time (153-155). In cuSCC, it was reported that hyaluronan-CD44 promoted miR-21 expression in cuSCC progression following UV irradiation (156). In agreement with previous findings, our data show that miR-21 and miR-31 are significantly overexpressed in three different subtypes of cuSCC, as compared to normal skin. Although widely observed to increase in cuSCC tumors, miR-21 and miR-31 functions in this cancer have not been characterized except for one study which showed that miR-31 increased in cuSCC and regulated cell motility and colony formation ability of tumor cells (141). Here, we found that the inhibition of miR-21 and miR-31 significantly suppressed cell proliferation and enhance cell apoptosis. More importantly, we showed that miR-21 and miR-31 inhibitors functioned in a combinatorial manner, suggesting that once validated, they can be used in cuSCC combined treatment.

Since microRNAs function through a network of target genes, it is important to identify these targets. PDCD4 is a confirmed target of miR-21 in many types of cancer including ovarian cancer, glioblastoma, breast cancer and many more (150, 157). Our proteomic data in SCCT8

cell line showed that PDCD4 expression increased when miR-21 was depleted and vice versa, which support previous findings. However, there are other proteins with higher magnitude of change. Among several potential miR-21 and miR-31 targets identified by proteomics approach, we identify that Myotubularin Related Protein 12 *MTMR12* and Molybdenum Cofactor Synthesis 2 *MOCS2* can be the common target of both miRNAs. However, there are many other potential candidates that have the similar magnitude of change as MTMR12. This can provide us with challenges when identifying additional potential targets of miR-21 and miR-31. The question is which genes are directly regulated by miR-21 and miR-31 and not as a secondary effect of the changes in other gene expression.

Because of this, we use pathway analysis to understand important pathways regulated by miR-21 and miR-31 and more importantly, connected these changes to potential target genes. In another way, these analyses might tell us how some cumulative modest changes in gene expression can lead to a more robust change in biological processes. Here, we found that cell cycle checkpoint pathways were positively enriched in cuSCC cells treated with inhibitors. When taking this result into the context of cell proliferation and apoptosis assay result, we reason that the cycle checkpoints were activated due to the damage caused by miRNA inhibitor. Taken together, this data suggests that these are the important processes where miR-21 and miR-31 function through and that predicted targets involved in cell cycle checkpoint pathways should be considered with greater weight.

Chapter 5: miR-181a promotes progression of cutaneous squamous cell carcinoma by targeting TGFβR3

5.1 INTRODUCTION

In the United States, over 700,000 cases of cutaneous squamous cell carcinoma (cuSCC) are diagnosed annually and account for about 15-20% of all skin cancers (158). Our understanding of the molecular and genetic events that lead to sequential progression of normal skin (NS) to precancerous actinic keratosis (AK) to cuSCC is limited. This represents a fundamental gap in our knowledge and understanding of this progression sequence is of relevance to understanding cancer development and developing more effective chemoprevention strategies. In an effort to identify transcriptional drivers of cuSCC development, we previously genomically profiled the development sequence from NS to AK to invasive cuSCC. This effort identified major microRNA drivers, as identified through functional pair analysis (17).

Our initial analysis suggested that miR-181a is upregulated during cuSCC development. The miR-181 family is highly evolutionarily conserved across vertebrates with roles in differentiation of hematopoietic cells, including lymphocytes, natural killer cells, and megakaryocytes (159). Pathway analysis reveals that miR-181 family target genes play important roles in cancer, axon guidance, actin cytoskeleton, MAPK signaling, and T cell receptor signaling pathways (160).

Several studies show upregulation of miR-181 expression in colorectal carcinoma (161), ovarian cancer(162) and hepatocarcinoma(163) with roles in cell cycle, apoptosis, proliferation, migration and invasion (164) through targets such as BCL2L11 (BIM) (165), BCL-2 (166), ATM (167), and KRAS (168). In a recent meta-analysis of 21 studies involving 1685 patients, elevated expression of miR-181a was identified as a negative prognostic molecular marker in human head and neck squamous cell carcinoma (HNSCC)(169), a disease that closely resembles cuSCC genomically(17, 170). Here, we define a mechanistic link between miR-181a, susceptibility to apoptosis, cellular motility and EMT, and TGFβR3. We show that miR-181a is able to confer several pro-tumorigenic properties upon epithelial cells, that these phenotypes are due to the direct regulation of TGFβR3 expression, and that inhibition of miR-181a compromises tumor growth *in-vivo*.

5.2 RESULTS

miR-181a overexpression is observed in cutaneous squamous cell carcinoma

First, we examined miR-181a expression in two different non-melanoma skin cancer cohorts (Fig. 26 A and B). A tissue microarray containing 37 evaluable cases of cuSCC and 9 normal skin controls (US Biomax) was hybridized with a locked nucleic acid (LNA, Exiqon) anti-miR-181a or nonspecific LNA anti-miR control and expression quantified within tumor cells and normal epidermis, respectively, using the Aperio Image system. We found that miR-181a was upregulated in the majority of cases, by a mean of 3.0 ± 0.5-fold ($P < 0.0001$, unpaired *t*-test) (Fig. 26 A and B). Furthermore, Taqman qPCR showed that miR-181a-5p was

81

increased in 8 out of 11 SCC cell lines when compared to normal human epithelial keratinocyte (NHEK) (Figure 25).
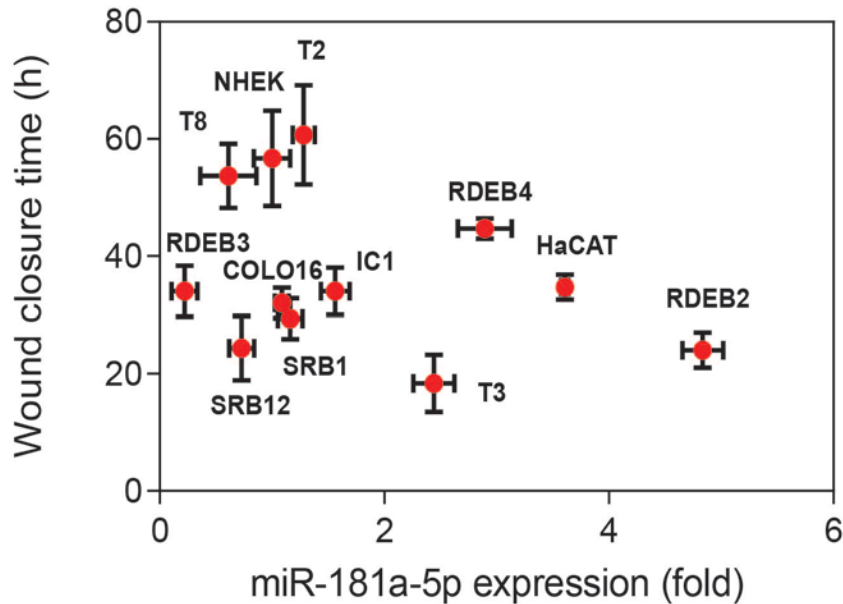
Figure 23

Corellation of relative miR-181a-5p (Taqman-qRT-PCR) expression levels in NHEK, HaCaT and cuSCC cell lines and wound closure time.

miR-181a overexpression increases colony formation efficiency and suppresses UV-induced apoptosis.

Next, we sought to determine the potential mechanism of action of miR-181a by assessing the pathways regulated by it. We performed microarray gene expression analysis (Illumina BeadArray) on lenti-miR-181a HaCat (miR-181a overexpressed) and lenti-miR-00 HaCat (negative control). Ingenuity Pathway Analysis (IPA, Qiagen) revealed enrichment of cell proliferation and cellular movement pathways (Fig. 26 C).

HaCaT cells overexpressing with miR-181a were tested for their survival in liquid culture and enhanced colony formation in soft agar. As a positive control we used Ha-Ras^{V12}-transformed HaCaT cells, which readily form colonies and tumors *in-vivo(171)*. Our results showed that HaCaT miR-181a overexpressing cell lines have an increased capability of colony formation in soft agar. miR-181a-overexpressing HaCaT cells produced 6.3 ± 0.6 fold more colonies (*P*< 0.0001, unpaired *t*-test) (Fig. 26D), reflective of a significant increase in anchorage-independent proliferation.
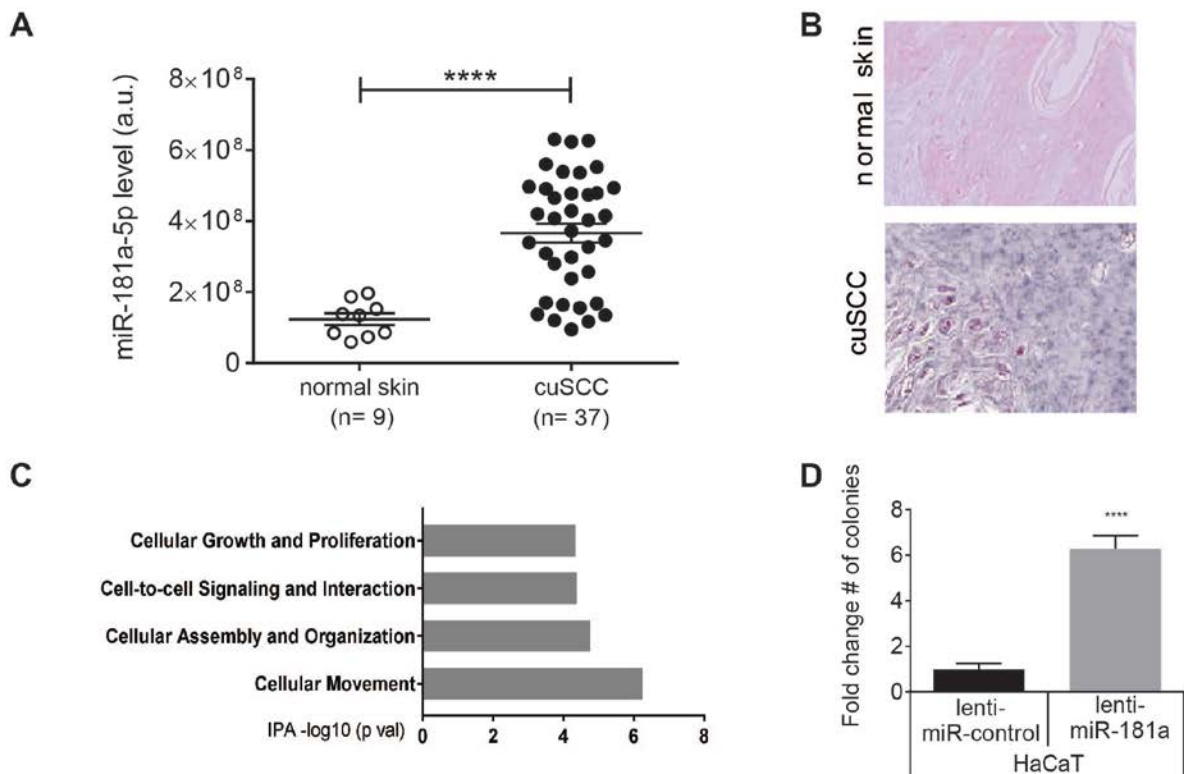
Figure 24

miR-181a is overexpressed in cuSCC. **A,** ISH detection using LNA detection probe (blue) or scramble-miR as negative control were performed on FFPE tissue microarray. Error bars

represent the mean (+) S.E.M.; **** $P<0.0001$ (unpaired t-test). **B,** Representative images show that cuSCC has higher miR-181a expression compared to normal skin. **C,** Transcriptome of HaCaT stable cell lines overexpressing lenti-miR-181a was analyzed by IPA for their associated molecular pathways. **D,** HaCaT stable cell lines overexpressing lenti-miR-181a or lenti-control were tested for their survival in liquid culture and enhance colony formation in soft agar. Error bars represent the mean (+) S.E.M.; **** $P<0.0001$ (unpaired t-test).

Exposure to UV radiation (UVR) can induce apoptosis of mammalian cells. Since UV exposure is the primary environmental cause of skin cancer, UV-induced apoptosis represents an important tumor suppressive mechanism. To identify a potential link between miR-181a expression and UV-induced apoptosis, we used NHEK and HaCaT overexpressing miR-181a and the negative lenti-miR-control. Cells were subjected to a flow cytometry-based apoptosis assay (Annexin V) 24 hours following 750 J/m^2 UV-irradiation (171). Overexpression of miR-181a strongly suppressed UV-induced apoptosis in both NHEK and HaCaT cells by 86.8% ± 3.5% ($P < 0.001$, unpaired t-test) and 45.4% ± 2.4 % ($P < 0.01$, unpaired t-test), respectively (Fig. 2A and B). Ataxia telangiectasia (ATM) is a key regulator of DNA damage signaling pathway that activates p53 (172, 173) and a validated target of miR-181a (174). ATM regulates cell cycle progression through phosphorylation of cell-cycle checkpoint kinase 1 (CHEK1) and p53, and DNA damage repair through phosphorylation histone H2AX(175). Here, we showed that ATM and p53 expression correlate conversely with miR-181a level. We also noticed that phosphorylation of DNA damage response proteins such as CHEK1, p53 and H2AX increased

84

to a lesser extent when cells with higher level of miR-181a were exposed to UV (Fig. 27C).
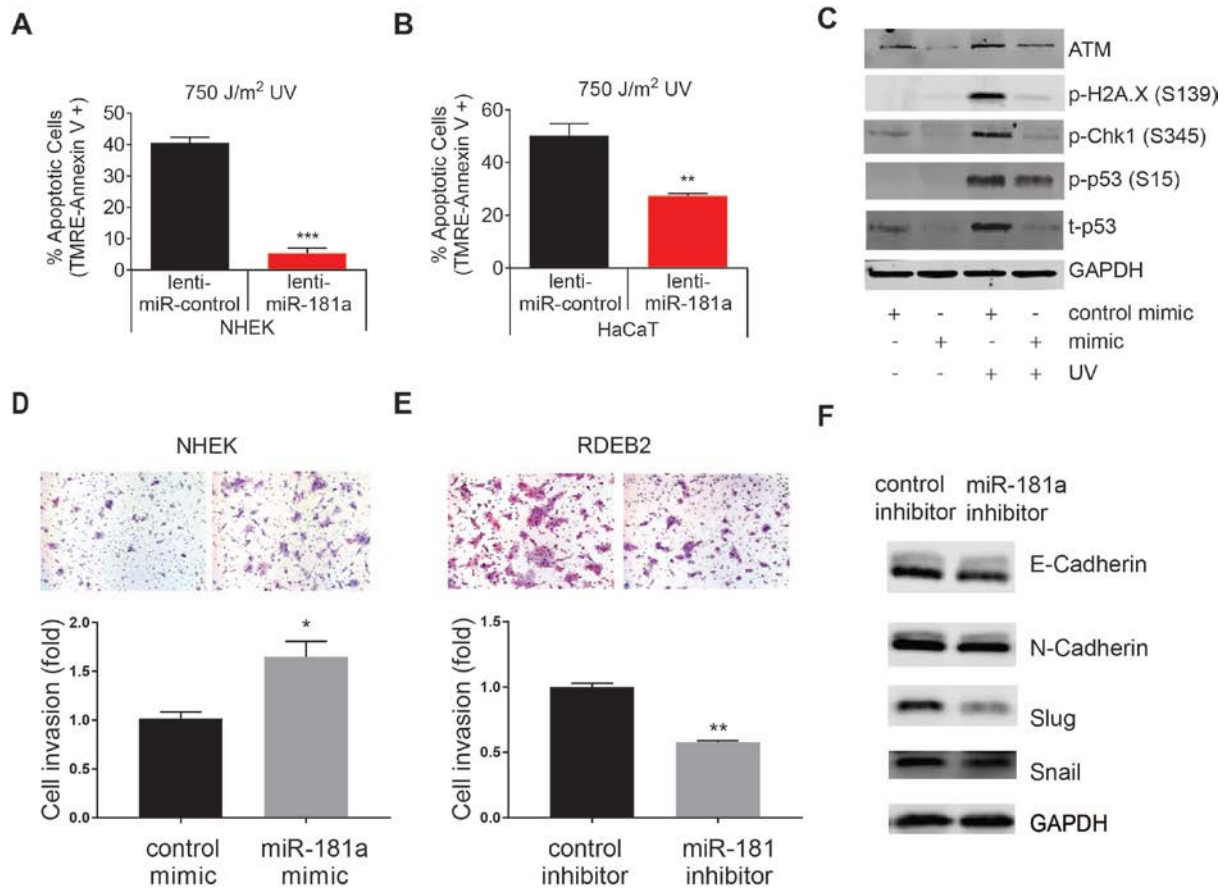
Figure 25

miR-181a suppresses UV-induced apoptosis and increases invasiveness of keratinocytes.

A-B, NHEK and HaCat cells were stably transfected with lenti-miR-181a or slenti-miR-control. Cells were sham irradiated or irradiated with 750 J/m^2 of UVB. Apoptotic cells were determined by flow cytometry. Error bars represent the mean (+) S.E.M.; *** $P < 0.001$, ** $P < 0.01$

85

(unpaired *t*-test). **C,** Western blots showed that overexpression impairs the proper induction of ATM, p-p53, p-His2AX, and p-Chk1 in response to UV exposure. **D-E,** Trans-well invasion assay was performed at 48 h after NHEK were transfected with control-mimic, or miR-181a-5p mimic and RDEB2 were transfected with control-inhibitor, or miR-181a-5p inhibitor. Error bars represent the mean (+) S.E.M.; * $P < 0.05$, ** $P < 0.01$ (unpaired *t*-test). **F,** Expression of EMT-markers was determined by western blot in transfected RDEB2. GAPDH served as the loading control.

miR-181a overexpression increases keratinocyte invasiveness

Because the cellular movement pathway was found to be highly enriched in miR-181a overexpressing HaCaT cells, we asked whether miR-181a affected keratinocyte morphology and motility and invasiveness. Interestingly, during the course of apoptosis assays, we observed that miR-181a overexpression induced morphological changes in NHEKs, with cells adopting a more spindled appearance. These observations suggested to us that miR-181a might also regulate keratinocyte epithelial-mesenchymal transition (EMT).

In order to address this, we performed Boyden chamber Matrigel invasion assays using NHEK and RDEB2 cuSCC cells (Fig. 27D and E). First, we overexpressed miR-181a in NHEK. We observed that miR-181a-5p increased NHEK invasiveness significantly by 1.7 ± 0.2-fold compared to non-targeting control-expressing NHEK ($P < 0.05$, unpaired *t*-test). We then depleted miR-181a in RDEB2 cuSCC cells. Depletion of miR-181a decreased RDEB2 invasiveness by 1.7 ± 0.1-fold compared to non-targeting control-expressing cells ($P < 0.01$,

unpaired *t*-test).

To investigate this further, we observed that this miR-181a depletion in RDEB2 resulted in decreased of Slug (SNAI2) expression (Fig. 27F). Slug is known to be particularly relevant to EMT in epidermal keratinocytes and our data reflect that in this context as well(176, 177). Taken together, these data show that the loss of miR-181a can induce decreases in EMT marker expression and cellular invasiveness.
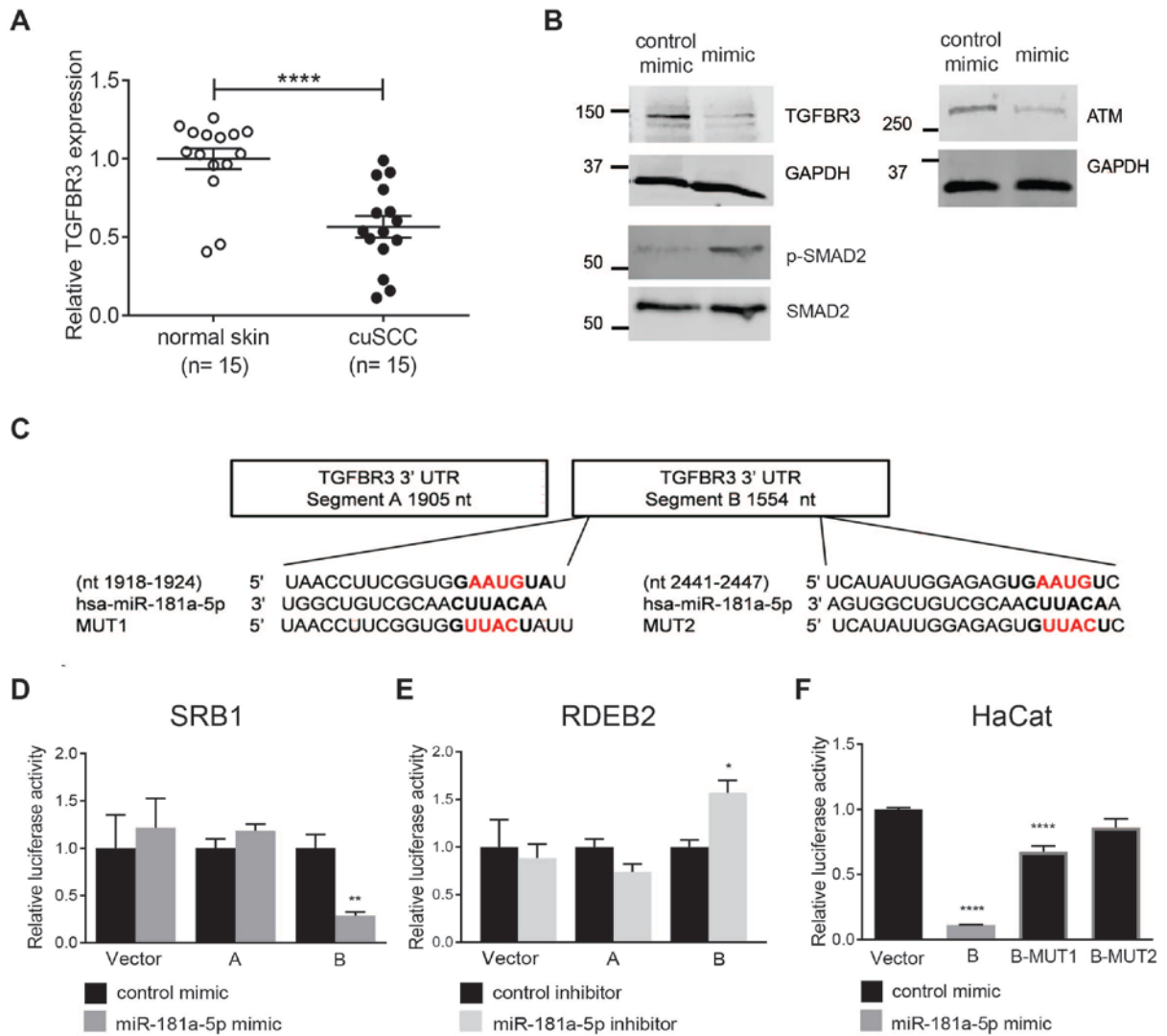
Figure 26

TGFβR3 is downregulated in cuSCC and is a direct target of miR-181a. **A,** Data obtained by RNA-sequencing shows TGFβR3 is downregulated in cuSCC relative to normal skin. Error bars represent the mean (+) S.E.M.; **** $P < 0.05$ (unpaired t-test). **B,** Western blot analysis of NHEK transiently transfected with control-mimic, or miR-181a mimic showed that miR-181a regulates TGFβR3 at the post-transcriptional level. **C,** Diagram of miR-181a predicted seed regions in the WT and MUT 3'UTR of TGFβR3. **D,** Reporter assay in SRB1 with cotransfection of WT reporter plasmid and control-mimic, or miR-181a-5p mimic. **E,** Reporter assay in RDEB2 with cotransfection of WT reporter plasmid and control-inhibitor or miR-181a-5p inhibitor. **F,** Reporter assay in HaCat, with cotransfection of WT-or MUT reporter and control-mimic, or miR-181a-5p mimic. Data represent the S.E.M. from three replicates. *$P < 0.05$; **$P < 0.01$; ****$P < 0.0001$ (unpaired t-test).

TGFβR3 is a direct target of miR-181a

Since the biological significance of miRNA-driven regulation relies on the effect upon their cognate mRNA targets, we then analyzed the predicted targets of miR-181a using Targetscan(178), PicTar(179) and miRanda (180). The predicted target genes of miR-181a included transforming growth factor beta receptor III, TGFβR3 which is highly relevant in skin cancer development (Appendix table 6 shows complete target list). By using RNA-seq data from human cuSCC samples (17), we confirmed that TGFβR3 expression is significantly decreased in cuSCC as compared to normal skin by 1.8 ± 0.2-fold ($P<0.0001$, unpaired t-test) (Fig. 3A). Western blot analysis demonstrated downregulation of TGFβR3 and increased

phosphorylation of downstream TGF-β-pathway target SMAD2 (181) in NHEK cells overexpressing miR-181a, consistent with upregulation of TGF-β signaling (Fig. 3B).

We then sought to address the hypothesis that TGFβR3 is a direct the target of miR-181a in keratinocytes and we asked whether the 3'-UTR of TGFβR3 could confer direct regulation by miR-181a. We used plasmids harboring the 3'-UTR of TGFβR3 upstream of a luciferase reporter gene (Fig. 28C). Because of the size of the 3'-UTR, we split it into two segments labeled "A" and "B". Only segment "B" contained the two predicted miR-181a binding sites. We use SCC cell line that has low miR-181a (SRB1) and high miR-181a (RDEB2) for the reporter assay. In SRB1, the wild-type (WT) reporter plasmids were co-transfected with a miR-181a mimic or, control-mimic. Reporter assays were performed 48hr post-transfection. Compared with the control-mimic, presence of the miR-181a mimic significantly decreased the relative luciferase activity by 3.5 ± 0.4-fold ($P<0.005$, unpaired t-test) when co-transfected with the WT reporter plasmid for segment "B" only (Fig. 28D). On the other hand, when we depleted miR-181a in RDEB2 and perform the same assay as with SRB1, luciferase activity increased by 1.6 ± 0.2-fold ($P<0.05$, unpaired t-test) (Fig. 28E).

To demonstrate the specificity of control conferred by the predicted miR-181 binding sites, we generated the mutant luciferase reporter plasmids for segment "B". The WT or mutant reporter plasmid was transfected into miR-181a constitutively overexpressing HaCat cells. While the WT reporter showed downregulation of luciferase activity these cells, the mutant reporters with site 1 and site 2 individually mutated did not show any significant decrease in luciferase activity

89

(Fig. 28E). These results show that miR-181a suppresses TGF☐R3 by targeting the two predicted sites within the 3'-UTR of TGFβR3.

TGFβR3 depletion phenocopies miR-181a effect in suppressing UV-induced apoptosis

Having demonstrated that TGFβR3 is a direct target of miR-181a, we then wanted to assess the degree to which phenotypes conferred by miR-181a-5p could be accounted for by downregulation of TGFβR3. To this end, we determined the effects of suppressing TGF☐R3 expression using shRNA in NHEK. Following UV-irradiation, we performed apoptosis assay and observed that TGFβR3 depletion suppressed UV-induced apoptosis in both NHEK and HaCaT cells by 63.6% ± 2.1% ($P < 0.005$, unpaired t-test) and 73.9% ± 1.8% ($P < 0.01$, unpaired t-test), respectively. Taken together, our data show that both overexpression of miR-181a and depletion of TGF☐R3 can suppress UV-induced apoptosis in keratinocytes (Fig. 29A and B).

TGFβR3 overexpression negates cell invasion promoted by miR-181a

Next we determined whether TGFβR3 overexpression would negate miR-181a-mediated effects on keratinocyte invasiveness. HaCaT cells were stably transfected with lenti-miR-181a (OE) or lenti-miR-00 (control) and subjected to Boyden chamber assays, using Matrigel-coated membranes. Our results showed that miR-181a overexpression significantly enhanced HaCaT invasion (2.6 ± 0.7 - fold, $P<0.01$, unpaired t-test). We then assessed whether miR-181a-induced enhancement of cell invasiveness could be blunted by TGFβR3 overexpression. In

90

these rescue experiments, we showed that overexpression of the TGFβR3 can essentially rescue the increased invasion nearly completely (1.3 ± 0.4-fold, P = 0.40, unpaired t-test) (Fig. 29 C and D). These data show that for the key phenotypes of miR-181a upregulation, including suppression of apoptosis and increased invasiveness can be attributed in large part to the downregulation of TGFβR3.
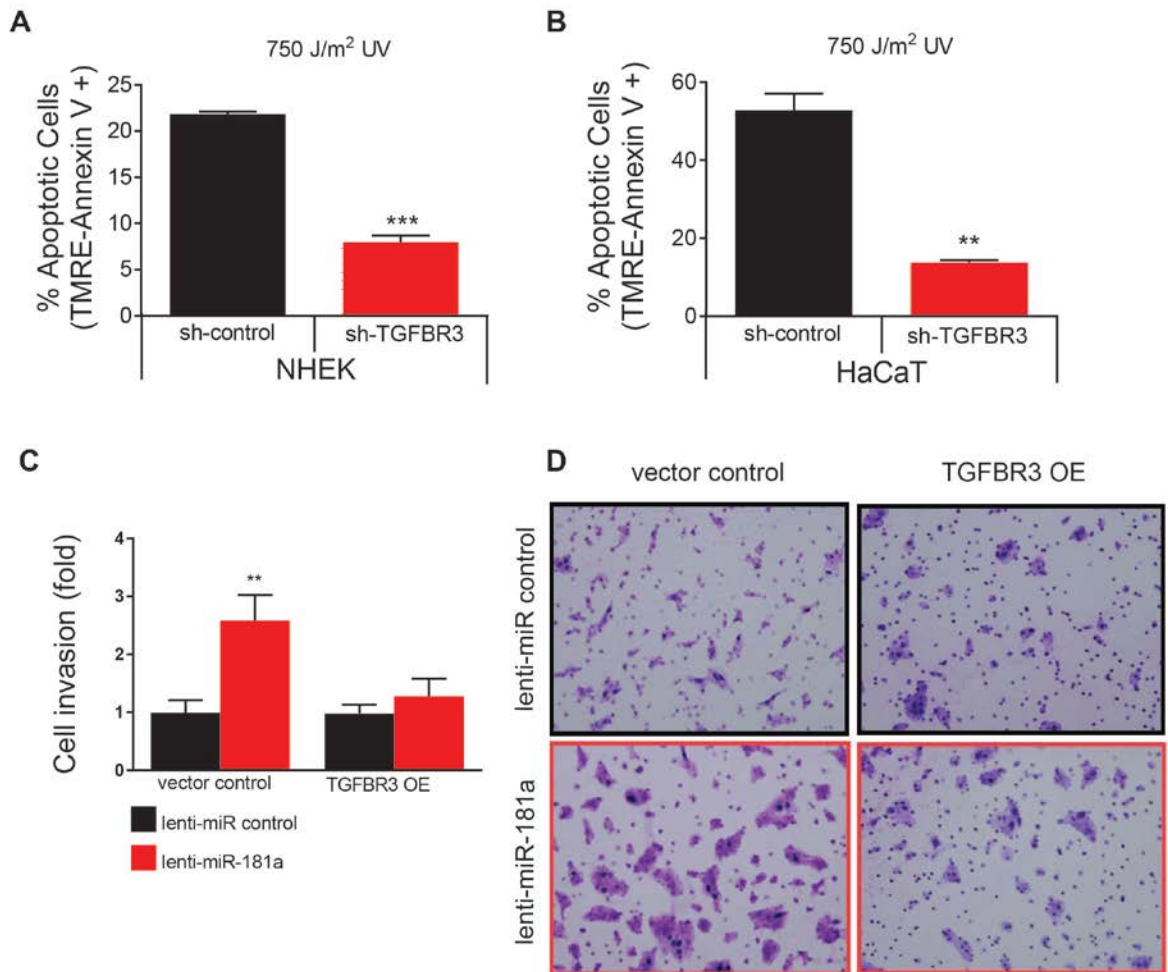
Figure 27

Downregulation of TGFβR3 phenocopies effect of miR-181a upregulation. A-B, Depletion of TGFβR3 phenocopies the suppression of UV-induced apoptosis by miR-181a in keratinocytes. NHEK and HaCat were transfected with sh-control, or sh-TGFβR3 After 24 h, cells were sham irradiated or irradiated with 750 J/m2 of UVB. Apoptotic cells were determined by flow cytometry. Error bars represent the mean (+) S.E.M.; *** $P<0.001$, ** $P<0.01$ (Student's t-test). **C-D,** TGFβR3 overexpression negates miR-181a effects in migration and invasion in keratinocytes. miR-181a stably expressed HaCat (lenti-miR-181a) and non-targeting control stably expressed HaCat (lenti-miR-control) were transfected with TGFβR3 expressed plasmid or vector control. Assays conducted 48 h after transfection. Error bars show SEMs. Asterisks represent a statistically significant difference from the control (**$P< 0.01$; ****$P < 0.0001$).

miR-181a inhibitor suppresses tumor growth in a xenograft SCC mouse model

To assess whether suppressing miR-181a expression would affect tumor growth *in-vivo*, we transiently transfected RDEB2 cells with miR-181a inhibitor or control inhibitor, and then injected them into flanks of NOD CRISPR *Prkdc Il2r gamma* (NCG) mice (Fig. 5A). We found that tumors derived from RDEB2 cells transfected with miR-181a inhibitor grew substantially more slowly, as compared to the negative control (Fig. 30B-D). By day 10, the average volume for tumors derived from cells transfected with miR-181a inhibitor was 2.1 ± 0.5-fold ($P < 0.05$, paired t-test) smaller than those derived from the cells transfected with the control inhibitor (Fig. 30B-D). Accordingly, TGFβR3 levels increased by 1.9 ± 0.5-fold ($P < 0.005$, two-way

ANOVA) in tumors derived from cells transfected with miR-181a inhibitor, as compared to control inhibitor (Fig. 30E). These results show that miR-181a plays an important role in cuSCC progression *in-vivo*.
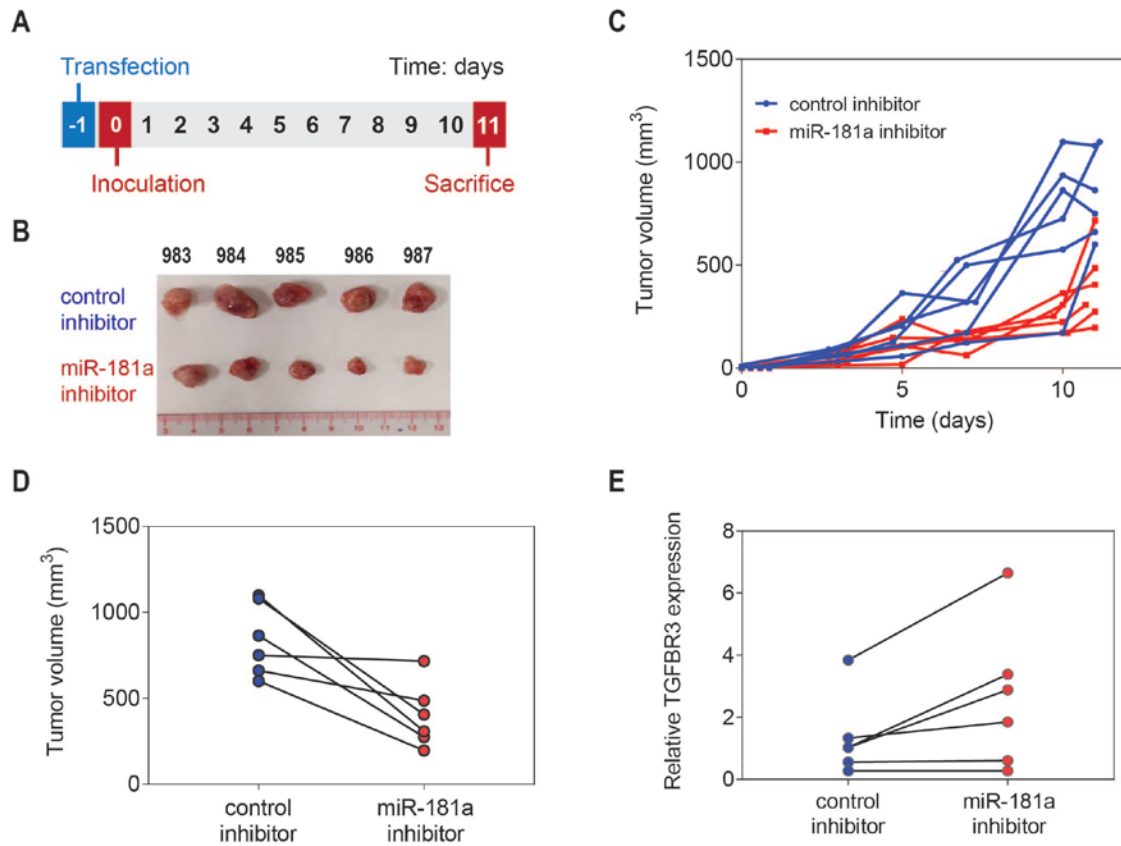
Figure 28

Inhibition of miR-181a function suppresses tumor progression *in-vivo*. A, Timeline of RDEB2 SCC cell line transfection and xenograft inoculation. **B,** Comparison of representative gross tumor xenografts at sacrifice. **C-D,** Xenograft tumor growth was significantly reduced ($P < 0.05$, paired Student's *t*-test, n=6 each) in tumors derived from cells transfected with miR-181a inhibitor than the control inhibitor. **E,** TGFBR3 expression increased significantly ($P <$

0.05, two-way ANOVA) in tumors derived from cells transfected with miR-181a inhibitor, compared to control inhibitor.

5.3 DISCUSSION

miR-181a overexpression has been associated with poor survival in oral and head and neck squamous cell carcinoma, which supports an oncogenic function (182). Individual studies have identified miR-181a to be upregulated in HNSCC, which is closely pathologically and genomically related to cuSCC (183, 184). Moreover, miR-181a serves as a putative biomarker for lymph-node metastasis of oral squamous cell carcinoma (182).

Our data show that miR-181a is significantly overexpressed in a subset of cuSCC, as compared to normal skin. The overexpression of miR-181a significantly suppressed UV-induced apoptosis (Fig. 2A-C), enhanced anchorage independent survival in keratinocytes (Fig. 1D), and significantly increased invasion (Fig. 2). Importantly, we showed that many of these phenotypes are due to the direct regulation of TGFβR3 by miR-181a (Fig. 4), which is conferred by two sites within the 3' UTR (Fig. 3C-F).

TGFβR3 is downregulated in various human cancers, including in HNSCC(185). In early-stage tumors, it has a suppressive role, serving as a homeostatic regulator of the TGF-β pathway. On the other hand, in late-stage tumors it increases TGF-β expression, promoting tumor progression(186). The TGF-SMAD2-Slug axis has been demonstrated in oral SCC, where SMAD2 is phosphorylated during pathway activation leading to increased migration(187). Phosphorylated SMAD2 is also increased in cuSCC arising in higher risk organ transplant recipients(188). Conversely, binding of cuSCC cells to collagen VII decreases features associated with tumor progression, with decreased SMAD2 activity(189). Also consistent with

a tumor-suppressive role, TGF□R3overexpression has been shown to enhance TGF-β signaling through the stimulation of SMAD-dependent signaling, resulting in upregulation of PAI-1 and p21Cip1(190). Nevertheless, there is also data that shows deletion of SMAD2 exacerbates cuSCC development *in-vivo*, reflecting the high complexity and context-dependent functions of this pathway(191).

Our data show that TGFβR3 expression is decreased in cuSCC as compared to normal skin (Fig. 3A) and that TGFβR3 is a direct and functional target of miR-181. Furthermore, we show that TGFβR3, as directly regulated by miR-181a, opposes TGF- β signaling, thus enhancing stress-induced apoptosis and suppressing invasiveness in cuSCC with increased miR-181a expression.

Chapter 6: DISCUSSION AND FUTURE DIRECTION

6.1 DISCUSSION

The research in this dissertation was designed and performed with the goal of using creative strategies to identify biomarkers for cuSCC prevention and treatment, studying how deregulated miRNA-mRNA functions to promote to cuSCC development. The findings in this thesis provide fresh perspective on the extent to how early changes in the expression level of miRNA-mRNA happen in UV-exposed skin and wound healing skin, prior to the development of cuSCC, providing solid experimental-based characterization of deregulated miRNAs mechanism of action in cuSCC development.

In chapter three, we showed that the transcriptomic deregulation observed in cuSCC was induced early in UV-exposed skin and wound healing skin, which are the two main prerequisites of cuSCC development. Importantly, we identified unprecedented evidence showing that the UV-exposed skin and wound healing skin showed significantly correlated. Even though in clinical setting, ultraviolet therapy has been used to disinfect the wound areas promote wound healing (115, 130, 192, 193), no studies have identified molecular correlation between UV-exposed skin and wound healing skin. Furthermore, we showed that UV-exposed skin, wound healing skin and cuSCC tumors have significant commons in their transcriptomes and canonical pathways. Our finding suggested that Oncostatin M signaling, a pathway found to be modified early in UV-exposed skin, wound healing and its deregulation exists in cuSCC tumors. This showed that Oncostatin M can be further evaluated as a novel target in cuSCC treatment.

In chapter four, we used TMT-based proteomics to identify novel targets of miR-21 and miR-31, the two most significantly and commonly regulated in various types of cuSCC tumors through our data. Although miR-21 and miR-31 expressions are often observed to be altered together in many tumors (194-198), our results showed for the first time that miR-21 and miR-31 exert synergistic effects in promoting proliferation and inhibit apoptosis in cuSCC. Our work from this part of the thesis will continue with the validation and characterization of the identified miR-21 and miR-31 targets in cuSCC cell lines and UV-induced hairless cuSCC mouse models.

Chapter five is the continuing work to complete the project initiated by Dr. Vida Chitsazzadeh at The University of Texas MD Anderson Cancer Center. Here, we investigated miR-181a, a microRNA upregulated in cuSCC and induced by UV-irradiation. We showed that miR-181a promotes migration and invasion of cuSCC cell lines through its novel target, TGFbR3. In xenografts mouse model, miR-181a inhibitor significantly reduce tumor size. This study offers evidence showing that miR-181a is important in promoting cuSCC development.

6.2 FUTURE DIRECTION

The discovery of miRNA genes in C. elegans and the subsequent recognition that this family of RNAs extends throughout all multicellular organisms has provided researchers with much more than a new class of regulatory RNAs. The substantial body of research over the last 17 years in the area of miRNA and cancer has constantly increased our knowledge base regarding the key roles of miRNA in tumor development. In this current era of genomics and targeted therapy, perhaps one of the more intriguing questions is how researchers can

incorporate prediction models and existing experimental data to ultimately generate therapeutic

values that miRNA research can provide. The key answer to this question depends on how well

we understand the miRNA network of targets. It has becoming more apparent that miRNAs

systematically regulate large networks of targets instead of predominantly suppress specific

major targets. With current technology, it is possible to record even the modest change in

transcriptome and proteome following miRNA modulation. Once the target gene and protein

networks were identified, it is important to determine whether the relationship among the

components a correlation or causation. This information will help build a reliable network of

miRNA targets, in order to choose most important genes to target. Although already in mature

phase, miRNA research still has many interesting unanswered questions that can be addressed

by future research.

In the near future, the continuing work for projects in chapter 3 includes validating the

functions of OSM in cuSCC development. Here, we plan to deplete OSM and study downstream

pathways and proceses that might be regulated by OSM such as EMT and proliferation. In

chapter 4, we plan to investigate whether MTMR12 as well as other potential targets are directly

targeted by miR-21 and miR-31 in cuSCC cell lines.

Appendix

Appendix 1

Detected miRNA in human skin at 24 hour following UV-exposure (fold change)

miRNA	Fold change at 24h post-SSL
hsa-miR-142-3p	6.29
hsa-miR-31	8.89
hsa-miR-132	2.93
hsa-miR-16	2.32
hsa-miR-93	1.77
hsa-miR-19a	1.8
hsa-miR-484	1.76
hsa-miR-150	2.45
hsa-miR-135b	3.41
hsa-miR-31-3p	2.99
hsa-miR-155	2.32
hsa-miR-886-3p	2.46
hsa-miR-451	18.53
hsa-miR-223	63.33
hsa-miR-652	3.1
hsa-miR-25	2.01
hsa-miR-340	3.55
hsa-miR-223-5p	11.8
hsa-miR-144-5p	19.43
hsa-miR-20b	7.52
hsa-miR-486	20.05
hsa-miR-425-5p	2.79
hsa-miR-15b	4.68
hsa-miR-142-5p	3.84
hsa-miR-539	0.53
hsa-miR-101	0.53
hsa-miR-27a	0.57
hsa-miR-1271	0.43
hsa-miR-455	0.5
hsa-miR-411	0.43

hsa-miR-328	0.54
hsa-miR-409-3p	0.54
hsa-miR-200a	0.53
hsa-miR-23a	0.46
hsa-miR-199a-3p	0.55
hsa-miR-214-5p	0.41
hsa-miR-221	0.57
hsa-miR-210	0.49
hsa-miR-365	0.57
hsa-miR-99a	0.45
hsa-miR-27b	0.53
hsa-miR-149	0.39
hsa-miR-23b	0.53
hsa-miR-152	0.52
hsa-miR-127	0.48
hsa-let-7c	0.56
hsa-miR-100	0.59
hsa-miR-146a	0.58
hsa-miR-214	0.3
hsa-miR-193b	0.55
hsa-miR-196b	0.51
hsa-miR-218	0.41
hsa-miR-139-5p	0.59
hsa-miR-489	0.24
hsa-miR-574-3p	0.44

Appendix 2

Detected miRNA in human skin at 1 hour following UV-exposure (log 2 fold change)

miRNA	log 2 fold change at 1 hour post-SSL
hsa-mir-145-5p	-0.54689
hsa-mir-668-3p	0.594605
hsa-mir-133a-3p	-0.61168
hsa-mir-23a-5p	-0.54239
hsa-mir-143-5p	-0.57547

Appendix 3

Detected miRNA in three subtypes of cuSCC (log 2 fold change)

miRNA	Xeroderma Pigmentosum cuSCC	Immunosuppressed cuSCC	UV-driven cuSCC
hsa-mir-6510-3p	-0.12	-1.82	3.2
hsa-mir-4532	1.29	-1	2.55
hsa-mir-6089	0.34	-0.8	2.48
hsa-mir-486-5p	-1.27	-3.76	2.35
hsa-mir-3621	0.48	-0.69	2.26
hsa-mir-204-5p	-3.08	-3.28	2.26
hsa-mir-184	0.17	-0.1	2.19
hsa-mir-218-1-3p	-0.15	-1.15	2.15
hsa-mir-6511a-3p	0.25	-1.34	2.1
hsa-mir-3656	1.32	-1.45	2.08
hsa-mir-3178	1.07	-0.83	2.06
hsa-mir-3195	1.69	-0.61	1.98
hsa-mir-214-3p	-1.19	-0.97	1.95
hsa-mir-3663-3p	0.28	-0.55	1.93
hsa-mir-145-5p	-2	-0.3	1.79
hsa-mir-211-5p	-4.91	-2.42	1.77
hsa-mir-1247-5p	-1.68	-1.86	1.75
hsa-mir-375	-0.22	-1.57	1.72
hsa-mir-149-5p	-0.48	-0.73	1.6
hsa-mir-718	0.23	-0.71	1.54
hsa-mir-574-3p	-1.39	-0.28	1.53
hsa-mir-3665	0.86	-1.09	1.53
hsa-mir-3196	1.05	-0.28	1.52
hsa-mir-125b-5p	-1.75	-1.32	1.5
hsa-mir-378a-5p	0.78	-0.84	1.5
hsa-mir-6087	1.63	-0.59	1.47
hsa-mir-6511b-3p	-0.1	-0.42	1.47
hsa-mir-652-3p	2.38	-2.12	1.46
hsa-mir-139-5p	-1.21	-1.48	1.46
hsa-mir-4655-3p	1.12	0.29	1.45
hsa-mir-100-5p	-1.16	-1.42	1.43
hsa-mir-762	0.28	-0.45	1.39
hsa-mir-1538	0.47	-0.5	1.37

hsa-mir-486-3p	-0.21	-2.77	1.34
hsa-mir-197-3p	-0.1	-0.35	1.33
hsa-mir-4508	1.83	-1.06	1.27
hsa-mir-193a-5p	0.35	-1.32	1.26
hsa-mir-5787	0.72	-0.28	1.25
hsa-mir-296-5p	1	-0.22	1.22
hsa-mir-664b-3p	0.01	-0.86	1.22
hsa-mir-4497	1.32	-0.34	1.21
hsa-mir-125a-5p	-1.24	-0.61	1.16
hsa-mir-4634	-0.9	-0.09	1.16
hsa-mir-4739	1.52	-0.43	1.11
hsa-mir-2110	0.43	-0.86	1.1
hsa-mir-664a-3p	-0.48	-0.89	1.1
hsa-mir-338-5p	-0.41	-1.39	1.09
hsa-mir-451a	0.53	-2.97	1.07
hsa-mir-509-3p	-0.78	-1.94	1.04
hsa-mir-497-5p	-0.5	-0.24	1.02
hsa-mir-1247-3p	0.02	-1.62	1.01
hsa-let-7d-3p	1.61	-0.53	0.99
hsa-mir-3605-3p	0.81	-0.78	0.97
hsa-mir-30a-3p	0.44	-1.09	0.97
hsa-mir-4707-5p	1.13	-0.5	0.93
hsa-mir-532-3p	1.07	-0.59	0.93
hsa-mir-485-5p	0	-0.74	0.93
hsa-mir-99a-3p	0	-0.66	0.93
hsa-mir-508-3p	-1.06	-1.53	0.92
hsa-mir-574-5p	2.17	0.01	0.89
hsa-mir-766-3p	0.75	-0.04	0.89
hsa-mir-320b	-0.48	-0.7	0.87
hsa-mir-99a-5p	-1.97	-1.1	0.86
hsa-mir-320a	-0.38	-0.68	0.86
hsa-mir-125b-1-3p	0.84	-0.88	0.84
hsa-mir-4516	3.27	-0.05	0.82
hsa-mir-195-5p	-2.57	-0.59	0.81
hsa-mir-146b-3p	0.88	-1.02	0.8
hsa-mir-664a-5p	-0.64	-0.87	0.78
hsa-mir-3609	0.07	0.2	0.78
hsa-let-7e-3p	0.88	0.09	0.77
hsa-mir-365a-5p	0.72	0.25	0.73

hsa-mir-30c-2-3p	0.33	-1.1	0.7
hsa-mir-193b-3p	0.52	0.58	0.69
hsa-mir-144-3p	3.54	-2.09	0.67
hsa-mir-1275	1.72	-0.27	0.67
hsa-mir-1915-3p	1.77	0.05	0.66
hsa-mir-214-5p	1.67	-0.03	0.66
hsa-mir-4492	2.91	-0.95	0.63
hsa-mir-432-5p	0.06	-0.81	0.63
hsa-mir-514a-3p	0.26	-1.16	0.6
hsa-mir-199a-5p	-0.01	-0.36	0.53
hsa-mir-140-3p	-0.53	-0.84	0.49
hsa-mir-378a-3p	-0.5	-0.72	0.49
hsa-mir-30d-5p	-0.9	-0.77	0.49
hsa-mir-365a-3p	1.7	-0.12	0.47
hsa-mir-365b-3p	1.7	-0.12	0.47
hsa-mir-99b-5p	-0.46	-0.15	0.47
hsa-mir-330-3p	0.89	-0.63	0.46
hsa-mir-6126	2.24	-0.03	0.35
hsa-mir-324-3p	2.12	0.25	0.31
hsa-mir-127-3p	-1.43	-0.46	0.3
hsa-mir-566	1.46	-0.03	0.28
hsa-mir-30a-5p	-1.49	-1.05	0.27
hsa-mir-331-3p	1.92	0.47	0.25
hsa-mir-129-2-3p	-0.87	0	0.24
hsa-mir-3158-3p	1.76	-0.77	0.21
hsa-mir-26a-5p	-1.35	-0.44	0.21
hsa-mir-4488	3.98	0.25	0.2
hsa-mir-3651	0.53	1.06	0.2
hsa-mir-191-5p	-0.62	-0.56	0.2
hsa-mir-324-5p	2.58	-0.21	0.16
hsa-mir-335-5p	0.72	-0.83	0.15
hsa-mir-125a-3p	1.48	0.01	0.14
hsa-mir-150-5p	-1.95	-1.08	0.13
hsa-mir-767-3p	1.14	1.55	0.11
hsa-mir-320c	0.91	0.1	0.1
hsa-mir-20b-5p	0.18	-2.12	0.1
hsa-mir-185-3p	1.26	0.01	0.09
hsa-mir-26b-3p	1.82	-0.11	0.09
hsa-mir-24-1-5p	1.58	0.83	0.08

hsa-mir-15b-5p	1.5	-0.08	0.06
hsa-mir-941	2.07	-0.36	0.05
hsa-mir-30c-5p	-0.62	-0.37	0.03
hsa-mir-150-3p	-0.26	-0.62	0.03
hsa-mir-93-3p	1.73	0.61	0
hsa-mir-3200-3p	0.23	-0.65	0
hsa-mir-339-5p	2.37	0.64	0.02
hsa-mir-10b-5p	-1.7	-0.59	0.06
hsa-mir-505-3p	2.17	0.01	0.08
hsa-mir-106a-5p	0.43	-1.18	0.08
hsa-mir-30b-5p	-0.18	-0.44	0.09
hsa-mir-129-5p	-0.28	0.03	0.1
hsa-mir-425-3p	1.58	-0.26	0.11
hsa-mir-363-3p	1.15	-2.12	0.11
hsa-mir-4326	1.16	0.27	0.15
hsa-mir-106b-3p	1.21	-0.26	0.16
hsa-let-7d-5p	0.42	-0.36	0.16
hsa-mir-99b-3p	1.86	0.35	0.18
hsa-mir-146a-5p	-0.58	-0.96	0.19
hsa-let-7g-3p	1.34	0.54	0.2
hsa-mir-33a-3p	1.76	0.99	0.2
hsa-mir-484	0.99	-0.23	0.21
hsa-mir-4746-5p	1.05	0.48	0.22
hsa-mir-409-3p	-1.1	-0.23	0.22
hsa-mir-550a-3p	1.81	-0.1	0.25
hsa-mir-3129-3p	0.56	1.05	0.26
hsa-mir-744-3p	0.73	0.91	0.26
hsa-mir-221-5p	2.06	0.28	0.26
hsa-let-7g-5p	0.89	-0.38	0.27
hsa-mir-641	1.19	0.28	0.27
hsa-mir-221-3p	1	0.46	0.28
hsa-mir-455-3p	1.77	0.43	0.29
hsa-mir-345-5p	1.85	-0.15	0.31
hsa-mir-576-5p	2.02	0.33	0.33
hsa-mir-185-5p	1.97	-1.04	0.34
hsa-mir-769-5p	-0.39	-0.41	0.36
hsa-mir-3117-3p	0.9	0.99	0.37
hsa-mir-6499-5p	0.94	0.74	0.37
hsa-mir-148b-3p	2.26	0.26	0.38

hsa-mir-369-3p	1.87	0.91	0.4
hsa-mir-200b-3p	0.56	0.62	0.41
hsa-mir-654-5p	-0.73	-0.14	0.42
hsa-mir-425-5p	0.33	-0.72	0.42
hsa-mir-2277-5p	1.01	0.38	0.43
hsa-mir-4478	4.13	0.19	0.44
hsa-mir-4784	1.49	1.1	0.44
hsa-mir-126-3p	-1.51	-0.29	0.44
hsa-mir-23a-3p	-0.22	0.59	0.45
hsa-mir-532-5p	1.46	-0.06	0.47
hsa-mir-4446-3p	0.24	0.01	0.49
hsa-mir-1185-1-3p	0.7	0.12	0.51
hsa-mir-132-3p	1.47	-0.22	0.51
hsa-mir-548av-3p	1.73	0.35	0.51
hsa-mir-98-5p	1.77	0.03	0.51
hsa-mir-708-5p	1.67	0.65	0.51
hsa-mir-24-3p	0.04	0.31	0.52
hsa-mir-548o-3p	1.74	0.38	0.52
hsa-mir-142-3p	1.79	0.12	0.52
hsa-mir-6724-5p	3.16	0.41	0.54
hsa-mir-1307-3p	2.73	0.18	0.55
hsa-mir-5701	3.24	0.56	0.55
hsa-mir-1293	0.66	0.4	0.56
hsa-mir-708-3p	3.6	0.63	0.58
hsa-let-7f-5p	0.68	0.02	0.59
hsa-mir-182-5p	0.63	-0.18	0.59
hsa-mir-25-3p	0.63	-0.06	0.6
hsa-mir-4443	2.91	0.29	0.61
hsa-mir-103a-3p	0.09	-0.11	0.61
hsa-mir-27b-3p	0.78	0.46	0.61
hsa-mir-614	4.07	1.42	0.62
hsa-mir-490-3p	2.3	1.82	0.63
hsa-mir-454-3p	2.04	0.26	0.64
hsa-mir-27a-5p	2.56	0.35	0.65
hsa-mir-107	0.73	-0.62	0.65
hsa-mir-28-5p	-0.1	0.08	0.66
hsa-mir-7-1-3p	1.73	0.67	0.67
hsa-mir-205-3p	2.12	1.53	0.68
hsa-mir-20a-5p	0.94	0.23	0.68

hsa-mir-1268a	1.99	0.77	0.7
hsa-mir-212-3p	2.68	0.08	0.71
hsa-mir-93-5p	0.54	-0.3	0.72
hsa-mir-330-5p	2.66	0.84	0.74
hsa-mir-181c-5p	0.75	0.06	0.74
hsa-mir-2355-5p	2.72	1.39	0.75
hsa-mir-4730	3.36	0.66	0.76
hsa-mir-181b-5p	0.61	0.5	0.76
hsa-mir-151a-3p	0.17	0.24	0.77
hsa-mir-3180	0.19	0.84	0.77
hsa-mir-3180-3p	0.19	0.84	0.77
hsa-mir-1307-5p	4.07	1.8	0.78
hsa-mir-200c-5p	1.4	1.25	0.8
hsa-mir-340-3p	2.01	0.25	0.8
hsa-mir-660-5p	1.07	0.18	0.82
hsa-mir-450b-5p	3.46	2.03	0.83
hsa-mir-25-5p	0.81	0.73	0.84
hsa-mir-665	1.06	1.01	0.85
hsa-mir-17-5p	0.71	0.17	0.86
hsa-mir-16-5p	-0.27	-0.5	0.86
hsa-let-7i-5p	1.04	0.4	0.87
hsa-mir-1246	1.4	1.46	0.87
hsa-mir-7-5p	1.79	1.98	0.88
hsa-mir-582-5p	2.99	0.61	0.88
hsa-mir-222-5p	1.01	-0.25	0.88
hsa-mir-146b-5p	-0.26	-0.53	0.89
hsa-mir-132-5p	1.76	0.02	0.9
hsa-mir-18a-5p	2.95	0.96	0.91
hsa-mir-148b-5p	2.75	0.78	0.91
hsa-mir-615-3p	2.48	1.38	0.92
hsa-mir-493-5p	1.21	0.7	0.92
hsa-mir-130b-5p	2.5	0.68	0.93
hsa-mir-17-3p	2.61	0.05	0.93
hsa-mir-493-3p	0.21	0.67	0.93
hsa-mir-3182	1.17	1.35	0.95
hsa-mir-454-5p	1.78	0.69	0.95
hsa-mir-181c-3p	2.02	0.58	0.96
hsa-mir-224-5p	0.5	0.94	0.96
hsa-mir-1303	1.58	0.67	0.96

hsa-mir-22-3p	0.38	0.45	0.98
hsa-mir-4448	1.08	1.47	1.03
hsa-mir-629-5p	1.5	-0.03	1.04
hsa-mir-106b-5p	1.67	0.26	1.05
hsa-mir-223-3p	1.17	-0.88	1.06
hsa-mir-196b-5p	0.78	1.29	1.06
hsa-mir-200a-5p	3.22	1.38	1.07
hsa-mir-331-5p	2.18	0.7	1.08
hsa-mir-1285-3p	3.4	1.13	1.09
hsa-mir-34c-5p	1.42	1.17	1.1
hsa-mir-944	3.78	1.63	1.14
hsa-mir-27a-3p	0.77	1.4	1.16
hsa-mir-193a-3p	2.78	0.92	1.17
hsa-mir-187-3p	0.78	0.81	1.17
hsa-mir-323b-3p	0.35	0.26	1.22
hsa-mir-431-5p	1.41	0.65	1.22
hsa-mir-15b-3p	2.09	1.46	1.23
hsa-mir-192-5p	-0.05	0.02	1.27
hsa-mir-141-5p	2.09	1.61	1.29
hsa-mir-27b-5p	0.26	0.57	1.29
hsa-mir-15a-5p	1.87	-0.46	1.31
hsa-let-7a-3p	3.84	1.45	1.34
hsa-mir-455-5p	1.92	1.18	1.37
hsa-mir-16-2-3p	2.85	-0.3	1.38
hsa-mir-135b-5p	3.14	3.41	1.41
hsa-mir-421	2.27	0.3	1.42
hsa-mir-452-5p	2.22	0.78	1.42
hsa-mir-450a-5p	2.75	1.71	1.44
hsa-mir-155-5p	0.88	0.36	1.46
hsa-mir-24-2-5p	2.63	0.84	1.52
hsa-mir-1269a	1.56	2.96	1.62
hsa-mir-130b-3p	1.58	0.59	1.63
hsa-mir-181a-3p	1.64	0.72	1.64
hsa-mir-196a-5p	0.43	1.55	1.65
hsa-mir-340-5p	2.26	0.37	1.68
hsa-mir-22-5p	2.72	1.35	1.73
hsa-mir-142-5p	-0.03	-0.56	1.77
hsa-mir-424-5p	3.36	1.95	1.82
hsa-mir-424-3p	2.4	1.37	1.88

	2.08	2.1	2.61
hsa-mir-21-5p			
hsa-mir-31-3p	4.16	3.96	2.73
hsa-mir-21-3p	5.2	2.56	3.01
hsa-mir-31-5p	2.64	3.47	3.28

Appendix 4

Potential miR-21 targets expression in SCCT8 treated with miR-21 inhibitor and mimic (log 2 fold change)

Proteins	miR-21 inhibitor	miR-21 mimic
ABI2	0.345161903	-0.265190391
ANP32E	0.553348599	-0.100458185
ANXA1	0.272606179	-0.432385806
AP1S2	0.336497486	-0.295161943
BID	0.55506518	-0.251256637
CAMSAP1	0.227075164	-0.203996023
CDS1	0.258788099	-0.162024316
CEP44	0.1440208	-0.247960871
CHM	0.555661009	-0.252766245
DAZAP2	0.356531027	-0.49251089
DCTN3	0.325878418	-0.114100454
FBXL2	0.25015208	-0.186006504
FGFR1OP2	0.153577475	-0.114399888
GINS1	0.186697023	-0.229961254
GNPDA2	0.612320893	-0.165388235
GSS	0.220859049	-0.124222386
GTPBP1	0.25680205	-0.292331839
GYG1	0.48055174	-0.147299543
IPO11	0.56435111	-0.314422377
MAPKAP1	0.122066129	-0.114405747
MTMR12	1.091099353	-1.112174201
MYEF2	0.29148543	-0.35450327
MYO1E	0.230829671	-0.112699661
NRIP1	0.1018217	-0.136875696
NSUN2	0.334317205	-0.135366843
PAN3	0.542806496	-0.118429218

POLD3	0.354945229	-0.271091152
PPP1R15B	0.457459773	-0.572173417
PPP1R9A	0.247218979	-0.479860937
PTPRE	0.362242838	-0.107814551
RAP2A	0.250560209	-0.214061809
SC5D	0.339750765	-0.10653511
SNIP1	0.145610548	-0.101109749
SUB1	0.171701999	-0.183746082
TIMP2	0.411778561	-0.295892187
TMEM192	0.270363104	-0.127320992
TMEM206	0.662488242	-0.183709032
TMEM63A	0.12315484	-0.126504127
TP53BP2	0.352457927	-0.131351061
TRAPPC8	0.700310521	-1.18224429
WDR7	0.155220126	-0.149321955

Appendix 5

Potential miR-21 tar3gets expression in SCCT8 treated with miR-31 inhibitor and mimic (log 2

fold change)

Protein	miR-31 inhibitor	miR-31 mimic
ABI2	0.271379139	-0.184046531
AHNAK2	0.167461929	-0.325298252
BAIAP2	0.110979987	-0.196978204
CNTN5	0.139161691	-0.219358741
CPNE8	0.110637696	-0.334887547
DENND1A	0.322071289	-0.192198154
EXOC7	0.104500081	-0.190625069
EXOC8	0.100481103	-0.11109884
FAM204A	0.156586526	-0.43724134
FAM210B	0.105067802	-0.138816402
FAM219A	0.278536732	-0.290551671

FOSL2	0.129112392	-0.117357719
GSE1	0.507165474	-0.656015902
HECTD3	0.189476314	-0.449661897
IER3IP1	0.11347451	-0.305169834
JDP2	1.032866941	-0.869091184
LPP	0.269905846	-0.121342165
LUC7L	0.114884396	-0.103246439
MANEAL	0.286967471	-0.192899519
MTM1	0.130448108	-0.163511833
NELFB	0.105361157	-0.155317708
PGM2L1	0.565088447	-0.167089403
PLEKHA1	0.24193254	-0.187203634
RAB38	0.233814069	-0.222847641
SEZ6L2	0.155522765	-0.226193472
SH3BGRL	0.125236086	-0.187369158
SHB	0.21462463	-0.1498071
SLC7A2	0.12151903	-0.333630398
SMAD3	0.152220698	-0.697041946
SNRNP27	0.39888721	-0.172124386
SPAST	0.122677515	-0.127890117
SSH1	0.984903464	-0.116403429
SUCO	0.180281183	-0.199824379
TOR2A	0.261281157	-0.123233029
UBE2B	0.145870993	-0.169010865
ZBTB10	0.172208086	-1.255087134
ZNF354C	0.17538168	-0.295982853

Appendix 6

Potential targets of miR-181a

	miR-181a predicted target genes
1	AFTPH
2	ANKRD13C
3	ARF6
4	ATP8A1
5	BAPX1
6	BCL2

7	BTBD3
8	CCDC6
9	CCNG1
10	CDX2
11	DDIT4
12	FAM160A2
13	FBX011
14	FBX028
15	FBX033
16	GATA6
17	GIGYF1
18	GPR1237B
19	KRAS
20	KIAA
21	KLADCS
22	LBR
23	LCLAT1
24	METAP1
25	MTMR12
26	NFYB
27	NLK
28	NOCH2
29	NOL4
30	NR6A1
31	NRP1
32	NUPL1
33	PDX3X
34	PITPNB
35	PLAG1
36	PLCL2
37	PLXDC2
38	PROX1
39	PUM1
40	RLF
41	RNF34
42	SCD
43	SFRS7
44	SLC37A3
45	SLC7A11

46	STCH
47	TGFBR3
48	TIAL1
49	TM9SF3
50	TMED4
51	TMEM64
52	YOD1
53	ZNF148
54	ZNF445

Reference

1. Rogers, H. W., M. A. Weinstock, S. R. Feldman, and B. M. Coldiron. 2015. Incidence Estimate of Nonmelanoma Skin Cancer (Keratinocyte Carcinomas) in the U.S. Population, 2012. *JAMA dermatology* 151: 1081-1086.
2. Lomas, A., J. Leonardi-Bee, and F. Bath-Hextall. 2012. A systematic review of worldwide incidence of nonmelanoma skin cancer. *The British journal of dermatology* 166: 1069-1080.
3. Karia, P. S., J. Han, and C. D. Schmults. 2013. Cutaneous squamous cell carcinoma: estimated incidence of disease, nodal metastasis, and deaths from disease in the United States, 2012. *Journal of the American Academy of Dermatology* 68: 957-966.
4. Stratigos, A., C. Garbe, C. Lebbe, J. Malvehy, V. del Marmol, H. Pehamberger, K. Peris, J. C. Becker, I. Zalaudek, P. Saiag, M. R. Middleton, L. Bastholt, A. Testori, and J. J. Grob. 2015. Diagnosis and treatment of invasive squamous cell carcinoma of the skin: European consensus-based interdisciplinary guideline. *European journal of cancer (Oxford, England : 1990)* 51: 1989-2007.
5. Glogau, R. G. 2000. The risk of progression to invasive disease. *Journal of the American Academy of Dermatology* 42: 23-24.
6. Jambusaria-Pahlajani, A., S. D. Hess, K. A. Katz, D. Berg, and C. D. Schmults. 2010. Uncertainty in the perioperative management of high-risk cutaneous squamous cell carcinoma among Mohs surgeons. *Archives of dermatology* 146: 1225-1231.
7. Schmults, C. D. 2005. High-risk cutaneous squamous cell carcinoma: identification and management. *Advances in dermatology* 21: 133-152.
8. Que, S. K. T., F. O. Zwald, and C. D. Schmults. 2018. Cutaneous squamous cell carcinoma: Incidence, risk factors, diagnosis, and staging. *Journal of the American Academy of Dermatology* 78: 237-247.

9.   Rowe, D. E., R. J. Carroll, and C. L. Day, Jr. 1992. Prognostic factors for local recurrence, metastasis, and survival rates in squamous cell carcinoma of the skin, ear, and lip. Implications for treatment modality selection. *Journal of the American Academy of Dermatology* 26: 976-990.

10.   Jensen, P., S. Hansen, B. Moller, T. Leivestad, P. Pfeffer, O. Geiran, P. Fauchald, and S. Simonsen. 1999. Skin cancer in kidney and heart transplant recipients and different long-term immunosuppressive therapy regimens. *Journal of the American Academy of Dermatology* 40: 177-186.

11.   Adamson, R., E. Obispo, S. Dychter, W. Dembitsky, R. Moreno-Cabral, B. Jaski, J. Gordon, P. Hoagland, K. Moore, J. King, J. Andrews, M. Rich, and P. O. Daily. 1998. High incidence and clinical course of aggressive skin cancer in heart transplant patients: a single-center study. *Transplantation proceedings* 30: 1124-1126.

12.   Smith, K. J., S. Hamza, and H. Skelton. 2004. Histologic features in primary cutaneous squamous cell carcinomas in immunocompromised patients focusing on organ transplant patients. *Dermatologic surgery : official publication for American Society for Dermatologic Surgery [et al.]* 30: 634-641.

13.   Martorell-Calatayud, A., O. Sanmartin Jimenez, J. Cruz Mojarrieta, and C. Guillen Barona. 2013. Cutaneous squamous cell carcinoma: defining the high-risk variant. *Actas dermo-sifiliograficas* 104: 367-379.

14.   Martinez, J. C., C. C. Otley, T. Stasko, S. Euvrard, C. Brown, C. F. Schanbacher, and A. L. Weaver. 2003. Defining the clinical course of metastatic skin cancer in organ transplant recipients: a multicenter collaborative study. *Archives of dermatology* 139: 301-306.

15.   Mullen, J. T., L. Feng, Y. Xing, P. F. Mansfield, J. E. Gershenwald, J. E. Lee, M. I. Ross, and J. N. Cormier. 2006. Invasive squamous cell carcinoma of the skin: defining a high-risk group. *Annals of surgical oncology* 13: 902-909.

16.   Lyakhovitsky, A., A. Barzilai, M. Fogel, H. Trau, and M. Huszar. 2004. Expression of e-cadherin and beta-catenin in cutaneous squamous cell carcinoma and its precursors. *The American Journal of dermatopathology* 26: 372-378.

17.   Chitsazzadeh, V., C. Coarfa, J. A. Drummond, T. Nguyen, A. Joseph, S. Chilukuri, E. Charpiot, C. H. Adelmann, G. Ching, T. N. Nguyen, C. Nicholas, V. D. Thomas, M. Migden, D. MacFarlane, E. Thompson, J. Shen, Y. Takata, K. McNiece, M. A. Polansky, H. A. Abbas, K. Rajapakshe, A. Gower, A. Spira, K. R. Covington, W. Xiao, P. Gunaratne, C. Pickering, M. Frederick, J. N. Myers, L. Shen, H. Yao, X. Su, R. P. Rapini, D. A. Wheeler, E. T. Hawk, E. R. Flores, and K. Y. Tsai. 2016. Cross-species identification of genomic drivers of squamous cell carcinoma development across preneoplastic intermediates. *Nature communications* 7: 12601.

18.   Pickering, C. R., J. H. Zhou, J. J. Lee, J. A. Drummond, S. A. Peng, R. E. Saade, K. Y. Tsai, J. L. Curry, M. T. Tetzlaff, S. Y. Lai, J. Yu, D. M. Muzny, H. Doddapaneni, E. Shinbrot, K. R. Covington, J. Zhang, S. Seth, C. Caulin, G. L. Clayman, A. K. El-Naggar, R. A. Gibbs, R. S. Weber, J. N. Myers, D. A. Wheeler, and M. J. Frederick. 2014. Mutational landscape of aggressive cutaneous squamous cell carcinoma. *Clinical cancer research : an official journal of the American Association for Cancer Research* 20: 6582-6592.

19.   Chen, H., Q. Y. Weng, and D. E. Fisher. 2014. UV signaling pathways within the skin. *The Journal of investigative dermatology* 134: 2080-2085.

20. Ashton, K. J., S. R. Weinstein, D. J. Maguire, and L. R. Griffiths. 2003. Chromosomal aberrations in squamous cell carcinoma and solar keratoses revealed by comparative genomic hybridization. *Archives of dermatology* 139: 876-882.

21. Purdie, K. J., S. R. Lambert, M. T. Teh, T. Chaplin, G. Molloy, M. Raghavan, D. P. Kelsell, I. M. Leigh, C. A. Harwood, C. M. Proby, and B. D. Young. 2007. Allelic imbalances and microdeletions affecting the PTPRD gene in cutaneous squamous cell carcinomas detected using single nucleotide polymorphism microarray analysis. *Genes, chromosomes & cancer* 46: 661-669.

22. Rehman, I., M. Takata, Y. Y. Wu, and J. L. Rees. 1996. Genetic change in actinic keratoses. *Oncogene* 12: 2483-2490.

23. Hameetman, L., S. Commandeur, J. N. Bavinck, H. C. Wisgerhof, F. R. de Gruijl, R. Willemze, L. Mullenders, C. P. Tensen, and H. Vrieling. 2013. Molecular profiling of cutaneous squamous cell carcinomas and actinic keratoses from organ transplant recipients. *BMC cancer* 13: 58.

24. Padilla, R. S., S. Sebastian, Z. Jiang, I. Nindl, and R. Larson. 2010. Gene expression patterns of normal human skin, actinic keratosis, and squamous cell carcinoma: a spectrum of disease progression. *Archives of dermatology* 146: 288-293.

25. Van Haren, R., D. Feldman, and A. A. Sinha. 2009. Systematic comparison of nonmelanoma skin cancer microarray datasets reveals lack of consensus genes. *The British journal of dermatology* 161: 1278-1287.

26. Hudson, L. G., J. M. Gale, R. S. Padilla, G. Pickett, B. E. Alexander, J. Wang, and D. F. Kusewitt. 2010. Microarray analysis of cutaneous squamous cell carcinomas reveals enhanced expression of epidermal differentiation complex genes. *Molecular carcinogenesis* 49: 619-629.

27. Abel, E. L., J. M. Angel, K. Kiguchi, and J. DiGiovanni. 2009. Multi-stage chemical carcinogenesis in mouse skin: fundamentals and applications. *Nature protocols* 4: 1350-1362.

28. Brown, K., A. Buchmann, and A. Balmain. 1990. Carcinogen-induced mutations in the mouse c-Ha-ras gene provide evidence of multiple pathways for tumor progression. *Proceedings of the National Academy of Sciences of the United States of America* 87: 538-542.

29. Spalding, J. W., J. Momma, M. R. Elwell, and R. W. Tennant. 1993. Chemically induced skin carcinogenesis in a transgenic mouse line (TG.AC) carrying a v-Ha-ras gene. *Carcinogenesis* 14: 1335-1341.

30. Ruggeri, B., J. Caamano, T. Goodrow, M. DiRado, A. Bianchi, D. Trono, C. J. Conti, and A. J. Klein-Szanto. 1991. Alterations of the p53 tumor suppressor gene during mouse skin tumor progression. *Cancer research* 51: 6615-6621.

31. Aldaz, C. M., D. Trono, F. Larcher, T. J. Slaga, and C. J. Conti. 1989. Sequential trisomization of chromosomes 6 and 7 in mouse skin premalignant lesions. *Molecular carcinogenesis* 2: 22-26.

32. Panteleyev, A. A., C. van der Veen, T. Rosenbach, S. Muller-Rover, V. E. Sokolov, and R. Paus. 1998. Towards defining the pathogenesis of the hairless phenotype. *The Journal of investigative dermatology* 110: 902-907.

33. Potter, G. B., G. M. Beaudoin, 3rd, C. L. DeRenzo, J. M. Zarach, S. H. Chen, and C. C. Thompson. 2001. The hairless gene mutated in congenital hair loss disorders encodes a novel nuclear receptor corepressor. *Genes & development* 15: 2687-2701.

34. de Gruijl, F. R., and P. D. Forbes. 1995. UV-induced skin cancer in a hairless mouse model. *BioEssays : news and reviews in molecular, cellular and developmental biology* 17: 651-660.

35. Ohtsuka, M., H. Ling, Y. Doki, M. Mori, and G. A. Calin. 2015. MicroRNA Processing and Human Cancer. *Journal of clinical medicine* 4: 1651-1667.

36. Ha, M., and V. N. Kim. 2014. Regulation of microRNA biogenesis. *Nature reviews. Molecular cell biology* 15: 509-524.

37. Yi, R., M. N. Poy, M. Stoffel, and E. Fuchs. 2008. A skin microRNA promotes differentiation by repressing 'stemness'. *Nature* 452: 225-229.

38. Wang, D., Z. Zhang, E. O'Loughlin, L. Wang, X. Fan, E. C. Lai, and R. Yi. 2013. MicroRNA-205 controls neonatal expansion of skin stem cells by modulating the PI(3)K pathway. *Nature cell biology* 15: 1153-1163.

39. Zhang, L., N. Stokes, L. Polak, and E. Fuchs. 2011. Specific microRNAs are preferentially expressed by skin stem cells to balance self-renewal and early lineage commitment. *Cell stem cell* 8: 294-308.

40. Lena, A. M., R. Shalom-Feuerstein, P. Rivetti di Val Cervo, D. Aberdam, R. A. Knight, G. Melino, and E. Candi. 2008. miR-203 represses 'stemness' by repressing DeltaNp63. *Cell death and differentiation* 15: 1187-1195.

41. Mardaryev, A. N., M. I. Ahmed, N. V. Vlahov, M. Y. Fessing, J. H. Gill, A. A. Sharov, and N. V. Botchkareva. 2010. Micro-RNA-31 controls hair cycle-associated changes in gene expression programs of the skin and hair follicle. *FASEB journal : official publication of the Federation of American Societies for Experimental Biology* 24: 3869-3881.

42. Volinia, S., G. A. Calin, C. G. Liu, S. Ambs, A. Cimmino, F. Petrocca, R. Visone, M. Iorio, C. Roldo, M. Ferracin, R. L. Prueitt, N. Yanaihara, G. Lanza, A. Scarpa, A. Vecchione, M. Negrini, C. C. Harris, and C. M. Croce. 2006. A microRNA expression signature of human solid tumors defines cancer gene targets. *Proceedings of the National Academy of Sciences of the United States of America* 103: 2257-2261.

43. Lu, J., G. Getz, E. A. Miska, E. Alvarez-Saavedra, J. Lamb, D. Peck, A. Sweet-Cordero, B. L. Ebert, R. H. Mak, A. A. Ferrando, J. R. Downing, T. Jacks, H. R. Horvitz, and T. R. Golub. 2005. MicroRNA expression profiles classify human cancers. *Nature* 435: 834-838.

44. Yang, W., X. Lan, D. Li, T. Li, and S. Lu. 2015. MiR-223 targeting MAFB suppresses proliferation and migration of nasopharyngeal carcinoma cells. *BMC cancer* 15: 461.

45. Li, X., Y. Zhang, H. Zhang, X. Liu, T. Gong, M. Li, L. Sun, G. Ji, Y. Shi, Z. Han, S. Han, Y. Nie, X. Chen, Q. Zhao, J. Ding, K. Wu, and F. Daiming. 2011. miRNA-223 promotes gastric cancer invasion and metastasis by targeting tumor suppressor EPB41L3. *Molecular cancer research : MCR* 9: 824-833.

46. Darido, C., S. R. Georgy, T. Wilanowski, S. Dworkin, A. Auden, Q. Zhao, G. Rank, S. Srivastava, M. J. Finlay, A. T. Papenfuss, P. P. Pandolfi, R. B. Pearson, and S. M. Jane. 2011. Targeting of the tumor suppressor GRHL3 by a miR-21-dependent proto-oncogenic network results in PTEN loss and tumorigenesis. *Cancer cell* 20: 635-648.

47. Wang, C. J., Z. G. Zhou, L. Wang, L. Yang, B. Zhou, J. Gu, H. Y. Chen, and X. F. Sun. 2009. Clinicopathological significance of microRNA-31, -143 and -145 expression in colorectal cancer. *Disease markers* 26: 27-34.

48. Rajewsky, N. 2006. microRNA target predictions in animals. *Nature genetics* 38 Suppl: S8-13.

49. Didiano, D., and O. Hobert. 2006. Perfect seed pairing is not a generally reliable predictor for miRNA-target interactions. *Nature structural & molecular biology* 13: 849-851.

50. Thomson, D. W., C. P. Bracken, and G. J. Goodall. 2011. Experimental strategies for microRNA target identification. *Nucleic acids research* 39: 6845-6853.

51. Kuhn, D. E., M. M. Martin, D. S. Feldman, A. V. Terry, Jr., G. J. Nuovo, and T. S. Elton. 2008. Experimental validation of miRNA targets. *Methods (San Diego, Calif.)* 44: 47-54.

52. Chou, C. H., S. Shrestha, C. D. Yang, N. W. Chang, Y. L. Lin, K. W. Liao, W. C. Huang, T. H. Sun, S. J. Tu, W. H. Lee, M. Y. Chiew, C. S. Tai, T. Y. Wei, T. R. Tsai, H. T. Huang, C. Y. Wang, H. Y. Wu, S. Y. Ho, P. R. Chen, C. H. Chuang, P. J. Hsieh, Y. S. Wu, W. L. Chen, M. J. Li, Y. C. Wu, X. Y. Huang, F. L. Ng, W. Buddhakosai, P. C. Huang, K. C. Lan, C. Y. Huang, S. L. Weng, Y. N. Cheng, C. Liang, W. L. Hsu, and H. D. Huang. 2018. miRTarBase update 2018: a resource for experimentally validated microRNA-target interactions. *Nucleic acids research* 46: D296-d302.

53. Papadopoulos, G. L., M. Reczko, V. A. Simossis, P. Sethupathy, and A. G. Hatzigeorgiou. 2009. The database of experimentally supported targets: a functional update of TarBase. *Nucleic acids research* 37: D155-158.

54. Vlachos, I. S., M. D. Paraskevopoulou, D. Karagkouni, G. Georgakilas, T. Vergoulis, I. Kanellos, I. L. Anastasopoulos, S. Maniou, K. Karathanou, D. Kalfakakou, A. Fevgas, T. Dalamagas, and A. G. Hatzigeorgiou. 2015. DIANA-TarBase v7.0: indexing more than half a million experimentally supported miRNA:mRNA interactions. *Nucleic acids research* 43: D153-159.

55. Xiao, F., Z. Zuo, G. Cai, S. Kang, X. Gao, and T. Li. 2009. miRecords: an integrated resource for microRNA-target interactions. *Nucleic acids research* 37: D105-110.

56. Cho, S., I. Jang, Y. Jun, S. Yoon, M. Ko, Y. Kwon, I. Choi, H. Chang, D. Ryu, B. Lee, V. N. Kim, W. Kim, and S. Lee. 2013. MiRGator v3.0: a microRNA portal for deep sequencing, expression profiling and mRNA targeting. *Nucleic acids research* 41: D252-257.

57. Dweep, H., N. Gretz, and C. Sticht. 2014. miRWalk database for miRNA-target interactions. *Methods in molecular biology (Clifton, N.J.)* 1182: 289-305.

58. Naeem, H., R. Kuffner, G. Csaba, and R. Zimmer. 2010. miRSel: automated extraction of associations between microRNAs and genes from the biomedical literature. *BMC bioinformatics* 11: 135.

59. Li, J. H., S. Liu, H. Zhou, L. H. Qu, and J. H. Yang. 2014. starBase v2.0: decoding miRNA-ceRNA, miRNA-ncRNA and protein-RNA interaction networks from large-scale CLIP-Seq data. *Nucleic acids research* 42: D92-97.

60. Sun, X., B. Dong, L. Yin, R. Zhang, W. Du, D. Liu, N. Shi, A. Li, Y. Liang, and L. Mao. 2013. PMTED: a plant microRNA target expression database. *BMC bioinformatics* 14: 174.

61. Pio, G., M. Ceci, D. Malerba, and D. D'Elia. 2015. ComiRNet: a web-based system for the analysis of miRNA-gene regulatory networks. *BMC bioinformatics* 16 Suppl 9: S7.

62. Hsu, S. D., F. M. Lin, W. Y. Wu, C. Liang, W. C. Huang, W. L. Chan, W. T. Tsai, G. Z. Chen, C. J. Lee, C. M. Chiu, C. H. Chien, M. C. Wu, C. Y. Huang, A. P. Tsou, and H. D. Huang. 2011. miRTarBase: a database curates experimentally validated microRNA-target interactions. *Nucleic acids research* 39: D163-169.

63. Reyes-Herrera, P. H., and E. Ficarra. 2012. One decade of development and evolution of microRNA target prediction algorithms. *Genomics, proteomics & bioinformatics* 10: 254-263.

64. Peterson, S. M., J. A. Thompson, M. L. Ufkin, P. Sathyanarayana, L. Liaw, and C. B. Congdon. 2014. Common features of microRNA target prediction tools. *Frontiers in genetics* 5: 23.

65. Betel, D., A. Koppal, P. Agius, C. Sander, and C. Leslie. 2010. Comprehensive modeling of microRNA targets predicts functional non-conserved and non-canonical sites. *Genome biology* 11: R90.

66. Bartel, D. P. 2009. MicroRNAs: target recognition and regulatory functions. *Cell* 136: 215-233.

67. Grimson, A., K. K. Farh, W. K. Johnston, P. Garrett-Engele, L. P. Lim, and D. P. Bartel. 2007. MicroRNA targeting specificity in mammals: determinants beyond seed pairing. *Molecular cell* 27: 91-105.

68.   Friedman, R. C., K. K. Farh, C. B. Burge, and D. P. Bartel. 2009. Most mammalian mRNAs are conserved targets of microRNAs. *Genome research* 19: 92-105.

69.   Lall, S., D. Grun, A. Krek, K. Chen, Y. L. Wang, C. N. Dewey, P. Sood, T. Colombo, N. Bray, P. Macmenamin, H. L. Kao, K. C. Gunsalus, L. Pachter, F. Piano, and N. Rajewsky. 2006. A genome-wide map of conserved microRNA targets in C. elegans. *Current biology : CB* 16: 460-471.

70.   Miranda, K. C., T. Huynh, Y. Tay, Y. S. Ang, W. L. Tam, A. M. Thomson, B. Lim, and I. Rigoutsos. 2006. A pattern-based method for the identification of MicroRNA binding sites and their corresponding heteroduplexes. *Cell* 126: 1203-1217.

71.   Kruger, J., and M. Rehmsmeier. 2006. RNAhybrid: microRNA target prediction easy, fast and flexible. *Nucleic acids research* 34: W451-454.

72.   Kertesz, M., N. Iovino, U. Unnerstall, U. Gaul, and E. Segal. 2007. The role of site accessibility in microRNA target recognition. *Nature genetics* 39: 1278-1284.

73.   Gaidatzis, D., E. van Nimwegen, J. Hausser, and M. Zavolan. 2007. Inference of miRNA targets using evolutionary conservation and pathway analysis. *BMC bioinformatics* 8: 69.

74.   Maragkakis, M., P. Alexiou, G. L. Papadopoulos, M. Reczko, T. Dalamagas, G. Giannopoulos, G. Goumas, E. Koukis, K. Kourtis, V. A. Simossis, P. Sethupathy, T. Vergoulis, N. Koziris, T. Sellis, P. Tsanakas, and A. G. Hatzigeorgiou. 2009. Accurate microRNA target prediction correlates with protein repression levels. *BMC bioinformatics* 10: 295.

75.   Kim, S. K., J. W. Nam, J. K. Rhee, W. J. Lee, and B. T. Zhang. 2006. miTarget: microRNA target gene prediction using a support vector machine. *BMC bioinformatics* 7: 411.

76.   Yan, X., T. Chao, K. Tu, Y. Zhang, L. Xie, Y. Gong, J. Yuan, B. Qiang, and X. Peng. 2007. Improving the prediction of human microRNA target genes by using ensemble algorithm. *FEBS letters* 581: 1587-1593.

77.   Yousef, M., S. Jung, A. V. Kossenkov, L. C. Showe, and M. K. Showe. 2007. Naive Bayes for microRNA target predictions--machine learning for microRNA targets. *Bioinformatics (Oxford, England)* 23: 2987-2992.

78.   Wang, X., and I. M. El Naqa. 2008. Prediction of both conserved and nonconserved microRNA targets in animals. *Bioinformatics (Oxford, England)* 24: 325-332.

79.   Yang, Y., Y. P. Wang, and K. B. Li. 2008. MiRTif: a support vector machine-based microRNA target interaction filter. *BMC bioinformatics* 9 Suppl 12: S4.

80.   Sturm, M., M. Hackenberg, D. Langenberger, and D. Frishman. 2010. TargetSpy: a supervised machine learning approach for microRNA target prediction. *BMC bioinformatics* 11: 292.

81.   Friedman, Y., G. Naamati, and M. Linial. 2010. MiRror: a combinatorial analysis web tool for ensembles of microRNAs and their targets. *Bioinformatics (Oxford, England)* 26: 1920-1921.

82.   Reyes-Herrera, P. H., E. Ficarra, A. Acquaviva, and E. Macii. 2011. miREE: miRNA recognition elements ensemble. *BMC bioinformatics* 12: 454.

83.   John, B., A. J. Enright, A. Aravin, T. Tuschl, C. Sander, and D. S. Marks. 2004. Human MicroRNA targets. *PLoS biology* 2: e363.

84.   Kanehisa, M., S. Goto, M. Furumichi, M. Tanabe, and M. Hirakawa. 2010. KEGG for representation and analysis of molecular networks involving diseases and drugs. *Nucleic acids research* 38: D355-360.

85.   Khatri, P., M. Sirota, and A. J. Butte. 2012. Ten years of pathway analysis: current approaches and outstanding challenges. *PLoS computational biology* 8: e1002375.

86.   Garcia-Campos, M. A., J. Espinal-Enriquez, and E. Hernandez-Lemus. 2015. Pathway Analysis: State of the Art. *Frontiers in physiology* 6: 383.

87. Mitrea, C., Z. Taghavi, B. Bokanizad, S. Hanoudi, R. Tagett, M. Donato, C. Voichita, and S. Draghici. 2013. Methods and approaches in the topology-based analysis of biological pathways. *Frontiers in physiology* 4: 278.

88. Berriz, G. F., O. D. King, B. Bryant, C. Sander, and F. P. Roth. 2003. Characterizing gene sets with FuncAssociate. *Bioinformatics (Oxford, England)* 19: 2502-2504.

89. Beissbarth, T., and T. P. Speed. 2004. GOstat: find statistically overrepresented Gene Ontologies within a group of genes. *Bioinformatics (Oxford, England)* 20: 1464-1465.

90. Castillo-Davis, C. I., and D. L. Hartl. 2003. GeneMerge--post-genomic analysis, data mining, and hypothesis testing. *Bioinformatics (Oxford, England)* 19: 891-892.

91. Pavlidis, P., J. Qin, V. Arango, J. J. Mann, and E. Sibille. 2004. Using the gene ontology for microarray data mining: a comparison of methods and application to age effects in human prefrontal cortex. *Neurochemical research* 29: 1213-1222.

92. Barabasi, A. L., and Z. N. Oltvai. 2004. Network biology: understanding the cell's functional organization. *Nature reviews. Genetics* 5: 101-113.

93. Subramanian, A., P. Tamayo, V. K. Mootha, S. Mukherjee, B. L. Ebert, M. A. Gillette, A. Paulovich, S. L. Pomeroy, T. R. Golub, E. S. Lander, and J. P. Mesirov. 2005. Gene set enrichment analysis: a knowledge-based approach for interpreting genome-wide expression profiles. *Proceedings of the National Academy of Sciences of the United States of America* 102: 15545-15550.

94. Kramer, A., J. Green, J. Pollard, Jr., and S. Tugendreich. 2014. Causal analysis approaches in Ingenuity Pathway Analysis. *Bioinformatics (Oxford, England)* 30: 523-530.

95. Draghici, S., P. Khatri, A. L. Tarca, K. Amin, A. Done, C. Voichita, C. Georgescu, and R. Romero. 2007. A systems biology approach for pathway level analysis. *Genome research* 17: 1537-1545.

96. Merico, D., R. Isserlin, O. Stueker, A. Emili, and G. D. Bader. 2010. Enrichment map: a network-based method for gene-set enrichment visualization and interpretation. *PloS one* 5: e13984.

97. Purdie, K. J., J. Pennington, C. M. Proby, S. Khalaf, E. M. de Villiers, I. M. Leigh, and A. Storey. 1999. The promoter of a novel human papillomavirus (HPV77) associated with skin cancer displays UV responsiveness, which is mediated through a consensus p53 binding sequence. *The EMBO journal* 18: 5359-5369.

98. Akgul, B., W. Lemme, R. Garcia-Escudero, A. Storey, and H. J. Pfister. 2005. UV-B irradiation stimulates the promoter activity of the high-risk, cutaneous human papillomavirus 5 and 8 in primary keratinocytes. *Archives of virology* 150: 145-151.

99. Kripke, M. L. 1994. Ultraviolet radiation and immunology: something new under the sun--presidential address. *Cancer research* 54: 6102-6105.

100. Arron, S. T., L. Jennings, I. Nindl, F. Rosl, J. N. Bouwes Bavinck, D. Seckin, M. Trakatelli, and G. M. Murphy. 2011. Viral oncogenesis and its role in nonmelanoma skin cancer. *The British journal of dermatology* 164: 1201-1213.

101. Purdie, K. J., C. Pourreyron, and A. P. South. 2011. Isolation and culture of squamous cell carcinoma lines. *Methods in molecular biology (Clifton, N.J.)* 731: 151-159.

102. Kim, D., G. Pertea, C. Trapnell, H. Pimentel, R. Kelley, and S. L. Salzberg. 2013. TopHat2: accurate alignment of transcriptomes in the presence of insertions, deletions and gene fusions. *Genome biology* 14: R36.

103. Trapnell, C., A. Roberts, L. Goff, G. Pertea, D. Kim, D. R. Kelley, H. Pimentel, S. L. Salzberg, J. L. Rinn, and L. Pachter. 2012. Differential gene and transcript expression analysis of RNA-seq experiments with TopHat and Cufflinks. *Nature protocols* 7: 562-578.

104.	Anders, S., P. T. Pyl, and W. Huber. 2015. HTSeq--a Python framework to work with high-throughput sequencing data. *Bioinformatics (Oxford, England)* 31: 166-169.

105.	Love, M. I., W. Huber, and S. Anders. 2014. Moderated estimation of fold change and dispersion for RNA-seq data with DESeq2. *Genome biology* 15: 550.

106.	Kozomara, A., and S. Griffiths-Jones. 2014. miRBase: annotating high confidence microRNAs using deep sequencing data. *Nucleic acids research* 42: D68-73.

107.	Agarwal, V., G. W. Bell, J. W. Nam, and D. P. Bartel. 2015. Predicting effective microRNA target sites in mammalian mRNAs. *eLife* 4.

108.	Cox, J., and M. Mann. 2008. MaxQuant enables high peptide identification rates, individualized p.p.b.-range mass accuracies and proteome-wide protein quantification. *Nature biotechnology* 26: 1367-1372.

109.	Welsh, E. A., S. A. Eschrich, A. E. Berglund, and D. A. Fenstermacher. 2013. Iterative rank-order normalization of gene expression microarray data. *BMC bioinformatics* 14: 153.

110.	Guy, G. P., Jr., S. R. Machlin, D. U. Ekwueme, and K. R. Yabroff. 2015. Prevalence and costs of skin cancer treatment in the U.S., 2002-2006 and 2007-2011. *American journal of preventive medicine* 48: 183-187.

111.	Muthusamy, V., and T. J. Piva. 2010. The UV response of the skin: a review of the MAPK, NFkappaB and TNFalpha signal transduction pathways. *Archives of dermatological research* 302: 5-17.

112.	Guerra, L., T. Odorisio, G. Zambruno, and D. Castiglia. 2017. Stromal microenvironment in type VII collagen-deficient skin: The ground for squamous cell carcinoma development. *Matrix biology : journal of the International Society for Matrix Biology* 63: 1-10.

113.	Watson, R. E., N. K. Gibbs, C. E. Griffiths, and M. J. Sherratt. 2014. Damage to skin extracellular matrix induced by UV exposure. *Antioxidants & redox signaling* 21: 1063-1077.

114.	Waster, P., K. Orfanidis, I. Eriksson, I. Rosdahl, O. Seifert, and K. Ollinger. 2017. UV radiation promotes melanoma dissemination mediated by the sequential reaction axis of cathepsins-TGF-beta1-FAP-alpha. *British journal of cancer* 117: 535-544.

115.	Gupta, A., P. Avci, T. Dai, Y. Y. Huang, and M. R. Hamblin. 2013. Ultraviolet Radiation in Wound Care: Sterilization and Stimulation. *Advances in wound care* 2: 422-437.

116.	Li, D., A. Wang, X. Liu, F. Meisgen, J. Grunler, I. R. Botusan, S. Narayanan, E. Erikci, X. Li, L. Blomqvist, L. Du, A. Pivarcsi, E. Sonkoly, K. Chowdhury, S. B. Catrina, M. Stahle, and N. X. Landen. 2015. MicroRNA-132 enhances transition from inflammation to proliferation during wound healing. *The Journal of clinical investigation* 125: 3008-3026.

117.	Nuutila, K., A. Siltanen, M. Peura, J. Bizik, I. Kaartinen, H. Kuokkanen, T. Nieminen, A. Harjula, P. Aarnio, J. Vuola, and E. Kankuri. 2012. Human skin transcriptome during superficial cutaneous wound healing. *Wound repair and regeneration : official publication of the Wound Healing Society [and] the European Tissue Repair Society* 20: 830-839.

118.	Brash, D. E. 2015. UV signature mutations. *Photochemistry and photobiology* 91: 15-26.

119.	Dawes, J. M., A. Antunes-Martins, J. R. Perkins, K. J. Paterson, M. Sisignano, R. Schmid, W. Rust, T. Hildebrandt, G. Geisslinger, C. Orengo, D. L. Bennett, and S. B. McMahon. 2014. Genome-wide transcriptional profiling of skin and dorsal root ganglia after ultraviolet-B-induced inflammation. *PloS one* 9: e93338.

120.	Ravnbak, M. H. 2010. Objective determination of Fitzpatrick skin type. *Danish medical bulletin* 57: B4153.

121. Degueurce, G., I. D'Errico, C. Pich, M. Ibberson, F. Schutz, A. Montagner, M. Sgandurra, L. Mury, P. Jafari, A. Boda, J. Meunier, R. Rezzonico, N. C. Brembilla, D. Hohl, A. Kolios, G. Hofbauer, I. Xenarios, and L. Michalik. 2016. Identification of a novel PPARbeta/delta/miR-21-3p axis in UV-induced skin inflammation. *EMBO molecular medicine* 8: 919-936.

122. Lin, K. Y., C. M. Chen, C. Y. Lu, C. Y. Cheng, and Y. H. Wu. 2017. Regulation of miR-21 expression in human melanoma via UV-ray-induced melanin pigmentation. *Environmental toxicology* 32: 2064-2069.

123. Guo, L., Z. X. Huang, X. W. Chen, Q. K. Deng, W. Yan, M. J. Zhou, C. S. Ou, and Z. H. Ding. 2009. Differential expression profiles of microRNAs in NIH3T3 cells in response to UVB irradiation. *Photochemistry and photobiology* 85: 765-773.

124. Yang, M., J. Chen, F. Su, B. Yu, F. Su, L. Lin, Y. Liu, J. D. Huang, and E. Song. 2011. Microvesicles secreted by macrophages shuttle invasion-potentiating microRNAs into breast cancer cells. *Molecular cancer* 10: 117.

125. Fine, J. D., L. Bruckner-Tuderman, R. A. Eady, E. A. Bauer, J. W. Bauer, C. Has, A. Heagerty, H. Hintner, A. Hovnanian, M. F. Jonkman, I. Leigh, M. P. Marinkovich, A. E. Martinez, J. A. McGrath, J. E. Mellerio, C. Moss, D. F. Murrell, H. Shimizu, J. Uitto, D. Woodley, and G. Zambruno. 2014. Inherited epidermolysis bullosa: updated recommendations on diagnosis and classification. *Journal of the American Academy of Dermatology* 70: 1103-1126.

126. Mootha, V. K., C. M. Lindgren, K. F. Eriksson, A. Subramanian, S. Sihag, J. Lehar, P. Puigserver, E. Carlsson, M. Ridderstrale, E. Laurila, N. Houstis, M. J. Daly, N. Patterson, J. P. Mesirov, T. R. Golub, P. Tamayo, B. Spiegelman, E. S. Lander, J. N. Hirschhorn, D. Altshuler, and L. C. Groop. 2003. PGC-1alpha-responsive genes involved in oxidative phosphorylation are coordinately downregulated in human diabetes. *Nature genetics* 34: 267-273.

127. Richards, C. D. 2013. The enigmatic cytokine oncostatin m and roles in disease. *ISRN inflammation* 2013: 512103.

128. Hermanns, H. M. 2015. Oncostatin M and interleukin-31: Cytokines, receptors, signal transduction and physiology. *Cytokine & growth factor reviews* 26: 545-558.

129. Whiteman, D. C., P. Valery, W. McWhirter, and A. C. Green. 1997. Risk factors for childhood melanoma in Queensland, Australia. *International journal of cancer* 70: 26-31.

130. Davidson, S. F., S. K. Brantley, and S. K. Das. 1991. The effects of ultraviolet radiation on wound healing. *British journal of plastic surgery* 44: 210-214.

131. Ding, J., and E. E. Tredget. 2015. The Role of Chemokines in Fibrotic Wound Healing. *Advances in wound care* 4: 673-686.

132. Behm, B., P. Babilas, M. Landthaler, and S. Schreml. 2012. Cytokines, chemokines and growth factors in wound healing. *Journal of the European Academy of Dermatology and Venereology : JEADV* 26: 812-820.

133. Zimolag, E., J. Borowczyk-Michalowska, S. Kedracka-Krok, B. Skupien-Rabian, E. Karnas, S. Lasota, J. Sroka, J. Drukala, and Z. Madeja. 2017. Electric field as a potential directional cue in homing of bone marrow-derived mesenchymal stem cells to cutaneous wounds. *Biochimica et biophysica acta* 1864: 267-279.

134. Guinea-Viniegra, J., M. Jimenez, H. B. Schonthaler, R. Navarro, Y. Delgado, M. J. Concha-Garzon, E. Tschachler, S. Obad, E. Dauden, and E. F. Wagner. 2014. Targeting miR-21 to treat psoriasis. *Science translational medicine* 6: 225re221.

135. Hatley, M. E., D. M. Patrick, M. R. Garcia, J. A. Richardson, R. Bassel-Duby, E. van Rooij, and E. N. Olson. 2010. Modulation of K-Ras-dependent lung tumorigenesis by MicroRNA-21. *Cancer cell* 18: 282-293.
136. Ma, X., M. Kumar, S. N. Choudhury, L. E. Becker Buscaglia, J. R. Barker, K. Kanakamedala, M. F. Liu, and Y. Li. 2011. Loss of the miR-21 allele elevates the expression of its target genes and reduces tumorigenesis. *Proceedings of the National Academy of Sciences of the United States of America* 108: 10144-10149.
137. Stojadinovic, O., H. Ramirez, I. Pastar, K. A. Gordon, R. Stone, S. Choudhary, E. Badiavas, K. Nouri, and M. Tomic-Canic. 2017. MiR-21 and miR-205 are induced in invasive cutaneous squamous cell carcinomas. *Archives of dermatological research* 309: 133-139.
138. Li, X., K. Huang, and J. Yu. 2014. Inhibition of microRNA-21 upregulates the expression of programmed cell death 4 and phosphatase tensin homologue in the A431 squamous cell carcinoma cell line. *Oncology letters* 8: 203-207.
139. Bruegger, C., W. Kempf, I. Spoerri, A. W. Arnold, P. H. Itin, and B. Burger. 2013. MicroRNA expression differs in cutaneous squamous cell carcinomas and healthy skin of immunocompetent individuals. *Experimental dermatology* 22: 426-428.
140. Lin, N., Y. Zhou, X. Lian, and Y. Tu. 2017. MicroRNA-31 functions as an oncogenic microRNA in cutaneous squamous cell carcinoma cells by targeting RhoTBT1. *Oncology letters* 13: 1078-1082.
141. Wang, A., N. X. Landen, F. Meisgen, W. Lohcharoenkal, M. Stahle, E. Sonkoly, and A. Pivarcsi. 2014. MicroRNA-31 is overexpressed in cutaneous squamous cell carcinoma and regulates cell motility and colony formation ability of tumor cells. *PloS one* 9: e103206.
142. Shi, J., X. Ma, Y. Su, Y. Song, Y. Tian, S. Yuan, X. Zhang, D. Yang, H. Zhang, J. Shuai, W. Cui, F. Ren, M. V. Plikus, Y. Chen, J. Luo, and Z. Yu. 2018. MiR-31 Mediates Inflammatory Signaling to Promote Re-Epithelialization during Skin Wound Healing. *The Journal of investigative dermatology*.
143. Valeri, N., C. Braconi, P. Gasparini, C. Murgia, A. Lampis, V. Paulus-Hock, J. R. Hart, L. Ueno, S. I. Grivennikov, F. Lovat, A. Paone, L. Cascione, K. M. Sumani, A. Veronese, M. Fabbri, S. Carasi, H. Alder, G. Lanza, R. Gafa, M. P. Moyer, R. A. Ridgway, J. Cordero, G. J. Nuovo, W. L. Frankel, M. Rugge, M. Fassan, J. Groden, P. K. Vogt, M. Karin, O. J. Sansom, and C. M. Croce. 2014. MicroRNA-135b promotes cancer progression by acting as a downstream effector of oncogenic pathways in colon cancer. *Cancer cell* 25: 469-483.
144. Lin, C. W., Y. L. Chang, Y. C. Chang, J. C. Lin, C. C. Chen, S. H. Pan, C. T. Wu, H. Y. Chen, S. C. Yang, T. M. Hong, and P. C. Yang. 2013. MicroRNA-135b promotes lung cancer metastasis by regulating multiple targets in the Hippo pathway and LZTS1. *Nature communications* 4: 1877.
145. Nezu, Y., K. Hagiwara, Y. Yamamoto, T. Fujiwara, K. Matsuo, A. Yoshida, A. Kawai, T. Saito, and T. Ochiya. 2016. miR-135b, a key regulator of malignancy, is linked to poor prognosis in human myxoid liposarcoma. *Oncogene* 35: 6177-6188.
146. Mazar, J., F. Qi, B. Lee, J. Marchica, S. Govindarajan, J. Shelley, J. L. Li, A. Ray, and R. J. Perera. 2016. MicroRNA 211 Functions as a Metabolic Switch in Human Melanoma Cells. *Molecular and cellular biology* 36: 1090-1108.
147. Diaz-Martinez, M., L. Benito-Jardon, L. Alonso, L. Koetz-Ploch, E. Hernando, and J. Teixido. 2018. miR-204-5p and miR-211-5p Contribute to BRAF Inhibitor Resistance in Melanoma. *Cancer research* 78: 1017-1030.

148. Wang, K., W. Jin, P. Jin, X. Fei, X. Wang, and X. Chen. 2017. miR-211-5p Suppresses Metastatic Behavior by Targeting SNAI1 in Renal Cancer. *Molecular cancer research : MCR* 15: 448-456.

149. Xu, N., F. Meisgen, L. M. Butler, G. Han, X. J. Wang, C. Soderberg-Naucler, M. Stahle, A. Pivarcsi, and E. Sonkoly. 2013. MicroRNA-31 is overexpressed in psoriasis and modulates inflammatory cytokine and chemokine production in keratinocytes via targeting serine/threonine kinase 40. *Journal of immunology (Baltimore, Md. : 1950)* 190: 678-688.

150. Lu, Z., M. Liu, V. Stribinskis, C. M. Klinge, K. S. Ramos, N. H. Colburn, and Y. Li. 2008. MicroRNA-21 promotes cell transformation by targeting the programmed cell death 4 gene. *Oncogene* 27: 4373-4379.

151. Ma, X., S. N. Choudhury, X. Hua, Z. Dai, and Y. Li. 2013. Interaction of the oncogenic miR-21 microRNA and the p53 tumor suppressor pathway. *Carcinogenesis* 34: 1216-1223.

152. Ma, X., D. J. Conklin, F. Li, Z. Dai, X. Hua, Y. Li, Z. Y. Xu-Monette, K. H. Young, W. Xiong, M. Wysoczynski, S. D. Sithu, S. Srivastava, A. Bhatnagar, and Y. Li. 2015. The oncogenic microRNA miR-21 promotes regulated necrosis in mice. *Nature communications* 6: 7151.

153. Bica-Pop, C., R. Cojocneanu-Petric, L. Magdo, L. Raduly, D. Gulei, and I. Berindan-Neagoe. 2018. Overview upon miR-21 in lung cancer: focus on NSCLC. *Cellular and molecular life sciences : CMLS*.

154. Piasecka, D., M. Braun, R. Kordek, R. Sadej, and H. Romanska. 2018. MicroRNAs in regulation of triple-negative breast cancer progression. *Journal of cancer research and clinical oncology*.

155. Panagal, M., R. S. S, S. P, B. M, K. M, V. Gopinathe, P. Sivakumare, and D. Sekar. 2018. MicroRNA21 and the various types of myeloid leukemia. *Cancer gene therapy*.

156. Bourguignon, L. Y., and D. Bikle. 2015. Selective Hyaluronan-CD44 Signaling Promotes miRNA-21 Expression and Interacts with Vitamin D Function during Cutaneous Squamous Cell Carcinomas Progression Following UV Irradiation. *Frontiers in immunology* 6: 224.

157. Mahmoud, E. H., A. Fawzy, and A. E. RA. 2018. Serum MicroRNA-21 Negatively Relates to Expression of Programmed Cell Death-4 in Patients with Epithelial Ovarian Cancer. *Asian Pacific journal of cancer prevention : APJCP* 19: 33-38.

158. Parikh, S. A., V. A. Patel, and D. Ratner. 2014. Advances in the management of cutaneous squamous cell carcinoma. *F1000prime reports* 6: 70.

159. Weng, H., K. Lal, F. F. Yang, and J. Chen. 2015. The pathological role and prognostic impact of miR-181 in acute myeloid leukemia. *Cancer Genet* 208: 225-229.

160. Yang, Z., X. Wan, Z. Gu, H. Zhang, X. Yang, L. He, R. Miao, Y. Zhong, and H. Zhao. 2014. Evolution of the mir-181 microRNA family. *Comput Biol Med* 52: 82-87.

161. Nishida, N., M. Nagahara, T. Sato, K. Mimori, T. Sudo, F. Tanaka, K. Shibata, H. Ishii, K. Sugihara, Y. Doki, and M. Mori. 2012. Microarray analysis of colorectal cancer stromal tissue reveals upregulation of two oncogenic miRNA clusters. *Clin Cancer Res* 18: 3054-3070.

162. Parikh, A., C. Lee, P. Joseph, S. Marchini, A. Baccarini, V. Kolev, C. Romualdi, R. Fruscio, H. Shah, F. Wang, G. Mullokandov, D. Fishman, M. D'Incalci, J. Rahaman, T. Kalir, R. W. Redline, B. D. Brown, G. Narla, and A. DiFeo. 2014. microRNA-181a has a critical role in ovarian cancer progression through the regulation of the epithelial-mesenchymal transition. *Nat Commun* 5: 2977.

163. Brockhausen, J., S. S. Tay, C. A. Grzelak, P. Bertolino, D. G. Bowen, W. M. d'Avigdor, N. Teoh, S. Pok, N. Shackel, J. R. Gamble, M. Vadas, and G. W. McCaughan. 2015. miR-181a mediates TGF-beta-induced hepatocyte EMT and is dysregulated in cirrhosis and hepatocellular cancer. *Liver*

international : official journal of the International Association for the Study of the Liver 35: 240-253.

164. Zhang, X., Y. Nie, Y. Du, J. Cao, B. Shen, and Y. Li. 2012. MicroRNA-181a promotes gastric cancer by negatively regulating tumor suppressor KLF6. *Tumour Biol* 33: 1589-1597.

165. Taylor, M. A., K. Sossey-Alaoui, C. L. Thompson, D. Danielpour, and W. P. Schiemann. 2013. TGF-beta upregulates miR-181a expression to promote breast cancer metastasis. *J Clin Invest* 123: 150-163.

166. Chen, G., W. Zhu, D. Shi, L. Lv, C. Zhang, P. Liu, and W. Hu. 2010. MicroRNA-181a sensitizes human malignant glioma U87MG cells to radiation by targeting Bcl-2. *Oncol Rep* 23: 997-1003.

167. Wang, Y., Y. Yu, A. Tsuyada, X. Ren, X. Wu, K. Stubblefield, E. K. Rankin-Gee, and S. E. Wang. 2011. Transforming growth factor-beta regulates the sphere-initiating stem cell-like feature in breast cancer through miRNA-181 and ATM. *Oncogene* 30: 1470-1480.

168. Shin, K. H., S. D. Bae, H. S. Hong, R. H. Kim, M. K. Kang, and N. H. Park. 2011. miR-181a shows tumor suppressive effect against oral squamous cell carcinoma cells by downregulating K-ras. *Biochem Biophys Res Commun* 404: 896-902.

169. Jamali, Z., N. Asl Aminabadi, R. Attaran, F. Pournagiazar, S. Ghertasi Oskouei, and F. Ahmadpour. 2015. MicroRNAs as prognostic molecular signatures in human head and neck squamous cell carcinoma: a systematic review and meta-analysis. *Oral Oncol* 51: 321-331.

170. Li, Y. Y., G. J. Hanna, A. C. Laga, R. I. Haddad, J. H. Lorch, and P. S. Hammerman. 2015. Genomic analysis of metastatic cutaneous squamous cell carcinoma. *Clin Cancer Res* 21: 1447-1456.

171. Vin, H., S. S. Ojeda, G. Ching, M. L. Leung, V. Chitsazzadeh, D. W. Dwyer, C. H. Adelmann, M. Restrepo, K. N. Richards, L. R. Stewart, L. Du, S. B. Ferguson, D. Chakravarti, K. Ehrenreiter, M. Baccarini, R. Ruggieri, J. L. Curry, K. B. Kim, A. M. Ciurea, M. Duvic, V. G. Prieto, S. E. Ullrich, K. N. Dalby, E. R. Flores, and K. Y. Tsai. 2013. BRAF inhibitors suppress apoptosis through off-target inhibition of JNK signaling. *Elife* 2: e00969.

172. Canman, C. E., and D. S. Lim. 1998. The role of ATM in DNA damage responses and cancer. *Oncogene* 17: 3301-3308.

173. Khanna, K. K., and G. Chenevix-Trench. 2004. ATM and genome maintenance: defining its role in breast cancer susceptibility. *Journal of mammary gland biology and neoplasia* 9: 247-262.

174. Bisso, A., M. Faleschini, F. Zampa, V. Capaci, J. De Santa, L. Santarpia, S. Piazza, V. Cappelletti, M. Daidone, R. Agami, and G. Del Sal. 2013. Oncogenic miR-181a/b affect the DNA damage response in aggressive breast cancer. *Cell Cycle* 12: 1679-1687.

175. Zhang, Z., Z. Yang, S. Jaamaa, H. Liu, L. G. Pellakuru, T. Iwata, T. M. af Hallstrom, A. M. De Marzo, and M. Laiho. 2011. Differential epithelium DNA damage response to ATM and DNA-PK pathway inhibition in human prostate tissue culture. *Cell cycle (Georgetown, Tex.)* 10: 3545-3553.

176. Hudson, L. G., K. M. Newkirk, H. L. Chandler, C. Choi, S. L. Fossey, A. E. Parent, and D. F. Kusewitt. 2009. Cutaneous wound reepithelialization is compromised in mice lacking functional Slug (Snai2). *J Dermatol Sci* 56: 19-26.

177. Shirley, S. H., E. A. Grimm, and D. F. Kusewitt. 2012. Ultraviolet radiation and the slug transcription factor induce proinflammatory and immunomodulatory mediator expression in melanocytes. *J Skin Cancer* 2012: 410925.

178. Iizuka, N., M. Oka, H. Yamada-Okabe, M. Nishida, Y. Maeda, N. Mori, T. Takao, T. Tamesa, A. Tangoku, H. Tabuchi, K. Hamada, H. Nakayama, H. Ishitsuka, T. Miyamoto, A. Hirabayashi, S. Uchimura, and Y. Hamamoto. 2003. Oligonucleotide microarray for prediction of early

intrahepatic recurrence of hepatocellular carcinoma after curative resection. *Lancet (London, England)* 361: 923-929.

179.   Roberts, L. R., and G. J. Gores. 2005. Hepatocellular carcinoma: molecular pathways and new therapeutic targets. *Seminars in liver disease* 25: 212-225.

180.   Griffiths-Jones, S., R. J. Grocock, S. van Dongen, A. Bateman, and A. J. Enright. 2006. miRBase: microRNA sequences, targets and gene nomenclature. *Nucleic acids research* 34: D140-144.

181.   Zhang, S., W. Y. Sun, J. J. Wu, Y. J. Gu, and W. Wei. 2016. Decreased expression of the type III TGF-beta receptor enhances metastasis and invasion in hepatocellullar carcinoma progression. *Oncol Rep* 35: 2373-2381.

182.   Yang, C. C., P. S. Hung, P. W. Wang, C. J. Liu, T. H. Chu, H. W. Cheng, and S. C. Lin. 2011. miR-181 as a putative biomarker for lymph-node metastasis of oral squamous cell carcinoma. *J Oral Pathol Med* 40: 397-404.

183.   Courthod, G., P. Franco, L. Palermo, S. Pisconti, and G. Numico. 2014. The role of microRNA in head and neck cancer: current knowledge and perspectives. *Molecules* 19: 5704-5716.

184.   Liu Y, L. Z., Liu M, Zhang L. 2016. Profiling of MicroRNA Expression in Head and Neck Cancer. . *MOJ Cell Sci Rep* 3.

185.   Meng, W., Q. Xia, L. Wu, S. Chen, X. He, L. Zhang, Q. Gao, and H. Zhou. 2011. Downregulation of TGF-beta receptor types II and III in oral squamous cell carcinoma and oral carcinoma-associated fibroblasts. *BMC Cancer* 11: 88.

186.   Bernabeu, C., J. M. Lopez-Novoa, and M. Quintanilla. 2009. The emerging role of TGF-beta superfamily coreceptors in cancer. *Biochim Biophys Acta* 1792: 954-973.

187.   Xue, M., F. Y. Zhu, L. Chen, and K. Wang. 2017. HoxB9 promotes the migration and invasion via TGF-beta1/Smad2/Slug signaling pathway in oral squamous cell carcinoma. *Am J Transl Res* 9: 1151-1161.

188.   Harradine, K. A., K. Ridd, E. F. Saunier, F. F. Clermont, J. Perez-Losada, D. H. Moore, E. H. Epstein, Jr., B. C. Bastian, and R. J. Akhurst. 2009. Elevated cutaneous Smad activation associates with enhanced skin tumor susceptibility in organ transplant recipients. *Clin Cancer Res* 15: 5101-5107.

189.   Martins, V. L., M. P. Caley, K. Moore, Z. Szentpetery, S. T. Marsh, D. F. Murrell, M. H. Kim, M. Avari, J. A. McGrath, R. Cerio, A. Kivisaari, V. M. Kahari, K. Hodivala-Dilke, C. H. Brennan, M. Chen, J. F. Marshall, and E. A. O'Toole. 2016. Suppression of TGFbeta and Angiogenesis by Type VII Collagen in Cutaneous SCC. *J Natl Cancer Inst* 108.

190.   Wang, F. D.-J. 2010. TGF-β receptor III enhances TGF-β and NF-κB signaling in head and neck squamous cell carcinoma. Yale Medicine Thesis Digital Library.

191.   Mordasky Markell, L., R. Perez-Lorenzo, K. E. Masiuk, M. J. Kennett, and A. B. Glick. 2010. Use of a TGFbeta type I receptor inhibitor in mouse skin carcinogenesis reveals a dual role for TGFbeta signaling in tumor promotion and progression. *Carcinogenesis* 31: 2127-2135.

192.   Nordback, I., R. Kulmala, and M. Jarvinen. 1990. Effect of ultraviolet therapy on rat skin wound healing. *The Journal of surgical research* 48: 68-71.

193.   Simmons, S., C. Dale, J. Holt, K. Velasquez, and M. Stibich. 2017. Role of Ultraviolet Disinfection in the Prevention of Surgical Site Infections. *Advances in experimental medicine and biology* 996: 255-266.

194.   Yuan, Y., W. Liu, Y. Zhang, Y. Zhang, and S. Sun. 2018. CircRNA circ_0026344 as a prognostic biomarker suppresses colorectal cancer progression via microRNA-21 and microRNA-31. *Biochemical and biophysical research communications*.

195. Schee, K., K. Boye, T. W. Abrahamsen, O. Fodstad, and K. Flatmark. 2012. Clinical relevance of microRNA miR-21, miR-31, miR-92a, miR-101, miR-106a and miR-145 in colorectal cancer. *BMC cancer* 12: 505.

196. Xu, X. M., J. C. Qian, Z. L. Deng, Z. Cai, T. Tang, P. Wang, K. H. Zhang, and J. P. Cai. 2012. Expression of miR-21, miR-31, miR-96 and miR-135b is correlated with the clinical parameters of colorectal cancer. *Oncology letters* 4: 339-345.

197. Odar, K., E. Bostjancic, N. Gale, D. Glavac, and N. Zidar. 2012. Differential expression of microRNAs miR-21, miR-31, miR-203, miR-125a-5p and miR-125b and proteins PTEN and p63 in verrucous carcinoma of the head and neck. *Histopathology* 61: 257-265.

198. Cottonham, C. L., S. Kaneko, and L. Xu. 2010. miR-21 and miR-31 converge on TIAM1 to regulate migration and invasion of colon carcinoma cells. *The Journal of biological chemistry* 285: 35293-35302.

VITA

Tran Nguyen was born in Vietnam. After completing her work at Le Hong Phong Highschool in 2063, she entered University of Medicine and Pharmacy in Ho Chi Minh City. She received the degree of Bachelor of Pharmacy in July, 2011. In August of 2012 she entered The University of Texas MD Anderson Cancer Center UTHealth Graduate School of Biomedical Sciences.

Permanent address:

67 Duong Van An

An Phu Ward, District 2

Ho Chi Minh City

Vietnam 70000